LOOK-AHEAD TRACKING CONTROLLERS FOR INTEGRATED LONGITUDINAL AND LATERAL CONTROL OF VEHICLE PLATOONS
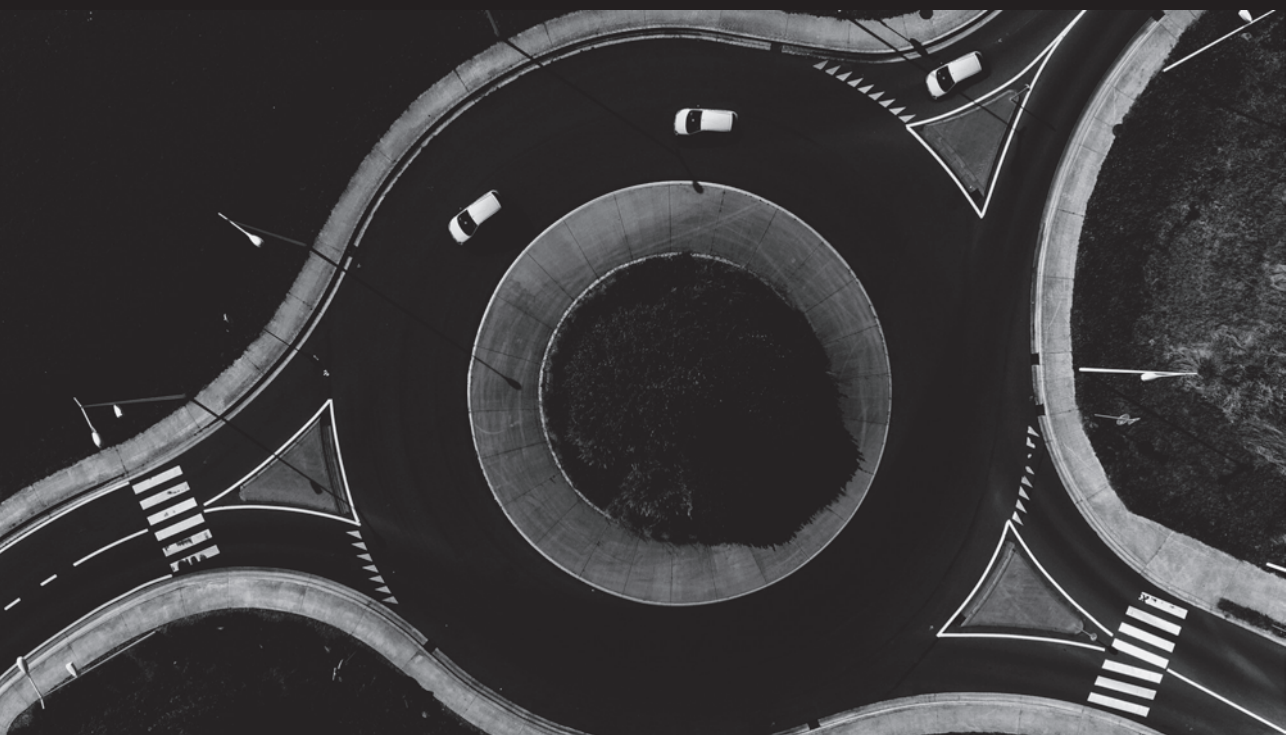
ANGGERA BAYUWINDRA

Look-ahead Tracking Controllers for Integrated Longitudinal and Lateral Control of Vehicle Platoons

Anggera Bayuwindra

disc

lpdp

Look-ahead Tracking Controllers for Integrated Longitudinal and Lateral Control of Vehicle Platoons

Dit proefschrift is goedgekeurd door de promotoren en de samenstelling van de promotiecommissie is als volgt:

voorzitter:	prof.dr. L.P.H. de Goey
promotor:	prof.dr. H. Nijmeijer
1$^{\text{e}}$ copromotor:	dr.ir. J. Ploeg
2$^{\text{e}}$ copromotor:	dr.ir. A.A.J. Lefeber
leden:	prof.dr. R.R. Negenborn (Technische Universiteit Delft)
	prof.dr. J.P. Huissoon (University of Waterloo)
	prof.dr. B. Jayawardhana (Rijksuniversiteit Groningen)
	prof.dr. J.J. Lukkien

Summary

Look-ahead Tracking Controllers for Integrated Longitudinal and Lateral Control of Vehicle Platoons

The increasing demand for mobility and a limited development of the existing road infrastructure leads to a growing interest in the improvement of ground transportation, with respect to safety, throughput, fuel consumption, and emissions. As a result, the field of Intelligent Transportation Systems (ITS) emerged in the past decade. As one of the promising ITS applications, Adaptive Cruise Control (ACC) was first invented for road vehicles as a safety and comfort system, by which a vehicle speed is automatically adjust to maintain a safe distance from vehicles ahead. In ACC, a radar or lidar measurements are used to measure the distance and the relative speed as inputs for a control system that automatically maintains a desired inter-vehicle distance.

During its development, ACC was further extended to Cooperative Adaptive Cruise Control (CACC) with the addition of information exchange between vehicles through a vehicle-to-vehicle (V2V) wireless communication. By providing the following vehicle with additional wireless information about its preceding vehicle, the addition of V2V communication has been proven to allow for reduction of the inter-vehicle distance while attenuating disturbances in upstream direction. A fully automated vehicle platoon, which can be described as a "follow the leader" strategy, is realized by exchanging information about the longitudinal (accelerating and decelerating) and lateral (turning) motion between vehicles. In most literature, the longitudinal control problem and the lateral control problem are treated independently. In particular, the longitudinal control problem is handled by CACC, while the lateral control problem is approached as a lane-keeping problem. Through radar/lidar and V2V communication, CACC minimizes the error between the desired distance and the actual distance between the vehicle and its preceding vehicle. On the other hand, the lateral control problem is solved by a vision-based lane-keeping system, which employs an image processing algorithm for lane detection. From a platooning viewpoint, there are several considerations regarding this lane-keeping method that should be taken into account. First,

it is not always possible to obtain an accurate measurement of lane markings, especially when vehicles in a platoon are driving close together, which is specifically aimed for with CACC. Secondly, the lane markings may be of bad quality, obstructed, or even not present (e.g., on intersections or at rural areas). Moreover, the longitudinal and lateral movement of the vehicle should not be treated independently, since the driving behavior includes the dynamics of longitudinal motion, lateral motion, and the combination of both (e.g, decelerating while turning).

To achieve fully automated vehicle following, there are two requirements that need to be considered: integrated longitudinal and lateral control design, and the robustness against loss of lane markings. Thus, a vehicle-following controller based on a look-ahead approach, in which the longitudinal and lateral vehicle dynamics are treated as coupled systems, is introduced. This look-ahead approach utilizes the current information about the position, orientation, velocity, and acceleration of the preceding vehicle such that the vehicle can follow its preceding vehicle while maintaining a safe inter-vehicle distance. However, without any information about the history of the path to be followed, the follower vehicle can deviate from the path of its preceding vehicle when cornering, thus resulting in corner-cutting. Therefore, this thesis focuses on the analysis and design of integrated longitudinal and lateral look-ahead tracking controllers that avoid corner-cutting behavior in vehicle platooning, in the situation where the lane-markings are not available.

In this thesis, the look-ahead tracking controllers are designed to follow a shifted reference point at a curved path, i.e., the vehicle is no longer following a rear bumper center of the preceding vehicle, but instead is following a point extended sideways from the rear bumper such that the corner-cutting behavior is avoided. The novel extended look-ahead controllers employ the position, velocity, and heading information of the preceding vehicle (which are available from camera and V2V), to create a "virtual vehicle" as the new tracking objective. As an important result, a vehicle in a platoon can perfectly track its preceding vehicle path, even where there are no lane-markings or no information about the path other than the current position of the preceding vehicle. The effectiveness of the resulting controllers is illustrated by means of numerical simulations and is extensively tested by means of experiments using a mobile robot platform.

Contents

<div align="right">

Chapter 1

</div>

Introduction

The concept of vehicle platooning is developed to improve road safety and traffic efficiency. The vehicle platoon consists of multiple controlled vehicles, where the control strategy for each vehicle is developed to maintain a desired inter-vehicle distance. Section 1.1 of this chapter briefly introduces the concept of vehicle platooning and essential aspects of autonomous vehicles in general. Section 1.2 describes the problem statement in designing the integrated longitudinal and lateral controllers for vehicle platooning. These challenges then are addressed in Section 1.3, by formulating the objectives. The main contributions of this thesis are presented in Section 1.4. Finally, Section 1.5 presents the outline of this thesis.

1.1 Vehicle platooning

The automobile has been a part of humankind since over a century ago. During its development, automobile manufacturers work towards cutting-edge technologies to improve the safety of the driver/passengers, to increase road safety, and also to increase highway capacity. Advanced Driver-Assistance Systems (ADASs) were designed and developed to automate, adapt and enhance vehicle systems for safer and more efficient driving. By minimizing human errors, ADASs have been shown to reduce road fatalities (ERSO (2016), Pascual (2009)). Research into ADASs has been initiated by automobile manufacturers, research organizations, and government-industry partnerships, and can be traced back to the 1980s, e.g.: the California PATH (Partners for Advanced Transit and Highway) project in the United States (Shladover et al. (1991)); the PROMETHEUS project in Europe (Williams (1988)); and the Advanced Safety Vehicle program in Japan (Iguchi et al. (1996)). As a part of ADASs, research on Automated Driving Systems, commonly referred to as autonomous or self-driving vehicles, has been conducted for several decades. Based on the degree of automation, a classification system of six different levels (from no automation to full automation) was defined by the

SAE level	Name	Narrative Definition	Execution of Steering and Acceleration/ Deceleration	Monitoring of Driving Environment	Fallback Performance of *Dynamic Driving Task*	System Capability (*Driving Modes*)
Human driver monitors the driving environment						
0	No Automation	the full-time performance by the *human driver* of all aspects of the *dynamic driving task*, even when enhanced by warning or intervention systems	Human driver	Human driver	Human driver	n/a
1	Driver Assistance	the *driving mode*-specific execution by a driver assistance system of either steering or acceleration/deceleration using information about the driving environment and with the expectation that the *human driver* perform all remaining aspects of the *dynamic driving task*	Human driver and system	Human driver	Human driver	Some driving modes
2	Partial Automation	the *driving mode*-specific execution by one or more driver assistance systems of both steering and acceleration/ deceleration using information about the driving environment and with the expectation that the *human driver* perform all remaining aspects of the *dynamic driving task*	System	Human driver	Human driver	Some driving modes
Automated driving system ("system") monitors the driving environment						
3	Conditional Automation	the *driving mode*-specific performance by an *automated driving system* of all aspects of the dynamic driving task with the expectation that the *human driver* will respond appropriately to a *request to intervene*	System	System	Human driver	Some driving modes
4	High Automation	the *driving mode*-specific performance by an automated driving system of all aspects of the *dynamic driving task*, even if a *human driver* does not respond appropriately to a *request to intervene*	System	System	System	Some driving modes
5	Full Automation	the full-time performance by an *automated driving system* of all aspects of the *dynamic driving task* under all roadway and environmental conditions that can be managed by a *human driver*	System	System	System	All driving modes

Figure 1.1: SAE classification and terminology for autonomous vehicles (source: 2014 SAE International).

US Society of Automotive Engineers (SAE), as shown in Figure 1.1. The bold line in the figure separates the intervention of a human driver from the automated system, based on which the levels of automation can be summarized as follows (NHTSA (2017)):

- Level 0: The human driver is in complete control of the vehicle;

- Level 1: The human driver is in control of the vehicle, but ADASs can assist the driver with either steering or braking/accelerating, but not both simultaneously;

- Level 2: The human driver is no longer in control of the steering and braking/accelerating of the vehicle, but still must continue to monitor the driving environment at all times, and control the vehicle if corrections are needed. ADASs of the vehicle control both steering and braking/accelerating simultaneously under some circumstances;

- Level 3: An Automated Driving System (ADS) of the vehicle can itself perform all aspects of the driving tasks, such as steering, braking/accelerating, and monitoring the driving environment under specific circumstances. In those circumstances, the human driver must be ready to intervene when requested by the system;

- Level 4: An ADS of the vehicle can itself perform all aspects of the driving tasks and monitor the driving environment in certain circumstances. The human driver need not pay attention and the system can choose to abort the driving (e.g., park the car) if the actual driving conditions exceed the performance boundaries;

- Level 5: An ADS of the vehicle can do all the driving in all circumstances. The human occupants are considered passengers and do not need to be involved in driving.

Traffic accidents and casualties caused by human errors, such as fatigues, tailgating, delayed reaction time, could be substantially reduced by increasing the degree of automation (ERSO (2016)). A study conducted by consulting firm McKinsey & Company concluded that the use of autonomous vehicles could eliminate 90% of road accidents in the United States (Ramsey (2015)), under assumptions that the vehicle automation is the perfect technology, never fails, always assesses traffic situations correctly, and works under all circumstances.

The concept of vehicle platooning employs automation of the longitudinal vehicle motion and optionally also the lateral vehicle motion, and is developed as an effective means to increase highway capacity by adopting a small inter-vehicle distance. A vehicle platoon can be described as an interconnected dynamical system, typically consisting of a leading vehicle (driven by a human), and follower vehicles, which are automated. Adaptive Cruise Control (ACC), which was initially introduced to increase driving comfort, then developed into the essential technology that enables platooning. ACC utilizes radar, lidar, or a camera to measure the actual distance from the preceding vehicle and automatically brakes or accelerates to keep a desired distance. Vehicles with ACC are considered as Level 1 autonomous vehicles since the driver still controls the steering wheel while the automated system controls speed.

ACC can be implemented with various inter-vehicle distances, where this distance is also commonly known as "spacing policy". The two most well-known spacing policies in literature are: a constant distance spacing policy (e.g., see Ren et al. (2007), Sheikholeslam and Desoer (1990), Swaroop and Hedrick (1999)); and a constant time-gap spacing policy (e.g., see Gehring and Fritz (1997), Huppe et al. (2003), Ploeg et al. (2014)). In a constant distance spacing policy, the desired following distance is independent of the velocity of the controlled vehicle. To increase the traffic capacity, a spacing policy of 1 meter was suggested in Shladover (2008). This small spacing, however, is not considered safe and would bring discomfort to passengers if vehicles are moving with high velocities (Zhao et al. (2009)). Thus, a constant time-gap spacing policy, where the desired inter-vehicle distance depends on the velocity of the follower vehicle, is adopted.

During the development of vehicle platooning, the notion of "string stability" is introduced as the attenuation along the string of vehicles of the effect of disturbances, such as speed variations or initial condition perturbations (Ploeg (2014)).

The choice of spacing policy is not only relevant for the safety and comfort of the vehicle, but also for string stability. In Sheikholeslam and Desoer (1990), it was shown that a vehicle platoon with a constant distance spacing policy may not exhibit string stability, which means that oscillations (by braking and accelerating) in the traffic flow may be amplified in upstream direction. Therefore, Cooperative Adaptive Cruise Control (CACC) was developed as an extension to ACC by adding vehicle-to-vehicle (V2V) communications, so that the vehicle has information (e.g., speed, acceleration) of preceding vehicles. It appeared that this extension was beneficial in view of string stability, depending on the spacing policy. In case of a constant distance spacing policy, the addition of V2V communication with the platoon leader could lead to string-stable behavior (Sheikholeslam and Desoer (1990)). In case of a constant time-gap spacing policy, the information of the preceding vehicle is used as a feed-forward term to attenuate disturbances along the platoon, which then leads to smaller string-stable inter-vehicle distance than ACC (Ploeg (2014)).

By definition, vehicles with CACC in a platoon should be considered as cooperative vehicles, rather than autonomous vehicles, since they depend on communication and cooperation with outside entities while the latter perform all of their functions independently and self-sufficiently (NHTSA (2017)). Thus, vehicles equipped with CACC can be categorized as Level 1 by SAE classification, since CACC only automates the longitudinal motion of vehicles. To realize a fully automated vehicle platoon, systems that automate both longitudinal (accelerating and decelerating) and lateral (steering) motion of vehicles need to be developed.

To achieve Level 2 vehicle platooning, several strategies have been introduced in literature and can generally be categorized into: path following, and vehicle following approaches, as illustrated in Figure 1.2. In the path following approach, the longitudinal and the lateral control of the vehicle are usually treated independently (see e.g., Hassanain (2017), Rajamani et al. (2000)). The longitudinal control is realized by ACC/CACC, while the lateral control can be realized by a lane-keeping method. The lateral control objective of lane keeping is to bring the lateral error (the lateral distance between the vehicle's position and the reference path) to zero. In Rajamani et al. (2000), the reference path is constructed by embedded magnetic markings which are used as a reference for the lateral controller, also known as a "look-down" approach. A drawback of this approach is the impracticality of embedding magnetic markers in each lane. Another approach is proposed by Tunçer et al. (2010), where a vision-based lane-keeping system is proposed. This technology is currently available on commercial vehicles and is known as Lane Keeping Assistance (LKA). However, the drawback of this vision-based lane-keeping method in the case of vehicle platooning with a short inter-vehicle distance, is that lane markings cannot be reliably detected by cameras as they are obstructed by the preceding vehicle (Solyom et al. (2013)). Moreover, lane markings are not always available on all roads, making it impossible for the controller to precisely track the path. To address this problem, a reference path constructed from the history of the preceding vehicle is proposed in several
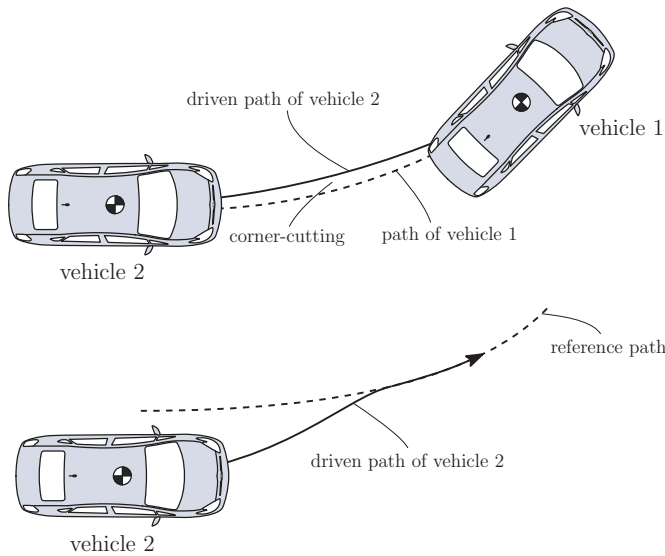
Figure 1.2: The vehicle following (top) and the path following approach (bottom).

publications. Gehrig and Stein (1998), for instance, proposed the Control Using Trajectory algorithm, where the path history associated with the respective time of the preceding vehicle is used as a reference trajectory for the follower vehicle. The position and the velocity of the preceding vehicle are stored to determine the past trajectory of the preceding vehicle. The results show a significant improvement in precision for lateral control at little computational expense. However, the approach relies on several assumptions: the path history of the preceding vehicle can be accurately obtained; all vehicles in the platoon maneuver with low velocity; and no inter-vehicle communication delay is involved. Lefeber et al. (2017) proposed a new approach by assuming that a virtual vehicle is driving along the trajectory of the preceding vehicle and is considered as a reference for the follower vehicle. The lateral control problem is then considered as a path following problem in the spatial domain, where the follower vehicle has to follow the path of the virtual vehicle. The longitudinal control problem is considered as controlling two points (of the virtual and the follower vehicle) on the same path towards a desired inter-vehicle distance in the time domain.

Instead of following the reference path or the path of a preceding vehicle, it is also possible to directly follow the preceding vehicle. In this vehicle-following approach, which is also known as a follow-the-leader approach, a vehicle tracks the orientation, position, and the velocity of the preceding vehicle, such that it steers towards its preceding vehicle. A desired spacing distance is used as a reference for the relative longitudinal inter-vehicle distance, known as a "look-ahead" distance. Although this approach is more reliable than the path-based following approach and relatively easy to implement, the main drawback of the

follow-the-leader approach is that the controller only uses the current relative position. Thus, the following vehicle can deviate on a curved path since it steers directly towards its preceding vehicle, resulting in corner-cutting. To address this corner-cutting, Petrov (2009), Pham and Wang (2006) propose a virtual point associated with the rear of the preceding vehicle as a reference point for the follower vehicle. By following this virtual point, the corner-cutting is compensated for small curvatures.

In summary, the path following and the vehicle following approaches, have their own advantages and disadvantages. The path following approach, where the path is either constructed from lane markings or generated by the preceding vehicle, has the main advantage that it does not suffer from corner-cutting: once the following vehicle is on the path, it stays on the path. The disadvantage of the path-following approach is that it relies heavily on the lane markings or the path history of the preceding vehicle, and sensors with high accuracy have to be installed in each vehicle in the platoon, which can be costly. On the other hand, the vehicle-following approach has advantages that it is relatively easy to implement and is cost efficient since it utilizes the already available information (e.g., position, velocity, and orientation of the preceding vehicle) from radar/camera and V2V communication. However, the vehicle-following approach suffers from corner-cutting.

1.2   Problem statement

To increase highway capacity, the main objective of the control design for vehicle platooning is to maintain a close and safe inter-vehicle distance. The designed controller should also consider the limitation in the sensors and actuators, and should be able to guarantee safety and comfort of the driver/passengers. The additional requirement for the control design of lateral and longitudinal vehicle platooning is that the follower vehicle should be able to accurately track the path of its preceding vehicle without corner-cutting.

As mentioned in the previous section, corner-cutting can be prevented by employing a path following approach, where the reference path (either constructed from lane markings or the path history of the preceding vehicle) is used as a target path for the follower vehicle. The longitudinal control problem is then separately treated from the lateral control problem. In practical situations, however, the longitudinal and lateral motion of vehicles should not be treated independently, since driving consists of a longitudinal motion (accelerating or decelerating on a straight path), a lateral motion (turning with a constant velocity), and a combination of both (accelerating or decelerating while turning). Moreover, the path following approach relies heavily on lane markings and accuracy of sensors or positioning systems, which renders a costly implementation. From the viewpoint of implementation and cost efficiency, a vehicle following approach is considered. The inherent corner-cutting problem is explicitly addressed, as becomes clear in the next section.
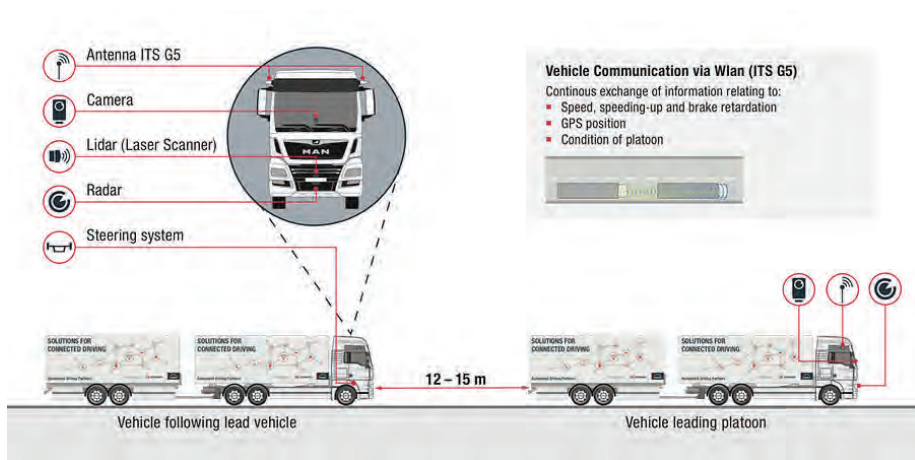
Figure 1.3: Vehicle platooning in logistics application (source: DB Schenker).

To guarantee the driver and passenger comfort, the maximum longitudinal and lateral acceleration/deceleration should be taken into account in the controller design. On a path with high curvature (i.e., small radius), for instance, a vehicle should drive with a lower velocity than on a path with a small curvature.

Vehicle platooning technology, regardless of the control strategy, typically involves sensors, localization services, V2V and V2I communications, control algorithms, hardware components, and a Human Machine Interface (HMI), as depicted in Figure 1.3. From a control perspective, the position of vehicles in two-dimensional space can be defined in either a global coordinate system or a local coordinate system. The global coordinate system is represented by two orthogonal axes that are rigidly connected to the origin point of the system. On the other hand, the local coordinate system is attached to the body of a vehicle, which translates and rotates with the body motion. The choice for either a global or local coordinate system results in different kinematics for the controller design, and depends on the available sensors in vehicles. Sensors such as lidar, radar, and camera work in conjunction to provide the vehicle with a relative distance to the preceding vehicle, and to provide a complete image of the surroundings. In case a global coordinate system is employed, the global location of the vehicle is determined by means of a global positioning system (GPS) and an inertial navigation system (INS). In low coverage areas or tunnels, a GPS can temporarily fail in which an INS can serve as a backup system to determine the vehicle orientation by using motion and rotation sensors. If an INS system also fails, a control strategy that is able to estimate the vehicle orientation using the remaining available sensors has to be deployed.

1.3   Research objectives

This thesis aims to develop an integrated longitudinal and lateral control strategy for vehicle platooning, based on a look-ahead vehicle-following approach, incorporating the perspective of the problem statement mentioned in Section 1.2. Consequently, the following objectives are defined:

- Design an integrated longitudinal and lateral controller for vehicles in a platoon that can compensate for corner cutting, both for a global and a local coordinate system;

- Take constraints on longitudinal acceleration, curvature, and yaw rate into account in the controller design;

- Design an orientation observer constructed from the position sensors such that the situation where the orientation sensor fails can be addressed,

- Experimentally validate the theoretical results regarding the integrated longitudinal and lateral control, together with the orientation observer, using a mobile robot (E-puck) platform;

- Formulate an adaptation of the designed controllers to a dynamic vehicle model, thereby facilitating the possibilities of implementing this controller to the actual vehicle platoon.

1.4   Contributions of the thesis

To achieve the objectives mentioned in the previous section, the vehicle platoon is modeled as a homogeneous platoon. First, each individual vehicle is modeled by a unicycle, which describes kinematics of the position and orientation, given the inputs of yaw rate and longitudinal velocity. Every vehicle is assumed to be equipped with radar, GPS, INS, and V2V communication. The radar, GPS, and INS are used to measure the inter-vehicle distance, position, orientation, longitudinal velocity, lateral velocity, and yaw rate of vehicles. V2V communication is used by the following vehicle to obtain the states of the preceding vehicle, and it is assumed that there are no delays involved in all sensors and the communication system. It should be noted that the requirement of these sensors depends on the controller design, in particular the coordinate system that is employed. The objectives mentioned in Section 1.3 are addressed by means of the following contributions:

- First, a novel extended look-ahead approach that addresses the corner-cutting problem in the vehicle-following approach for vehicle platooning is formulated. The extended look-ahead reference point, which extends a target reference position to a point sideways of the preceding vehicle, can be viewed as a virtual vehicle which is characterized by the position and

orientation of the preceding vehicle. The integrated longitudinal and lateral control of vehicles in a platoon, using the extended look-ahead approach, is designed in a global coordinate system through input-output linearization. Using Lyapunov techniques, the stability analysis of the internal dynamics is proven, under constraints of longitudinal acceleration, lateral jerk, and curvature of the preceding vehicle. These theoretical contributions are validated by means of extensive simulations and experiments on a mobile robot platform.

- Second, it is shown that employing a local coordinate system instead of a global one solves the unavailability of a global positioning system. The integrated longitudinal and lateral control strategy is designed in this local coordinate system using input-output linearization. Lyapunov stability of the internal dynamics is proven, resulting in asymptotic stability given that the initial position error, orientation error, lateral jerk and longitudinal acceleration of the preceding vehicle are bounded. To address the situation where the orientations (of both the preceding and the follower vehicle) are not available or disturbed by noise, an orientation-error observer is designed. The potential of the extended look-ahead approach for a local coordinate system, together with the orientation-error observer, is illustrated by means of extensive simulations and experiments on a mobile robot platform.

- Third, the adaptation of the extended look-ahead controllers to a single-track dynamic model, where the lateral tire forces are taken into account, is studied. This work is considered as an important contribution towards the practical implementation of the proposed controllers to actual vehicles. To be able to adapt the control strategy, the center-of-gravity point of a single-track model is chosen as a control point. The outputs of the extended look-ahead controllers are then transformed to the inputs of the single-track model, using a state/input inversion. Due to the nonlinearity of the single-track model, the inversion is implemented using several approaches: a numerical approach, a first-order Taylor approximation, and a second-order Taylor approximation. The tracking performance and computation time of the three inversion approaches are evaluated and compared. To demonstrate the flexibility of the approach, a rear axle center and a front axle center point are also evaluated as a control point, and the corresponding input inversion is applied.

1.5   Outline

This thesis is organized as follows. Chapter 2 presents a categorized overview of available literature on vehicle platooning control strategies. Two main approaches commonly used in vehicle platooning, the path-following and the preceding-vehicle following approaches, are discussed. Moreover, an overview of the current state-of-the-art in the field of vehicle platooning is presented in this chapter.

Chapter 3, which is based on Bayuwindra et al. (2016) and Bayuwindra et al. (2019b), presents the extended look-ahead concept for combined longitudinal and lateral vehicle-following control for vehicle platooning. A nonlinear controller structure, which is based on Cooperative Adaptive Cruise Control (CACC), is designed for the lateral and longitudinal direction. To overcome the cutting-corner problem, the look-ahead point is extended to a point perpendicular to the direction of the preceding vehicle, which can be viewed as a virtual preceding vehicle tracking objective. A stability analysis on the internal dynamics is employed using Lyapunov's second theorem. To demonstrate the effectiveness of the designed controller with the extended look-ahead approach, simulations are performed and further validated with experiments on a mobile robot (E-puck) platform.

Chapter 4, which is based on Bayuwindra et al. (2019a), focuses on the extended look-ahead vehicle-following controller design for combined longitudinal and lateral vehicle control in a local/moving coordinate frame. To address the situation where the orientation is not measurable or corrupted by noise, an orientation-error observer, constructed from the position error measurement, is designed. The performance of the extended look-ahead controller and the orientation-error observer is investigated by means of a simulation study, and further validated with experiments on the E-puck platform.

As an important step towards the application of the extended look-ahead controller to a real vehicle, Chapter 5 extends the vehicle models to a dynamic single-track model, where the lateral forces generated by tires are taken into account. To be able to adapt the controllers designed in previous chapters, a state/input inversion method is applied to a control point on a single-track model. Due to the nonlinearity of the single-track model, the inversion can only be determined numerically or by Taylor approximations. The tracking performance and the computation time of the approaches are evaluated. Moreover, to demonstrate the flexibility of the adopted approach, three control points within a single-track model are chosen, being the center-of-gravity, the rear axle center, and the front axle center.

Finally, Chapter 6 summarizes the main conclusions of this thesis and presents recommendations for further research.

<div align="right">

Chapter 2

</div>

Literature review

In this chapter, we present a literature review related to vehicle platooning. First, the societal context related to transportation development and vehicle production, including benefits and problems, is presented. Section 2.2 introduces the concept of vehicle platooning as one of the solutions to handle the problems incurred from transportation development. A longitudinal control strategy of vehicle platooning is explained in Section 2.3. Section 2.4 presents related works on control strategies of lateral and longitudinal control of vehicle platooning.

2.1 Background

During the past decades, worldwide vehicle production has relatively risen in parallel with the development of the automobile industry. In 1999, more than 30 million passenger cars were produced worldwide, and in 10 years the number rose to 47 million (see Figure 2.1). The number was growing steadily between 2010 and 2016, reached over 70 million passenger cars that were produced in a single year for the first time in history, and is predicted to grow steadily in the future (OICA (2018)). In general, the development of the automobile industry improves overall accessibility of both personal needs (e.g., improve people's ability to access employment, education and services) and economic productivity (e.g., improve business ability to provide goods and services). The transport development brings a wide range of direct, indirect, and induced benefits to the economic productivity (Rodrigue (2017)). The direct benefits are related to capacity and efficiency improvements, in terms of the time and costs savings. The indirect benefits, on the other hand, are related to accessibility gains and better economies of scale. Lastly, the induced impacts are related to economic multipliers and increased opportunities.

The development of the automobile industry, however, also brings costs to society. According to Commision of the European Communities (2006b), the most
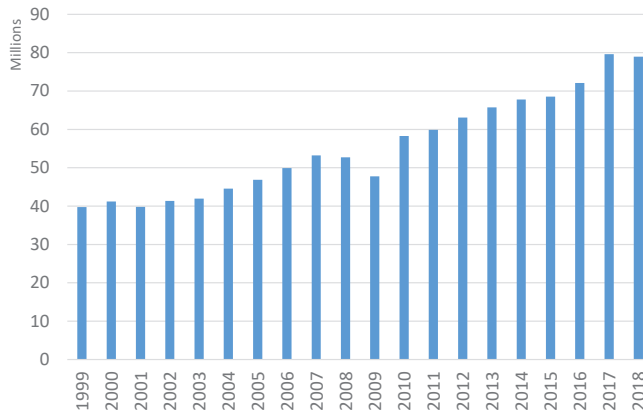
Figure 2.1: Passenger cars production in the world (source: OICA (2018)).

impact of road transportation is the environmental cost, which is mainly related to traffic emission and energy consumption. It was investigated that up to 50% of fuel consumption in road transportation is caused by traffic congestion and non-optimal driving behavior (Commision of the European Communities (2006c)). As a result, traffic congestion has been regarded as one of the most serious economic and environmental problems in the world. One of the proposed solutions to traffic congestion is to build adequate highways and roads. For both financial and environmental aspects, however, it becomes gradually more difficult to build new highways and roads. Among all transport problems, traffic safety is considered as one with the most severe impact on the daily lives of society. Although road fatalities have declined by more than 17% since 2001, road transport still remains the least safe mode of transport (Commision of the European Communities (2006a)). A research conducted by the German In-Depth Accident Study (GIDAS) indicates that a human error is involved in almost 93% of accidents, concluding the limitation of humans as drivers (Commision of the European Communities (2006c)).

The reaction of human drivers is subjected to error, delay, and indecisiveness. For several drivers even with full attention, it is not trivial to find the optimal maneuver in terms of safety and fuel efficiency. The reaction of a particular driver usually is made based on his/her perception of the environment, and consequently, limitation in the information that can be accessed by the driver can lead to a delay in the reaction, resulting in a non-optimal decision. This decision can have a great impact on the traffic flow, ranging from traffic congestion to accidents. Based on the consideration of environmental cost, traffic congestion, and traffic safety, the solution to the traffic problem must involve optimizing the use of available highways/roads, ensuring traffic safety, while also having minimal impact on environment and fuel consumption.
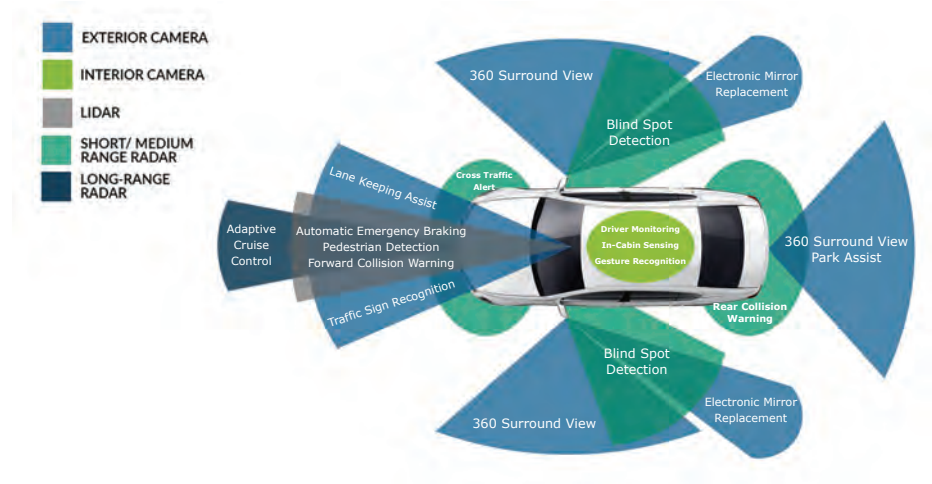
Figure 2.2: Advanced Driver-Assistance Systems (ADAS) in a modern vehicle (source: Jabil (2019)).

2.2 Vehicle platooning

One proposed solution to the traffic problems is to introduce intelligent vehicles, as a part of an Intelligent Transportation System (ITS). Studies conducted by Unsal (1998) and Pascual (2009) indicate that this intelligent solution is believed to reduce emissions by 15%, fuel consumption by 12%, and traffic accidents by 18%. Since most traffic accidents are caused by human errors, Advanced Driver-Assistance Systems (ADAS) were designed to aid human drivers by automating, adapting, and enhancing vehicle systems for safety and better driving. Based on the type of assistance, ADAS can be classified into (Vugts (2010)):

- information systems, which provide the driver with information about the vehicle and environments.

- warning systems, which alert the driver to potential problems.

- driver assistance or intervention systems, which take partial control of the vehicle (such as acceleration or deceleration, while the driver is still in charge of steering).

Figure 2.2 shows the feature of ADAS in a modern vehicle, and Table 2.1 presents some examples of ADAS and its classification. Some of the systems, for example, a driver monitoring system, can be classified as both an information and a warning system since it monitors and gives information about the attentiveness of the driver, and also warns the driver if he/she is not paying attention to the road ahead or a dangerous situation is detected. A collision avoidance system also can

Table 2.1: Classification of Advanced Driver-Assistance Systems (source: Vugts (2010)).

type of assistance system		
Information	**Warning**	**Driver assistance / intervention**
Navigation (dynamic routing)	Blind spot monitor	Anti-lock Braking System (ABS)
Night vision	Driver monitoring	Electronic Stability Program (ESP)
Merging lane	Collision warning	Traction Control System (TCS)
Pedestrian detection	Turning assistance	Adaptive Cruise Control (ACC)
Driver monitoring	Lane change warning	Collision avoidance

be classified as both a warning and a driver assistance systems, since it works first by providing a warning to the driver if an impending collision is detected. The system then takes action autonomously (by braking or steering or both) when the collision becomes imminent. During the last two decades, the rapid development of sensors, embedded systems, communication technology, and control systems has led to the advancement of ADAS to a higher degree of vehicle automation. In this thesis, we focus on the design of the control of vehicles which enables vehicle platooning: longitudinal (accelerating or braking) and lateral (steering) control.

Vehicle platooning can be defined as grouping automated vehicles which drive at a shorter distance than human drivers would, thus forming a compact formation that travels (part of) a designated route. Automated vehicles in a platoon can be considered as an intermediate step between manual vehicles and autonomous vehicles (Kianfar (2014)). By moving together, a vehicle platoon can help to reduce traffic congestion and increase safety. A vehicle platoon consists of a leader vehicle (can be either driven by a human or an autonomous vehicle) and several follower vehicles, which are automated. Follower vehicles measure their position with respect to their preceding vehicle using onboard sensors (e.g., radar, lidar, or a camera) and maintain a safe distance to their preceding vehicle by actively controlling their distance. By enabling automation, the main advantages of vehicle platooning are (Kianfar (2014)):

- increasing traffic flow. Vehicle platooning can reduce the inter-vehicle distance and can eliminate phantom traffic jams. A study conducted by Varaiya (1993) shows that vehicles traveling in closely packed platoons can increase the traffic flow to three times the flow of a typical highway. The study is supported by Tientrakool et al. (2011), stated that the traffic flow can be increased up to 43% if all vehicles in the highway enable platooning. A phantom traffic jam begins when a vehicle in dense traffic slows down even slightly, which causes the following vehicle to slow even more, due to the delayed reaction of the driver. As a result, the deceleration action spreads backward through the lane of traffic and escalates the farther it spreads. By automating acceleration or deceleration, vehicle platooning can eliminate phantom traffic jams by eliminating the delayed reaction of

human drivers (Stern et al. (2018), Sugiyama et al. (2008)).

- reducing fuel consumption. Vehicle platooning can reduce the aerodynamic drag by reducing inter-vehicle distances, especially in heavy-duty vehicles. By driving close together at a constant speed, the leader vehicle cuts through the air and reduces the amount of air flowing between the following vehicles. The reduced aerodynamic drag then leads to the reduction of fuel consumption. A research conducted by Alam et al. (2010) shows that the fuel consumption of a two heavy-duty vehicles in a platoon can be reduced up to 7%.

- increasing safety. Human error is involved in more than 90% of accidents (Commision of the European Communities (2006c)). By reducing the involvement of a human driver, vehicle platooning can reduce errors and delays which are naturally subjects to human reaction. It is expected that the employment of a well-designed automated vehicle (under assumptions that it never fails, always assesses traffic situations correctly, and works under all circumstances) would certainly improve traffic safety.

2.3   Longitudinal control in vehicle platooning

The research of automated longitudinal control of a vehicle can be traced back to the 1980s. In the US, the rapid development of vehicle technology and the emerging traffic problem has led to the PATH (Partners for Advanced Transit and Highway) project, first created by the California Department of Transportation in collaboration with the University of California in 1986 (Shladover et al. (1991)). In 1997, the PATH project conducted a demonstration of a vehicle platoon consisting of eight fully automated vehicles, traveling together at a tightly spaced distance, within a 20 cm RMS error, guided by the magnetic markers on the center of the road. This demonstration showed the feasibility of automated vehicles and is regarded as the first milestone in automated vehicle platooning. In 2004, PATH platooning research has focused on heavy-duty vehicles, with the objective to reduce fuel consumption associated with the aerodynamic drag. The experiments conducted by Browand et al. (2004) have shown the technical feasibility of driving two trucks at a gap of 3 m, resulting in fuel consumption savings of 5% for the lead truck and 10-15% for the following truck, under conservative assumptions.

In Europe, several projects on automated vehicles have been carried out since the 1970s. One of the early projects is PROMETHEUS (Programme for a European Traffic with Highest Efficiency and Unprecedented Safety), which was implemented during 1986 and 1994. The objective of this project was to improve traffic safety and the efficiency of road transport Williams (1988). In 2011, a Grand Cooperative Driving Challenge (GCDC) was conducted in Helmond, the Netherlands. The GCDC is an open competition between teams from industry and academia to develop a vehicle controller that performs longitudinal controller in a platooning setup (Lauer (2011)). The focus of 2011 GCDC was to enable the

(a)   (b)
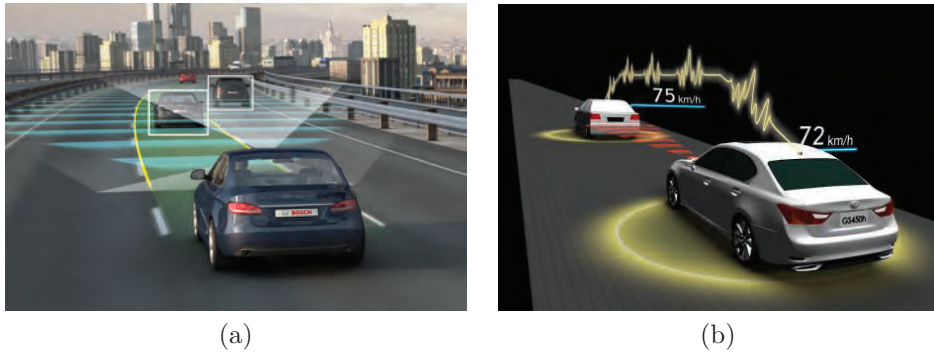
Figure 2.3: (a) Adaptive Cruise Control (ACC) (source: Braun (2014)), and (b) Cooperative Adaptive Cruise Control (CACC) (source: Toyota (2014)).
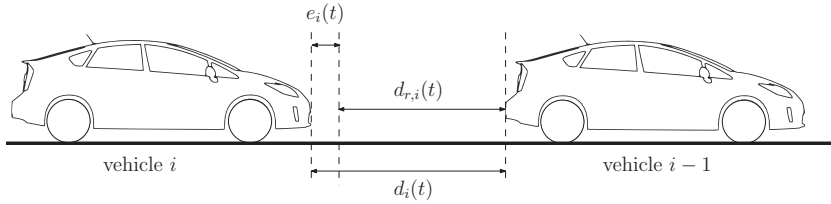
Figure 2.4: Spacing error in longitudinal vehicle platooning.

formation of vehicle platoons with small inter-vehicles distance while attenuating disturbances along the platoon (Ploeg et al. (2012), van Nunen et al. (2012)). The second GCDC was organized in 2016 as apart of the European Seventh Framework Programme i-GAME project (Englund et al. (2016)), demonstrating advance realistic traffic scenarios, such as: cooperative platoon merging; automated intersection crossing; and automatically giving way to emergency and special vehicles (Morales Medina et al. (2018), Ploeg et al. (2018)). In this project, a multi-brand approach was adopted and vehicles from different manufacturers were allowed to cooperate based on a minimum set of common rules, such as safety regulations and communication protocols (Englund et al. (2016), Morales Medina (2018)). In 2015, DAF Trucks, together with NXP Semiconductors, TNO (the Netherlands Organization for Applied Scientific Research), and the safety consultancy firm Ricardo, created the truck platooning EcoTwin project. This project was followed up by the European ENSEMBLE project, an EU multi-brand platooning project, with the goal to improve fuel economy, traffic safety, and traffic output of heavy-duty transportation in the whole EU (ENSEMBLE (2018)).

Longitudinal vehicle platooning, in the sense that it only automates the longitudinal control of vehicles, was first realized by Adaptive Cruise Control (ACC). In a vehicle equipped with ACC, the distance and relative velocity between its position and the preceding vehicle are measured using radar, lidar, or a camera (Figure 2.3(a)). Based on this measurement, the system then controls the throttle

and brake to maintain the desired spacing distance from the preceding vehicle. The actual inter-vehicle distance $d_i(t)$ is defined by

$$d_i(t) = x_{i-1}(t) - x_i(t) - L_i, \tag{2.1}$$

where $x_i(t)$ is the curvilinear position of vehicle i, and L_i is the length of vehicle i. The primary control objective of a longitudinal vehicle platooning is commonly to minimize the spacing error, which is defined as (see Figure 2.4)

$$e_i(t) = d_i(t) - d_{r,i}(t), \tag{2.2}$$

where $d_{r,i}(t)$ is the desired inter-vehicle spacing distance, which can be either a constant or a function that depends on the states of the vehicle.

The functionality of ACC was then extended to CACC by adding V2V communications (Figure 2.3(b)), so that the follower vehicle can obtain the information (acceleration and velocity) of the preceding vehicle or even other vehicles in the platoon. A detailed review conducted by Shladover (1995) introduces longitudinal control strategies that were classified into 12 structures, depending on the sources of the feedback information of the control. Among the control strategies, the control structure with feedback of spacing and velocity (relative to the preceding vehicle) is considered as a popular controller structure due to its simplicity and potential for its usage in mixed traffic. In a more centralized approach, the control may depend on the spacing and the velocity of the follower vehicle with respect to all vehicles in the platoon.

In longitudinal vehicle platooning, depending on the control strategy, the typical information that is usually considered is: (1) the velocity and acceleration of the follower vehicle; (2) the relative distance to the preceding vehicle; (3) the velocity and acceleration of the preceding vehicle (Huang (2012)). The velocity and acceleration of the follower vehicle can be measured by speed sensors and accelerometers on the vehicle. The relative distance to the preceding vehicle can be measured by radar (radio detection and ranging), lidar (light detection and ranging), or cameras. Radar uses radio waves to determine the velocity, range, and angle of objects. From the viewpoint of computational processing, radar is lighter than a camera and uses far less data than a lidar (Santo (2016)). Radar can work in every condition and even use reflection to see beyond obstacles. However, radar is less accurate than lidar. Lidar, on the other hand, measures the distance to the target (in this case, the preceding vehicle) by illuminating the target with pulsed laser light and measuring the reflected pulses with a sensor. Lidar can also scan more than 100 meters in all directions, generating a precise 3D map of the environment surrounding the vehicle (Santo (2016)). The drawback of lidar is that it generates a large amount of data and is quite expensive for the implementation. Moreover, the performance of lidar is often affected by weather conditions. Cameras, are the cheapest of the three (but not the cheapest in processing) and are also the best for scene interpretation. However, cameras use massive amounts of data and can lead to an intense and algorithmically complex

computational processing. In addition, they are also affected by variation in environmental conditions, such as brightness, rain or snow.

The velocity of the preceding vehicle can be directly measured by a doppler radar, which has been applied in most commercially available ACC systems. The acceleration of the preceding vehicle, on the other hand, cannot be measured directly by onboard sensors and theoretically can only be estimated from the velocity and acceleration of the follower vehicle and the relative distance measurements. However, it cannot be accurately estimated due to the noise from velocity and distance measurement. With the advances in wireless communication, vehicles can now send and receive information (including the acceleration of the preceding vehicle) through V2V communication based on the communication standard protocol IEEE 802.11p. A V2V communication, also known as VANET (vehicular ad-hoc network), can transmit the information in real-time and can also provide additional useful information to the vehicle that is beyond information obtained from the onboard sensors.

2.3.1 Spacing policies

The longitudinal controller in vehicle platooning determines the acceleration or velocity of the follower vehicle such that the desired inter-vehicle distance is maintained. This desired inter-vehicle distance is commonly termed as the spacing policy, and can be: a constant distance; a function of the vehicle velocity; or a function of other variables (such as relative velocity between the follower and the preceding vehicle). The spacing policy is an important aspect in the longitudinal control of a vehicle platoon since it affects vehicle safety, traffic capacity and string stability. Therefore, this section presents a variety of spacing policies in literature.

A constant distance spacing policy has been proposed in early literature (see, e.g., Sheikholeslam and Desoer (1990), Godbole and Lygeros (1994), Warnick and Rodriguez (1994)) and was chosen because of its simplicity from the viewpoint of control design. However, maintaining a constant distance spacing for different velocity can lead to unsafe driving. Regarding the safety aspect, vehicles driving at high speed are not safe if the inter-vehicle distance is small. Increasing the inter-vehicle distance would lead to safe driving, but decreases the traffic capacity. Studies conducted by Sheikholeslam and Desoer (1990), Swaroop and Hedrick (1999), and Naus et al. (2010b) have concluded that the constant distance spacing policy would not lead to a string-stable behavior without communication with other vehicles. String stability can be achieved if the communication with the leader vehicle is enabled, and marginal string stability can be achieved if the communication with only the preceding vehicle is enabled.

A constant time-gap spacing policy has been adopted in a vast amount of literature (see, e.g., Gehring and Fritz (1997), Shaw and Hedrick (2007), Ren et al. (2007), Ploeg (2014), Morales Medina (2018), Lefeber et al. (2017)), where the desired

inter-vehicle distance $d_{r,i}(t)$ is linearly dependent on the velocity of the follower vehicle. The desired inter-vehicle distance in a constant time-gap spacing policy is defined as

$$d_{r,i}(t) = r_i + h_i v_i(t), \tag{2.3}$$

where r_i is the desired standstill distance, h_i is the time-gap, and $v_i(t)$ is the velocity of vehicle i at time t. The constant time-gap spacing policy includes a safety requirement, which is the increased distance with increasing velocity. Moreover, a constant time-gap spacing policy has been shown to exhibit string-stable behavior using communication with the preceding vehicle. Since, however, the desired distance increases linearly with the velocity of the follower vehicle, the time-gap spacing policy can become disadvantageous in a high-speed driving environment, such as highways, where the traffic throughput and road capacity are considered to be important.

Eyre et al. (1998) proposed a varying time-gap spacing policy, where the time-gap is a function of the relative velocity between the follower and the preceding vehicle. The varying time-gap spacing policy is defined as

$$d_{r,i} = r_i + h_i(t)v_i(t) \tag{2.4}$$
$$h_i(t) = h_{0,i} - c_i v_{r,i}(t), \tag{2.5}$$

where $h_{0,i}$ and c_i are positive constants, and $v_{r,i}(t) = v_{i-1}(t) - v_i(t)$ is the velocity of vehicle $i-1$ at time t. By introducing the velocity-dependent time-gap, the follower vehicle is expected to reduce the time-gap if the preceding vehicle is moving faster. Thus, the inter-vehicle distance decreases and the traffic throughput is expected to increase. To prevent the negative time-gap, the results are then elaborated in Yanakiev and Kanellakopoulos (1998) to limit the time-gap $h_i(t)$ in the interval $[0,1]$ by introducing the saturation function as

$$h_i(t) = \text{sat}\,(h_{0,i} - c_i v_{r,i}(t)) = \begin{cases} 1, & \text{if } h_{0,i} - c_i v_{r,i}(t) \geq 1 \\ h_{0,i} - c_i v_{r,i}(t), & \text{if } 0 < h_{0,i} - c_i v_{r,i}(t) < 1 \\ 0, & \text{otherwise.} \end{cases} \tag{2.6}$$

Zhao et al. (2009) proposed the safety spacing policy, which takes the deceleration of the follower vehicle into account. The safety spacing policy is defined as

$$d_{r,i}(t) = r_i + t_i v_i(t) + \frac{\gamma_i}{2b_i} v_i^2(t), \tag{2.7}$$

where t_i is the time delay constant of the longitudinal control system consisting of a time delay in brake actuator and a time delay in driveline dynamics, γ_i is the safety coefficient relevant to the road condition and vehicle position in the platoon, $b_i < 0$ is the deceleration constant of vehicle i under the maximum brake action. It can be observed that this spacing policy is a modified version of the time-gap spacing policy, with the inclusion of the deceleration of vehicle i and the safety coefficient. Zhao et al. (2009) suggested to set a bigger value of γ for the leading vehicle to improve platoon safety, and a smaller γ for the follower vehicles to improve traffic capacity.

2.4 Longitudinal and lateral control in vehicle platooning

For a higher degree of automation in vehicle platooning, an integration of longitudinal and lateral control needs to be considered. In addition to all information considered for longitudinal vehicle platooning, lateral control of a vehicle needs also to consider the orientation and a relative lateral position of the follower and the preceding vehicle, known as a localization system. For localization, the global position of a vehicle can be measured by a global positioning system (GPS) and an inertial navigation system (INS). A commercial GPS has about 5–15 meter accuracy, while the differential global positioning system (DGPS) enhances the accuracy to about 10 centimeters (in case of the best implementations) by using a static base station with a fixed, known position to eliminate positional errors in GPS. In a condition where GPS fails temporarily, an INS can take over to obtain the information of vehicle orientation by using accelerometers and gyroscopes.

Regarding the controller design, Rajamani et al. (2000) proposed a longitudinal controller based on a constant distance spacing policy, and a separated lane-keeping controller based on a path following approach. A magnetic marker sensing system is used to determine the path of the preceding vehicle. The proposed controllers were demonstrated with a platoon consisting of eight vehicles and successfully maintained the inter-vehicle spacing distance to within an accuracy of 20 cm and a lateral deviation within a margin of 15 cm. The major drawback of this approach is that it is impractical for use on varying routes since lanes need to be embedded with magnetic markers. In Bom et al. (2005), RTK GPS (Real Time Kinematic Global Positioning System) is used to determine vehicle localization with a centimeter accuracy. The lateral and longitudinal control problems are decoupled using a chained form technique, where the longitudinal control is based on the constant distance spacing policy and the lateral control is treated separately using the path following approach. Under the assumption that the velocity of the vehicle never goes to zero, the results show that the proposed approach managed to maintain the lateral error within an accuracy of 2 cm. However, this approach may be difficult for implementation since RTK GPS is not commonly available in commercial vehicles due to the high cost of such a system. Tunçer et al. (2010) proposed a lateral control using a vision based lane-keeping system. Using a camera, image processing algorithm, and composite Bezier curves to fit curved lanes, the proposed approach is shown to have a small lateral deviation with a margin of 5 cm and a yaw rate error with a margin of 0.03 rad/s. Regardless of high tracking accuracy, lateral control based on a path following approach relies heavily on the path information (either the path constructed from lane markers or from the path history of the preceding vehicle), and could render a costly implementation.

In a case lane markings and path information are not available, a direct vehicle following approach is proposed (see, e.g., Fujioka and Omae (1998), Pham and Wang (2006), Petrov (2008), Solyom et al. (2013)). In a direct vehicle following

approach, a follower vehicle tracks the current position and possibly orientation of the preceding vehicle and steers towards the preceding vehicle within the desired inter-vehicle distance. The position of vehicles and the desired inter-vehicle distance are defined in a two-dimensional space, and the relative position can be defined in either a global coordinate system or a local coordinate system, e.g., a frame attached to the follower vehicle. A direct vehicle following approach is also known as the "pure-pursuit" method, which is widely adopted in the tracking algorithm of an aircraft for defense purposes (Yamasaki and Balakrishnan (2010), Yamasaki et al. (2012)). The direct vehicle following approach is considered as a cost-effective and high-feasibility approach since it utilizes the already available information from an ACC/CACC setup (Solyom et al. (2013)). As explained in Chapter 1, however, the vehicle following approach is prone to corner-cutting.

2.4.1 Path following

This subsection introduces and generalizes the path following method commonly used in vehicle platooning (see, e.g., Chatzikomis and Spentzas (2009), Fukao et al. (2013), Morales Medina (2018), Plaskonka (2015)). Consider the kinematic model of a vehicle as follows

$$\dot{x}_i = v_i \cos \theta_i \tag{2.8a}$$

$$\dot{y}_i = v_i \sin \theta_i \tag{2.8b}$$

$$\dot{\theta}_i = \omega_i, \tag{2.8c}$$

where (x_i, y_i) is the coordinate of the vehicle in a fixed Cartesian frame, θ_i is the orientation of the vehicle, v_i is the longitudinal velocity input, and ω_i is the yaw rate input of the vehicle. The positive heading direction θ_i is taken counter clockwise from the global X positive axis. Consider a planar path $\mathcal{C}$ and let us define three frames as follows: $\mathcal{F}_0 = \{0, \mathbf{i}, \mathbf{j}\}$ is a fixed Cartesian coordinate frame, $\mathcal{F}_{v,i} = \{P_{v,i}, \mathbf{i_{v,i}}, \mathbf{j_{v,i}}\}$ is a moving frame attached to vehicle i, and $\mathcal{F}_{s,i} = \{P_{s,i}, \mathbf{i_{s,i}}, \mathbf{j_{s,i}}\}$ is a moving frame attached to the orthogonal projection of point $P_{v,i}$ on the path $\mathcal{C}$, see Figure 2.5. The frame $\mathcal{F}_{s,i}$ is known as a Serret-Frenet frame. The path $\mathcal{C}$ itself is characterized by the parameter s_i as the curvilinear distance between point $P_{s,i}$ and the beginning point of the path. The parameter d_i is defined as the minimum ordinate of $P_{v,i}$ in the frame $\mathcal{F}_{s,i}$, where it is assumed that d_i is small, and the orientation error between the actual vehicle and the projection is defined as $\theta_{e,i} := \theta_i - \theta_{s,i}$. The kinematic model of the vehicle expressed in the Serret-Frenet frame is given by (Morin and Samson (2008))

$$\dot{s}_i = \frac{v_i}{1 - d_i \kappa_i(s_i)} \cos \theta_{e,i}, \tag{2.9a}$$

$$\dot{d}_i = v_i \sin \theta_{e,i}, \tag{2.9b}$$

$$\dot{\theta}_{e,i} = \omega_i - \dot{s}_i \kappa_i(s_i), \tag{2.9c}$$

where $d_i \kappa_i(s_i) < 1$, and $\kappa_i(s_i)$ is the curvature of the path at point s_i. Using this kinematic model, the path following control objective is to asymptotically
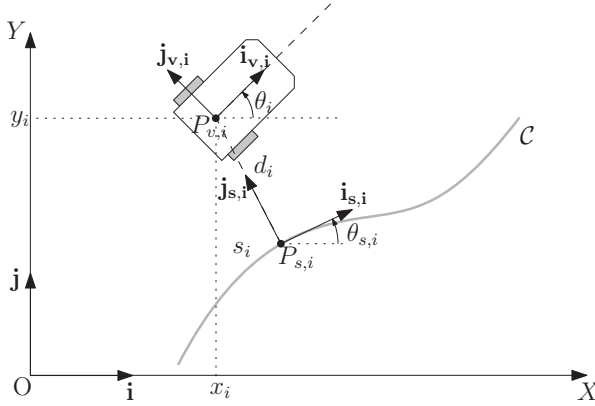
Figure 2.5: Projection of a vehicle in a Serret-Frenet frame.

stabilize $(d_i, \theta_{e,i})$ at zero, and the longitudinal control problem can be solved by associating the path $\mathcal{C}$ with the path driven by the preceding vehicle, and associating the curvilinear distance s_i with the traveled distance x_i in (2.1).

The path following approach needs to consider the following information: positions and curvatures of the path $\mathcal{C}$ at any given point; the distance of the follower vehicle to that path; velocity and yaw rate of the follower vehicle; and the orientation error between the follower vehicle and the desired orientation on the path. The desired path $\mathcal{C}$ can be a path constructed from either lane markers or the path history of the preceding vehicle, which can obtained from vision systems and RTK GPS (see, e.g., Bom et al. (2005), Fahmy et al. (2018), Omae et al. (2006), Ranjitkar et al. (2002), Tunçer et al. (2010)). The shortcomings of a path following approach are: firstly, the lane markings are not always available, especially in bad weather conditions; secondly, related to the short inter-vehicle distance of vehicle platooning, lane markings may not be reliably detected by the vision systems (Solyom et al. (2013)); lastly, the RTK GPS is expensive and not available in commercial vehicles.

2.4.2 Direct vehicle following

In a direct vehicle following approach, the relative position between vehicles can be derived in either a global coordinate system or a local coordinate system. Consider the follower vehicle i and preceding vehicle $i-1$ with the kinematics as in (2.8). In a global coordinate system (Figure 2.6(a)), the position error states are defined as

$$e_{x,i} = x_{i-1} - x_i - d_{rx,i} \tag{2.10a}$$

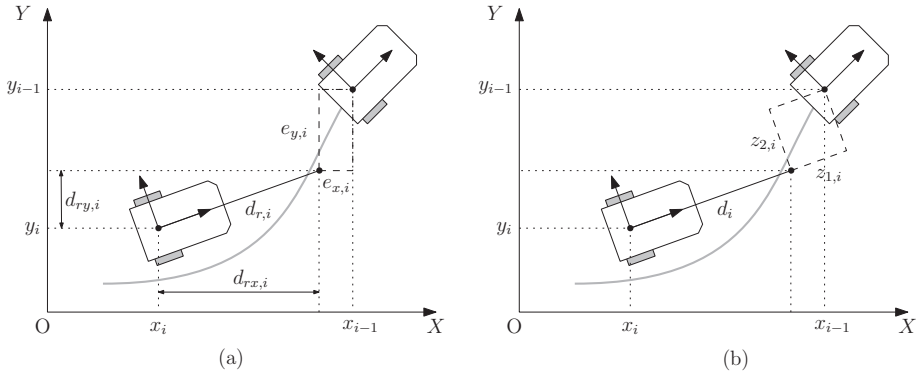$$e_{y,i} = y_{i-1} - y_i - d_{ry,i}, \tag{2.10b}$$

Figure 2.6: A direct vehicle following errors definition: (a) in a global coordinate system; (b) in a local coordinate system.

where $(d_{rx,i}, d_{ry,i})$ are the components of the desired inter-vehicle distance, either a constant or a function depending on the states of the vehicle. The control objective is then to asymptotically stabilize $(e_{x,i}, e_{y,i})$ at zero. It should be noted that the direct vehicle following approach in a global coordinate system still needs to utilize the information of the global position of all vehicles, which can be obtained with a GPS.

On the other hand, in a local coordinate system, the relative position between vehicles can be determined with respect to the follower vehicle frame (see, e.g., Jiang and Nijmeijer (1997), Kanayama et al. (1990), Loría and Panteley (2005), Panteley et al. (1998)), the preceding vehicle frame (see, e.g., Morin and Samson (2008), Petrov (2009)), or any moving frame, which results in different error kinematics and control design. The relative position error states with respect to the follower vehicle frame are defined as (see Figure 2.6(b))

$$\begin{bmatrix} z_{1,i} \\ z_{2,i} \end{bmatrix} = \begin{bmatrix} \cos\theta_i & \sin\theta_i \\ -\sin\theta_i & \cos\theta_i \end{bmatrix} \begin{bmatrix} x_{i-1} - x_i \\ y_{i-1} - y_i \end{bmatrix} - \begin{bmatrix} d_{r,i} \\ 0 \end{bmatrix}, \tag{2.11}$$

where $d_{r,i}$ is the desired inter-vehicle distance. In contrast to the global coordinate system, global positions of vehicles are not needed for this local coordinate system.

A direct vehicle following approach, either defined in a global or local coordinate system, does not need the path information of the preceding vehicle. However, the follower vehicle may cut corners, as becomes clear in the next chapter. To compensate corner cutting in a direct vehicle following approach, several strategies have been proposed in literature. Pham and Wang (2006) proposed a virtual focus point positioned at a desired distance behind the preceding vehicle, which then serves as a reference point where the follower vehicle should follow. The results show that the proposed controller is able to compensate for corner cutting for a small desired inter-vehicle distance (less than 2.5 m). Using similar techniques, Petrov (2009) introduced a reference virtual point, which is positioned at a de-

sired known distance behind the preceding vehicle, and a look-ahead point, which is positioned at a desired distance in front of the follower vehicle. The proposed controller is based on a reduced-order system, with the objective to asymptotically track the reference virtual point with respect to the look-ahead point. The shortcomings are: the controllers do not compensate for corner cutting on paths with varying curvature; the constraints on curvatures, accelerations, and yaw rate are not formulated; the controllers do not address the situation where the orientation sensor is not reliable; and the proposed approaches did not take the dynamic vehicle model into account.

2.5 Conclusion

This chapter reviewed the development of control strategies of vehicle platooning. At first, the background of the current transportation development situation and problems are introduced. Secondly, the concept of vehicle platooning, which was considered as the most promising solution to traffic problems, is introduced. Lastly, the evaluation of the existing research and development in both longitudinal only and lateral and longitudinal control strategies of vehicle platooning are discussed in details.

The longitudinal and lateral control strategies in vehicle platooning can be mainly categorized into two strategies: the path following and the direct vehicle following approach. Based on the consideration of cost-effectiveness, ease of implementation, sensors availability, and the uncertainty of path information, the direct vehicle following approach is preferred in the case a preceding vehicle is present. Several strategies have been proposed in the literature to compensate corner-cutting, with some aforementioned shortcomings. In the following chapter, we address the shortcomings by first explaining the cutting corner problem in a direct vehicle following approach, introducing the concept of the extended look-ahead as a solution to prevent corner cutting, and formulating constraints related to the control design.

Longitudinal and lateral control for car-like vehicle platooning with extended look-ahead in a global coordinate system

Abstract[1] - This chapter presents a novel look-ahead concept for combined longitudinal and lateral vehicle following control for a car-like platoon. A nonlinear controller structure, which is based on Cooperative Adaptive Cruise Control (CACC), is designed for the lateral and longitudinal direction. For practical implementation and cost-efficiency, a preceding vehicle look-ahead approach is considered since it utilizes the already available information (such as preceding vehicle position, orientation, and velocity) from radar and V2V communication. However, due to the position control in the look-ahead approach, the follower vehicle may cut corners. To overcome this problem, the look-ahead is extended to a point perpendicular to the direction of the preceding vehicle, which can be viewed as a virtual preceding vehicle tracking objective. To demonstrate the effectiveness of the designed controller with the extended look-ahead approach, simulations are performed and further validated with experiments on a mobile robot platform. The results prove the effectiveness of the extended look-ahead approach.

3.1 Introduction

The increasing needs of transportation that are not balanced by the growth of highway capacity lead to traffic congestion. Hence, vehicle platooning is developed as an effective means to increase highway capacity by maintaining the inter-vehicle distance (Vahidi and Eskandarian (2003)). The concept of maintaining a desired inter-vehicle distance is first introduced by the invention of Adaptive Cruise Control (ACC). By means of a radar and lidar, ACC measures the distance

---

[1]This chapter is based on Bayuwindra et al. (2016) and Bayuwindra et al. (2019b).

and the relative speed of the preceding vehicle and adapts the velocity of the following vehicle in order to maintain a desired distance. As an extension to ACC, Cooperative Adaptive Cruise Control (CACC) was developed by adding Vehicle-to-vehicle (V2V) communication. By providing the following vehicle with more information about its preceding vehicle, the addition of V2V communication has been proven to reduce the inter-vehicle distance while attenuating disturbances in upstream direction (Naus et al. (2010a), Ploeg et al. (2011)). In addition, by driving closer behind one another, the aerodynamic drag force between vehicles can be reduced, especially for heavy-duty vehicles, thus resulting in lower emissions and fuel consumption of all vehicles in a platoon (Alam et al. (2010), Shladover (2006)).

Vehicle platooning, which can be described as a "follow the leader" strategy, is realized by exchanging information about the longitudinal and lateral properties between vehicles. To achieve a fully automated vehicle platooning, several strategies have been introduced in literature. In Rajamani et al. (2000), the longitudinal and lateral control system for automated vehicles in a platoon are introduced as independent systems. The longitudinal controller is based on CACC, with the objective of maintaining constant spacing between vehicles, while the lateral control is developed based on a lane-keeping approach. In other literature, longitudinal and lateral controllers are treated as coupled systems. The studies in Lim and Hedrick (1999), Sheikholeslam and Desoer (1992b) show that the coupling compensation improves the control performance. In general, the longitudinal controller of vehicle platooning is designed based on CACC, with an objective to maintain a desired longitudinal inter-vehicle spacing. On the other hand, the lateral controller can be designed either based on: lane-keeping (e.g., Kianfar et al. (2014), Rajamani et al. (2000), Tunçer et al. (2010)) or vehicle following (e.g., Petrov (2008), Solyom et al. (2013)). In Rajamani et al. (2000), a lane-keeping method with a magnetic marker system is used for the lateral control system. The magnetic marker system uses magnetometers mounted on the vehicles and senses the magnetic field intensity from magnets embedded in the lane to measure the lateral distance from the center of the lane, hence earns the nickname "look-down" sensing system. Although the proposed control system had been proven to be reliable and robust, this approach is impractical because every lane needs to be embedded with magnets. In another approach (Tunçer et al. (2010)), the lateral control is developed using a vision based lane-keeping system. Instead of embedding magnets in lanes, this vision based look-down system employs a camera based image processing algorithm for lane detection. This approach is analogous to the path-tracking approach that has been widely adopted in robot motion. From a platooning viewpoint, there are several considerations in a lane-keeping method that should be taken into account. First, when the vehicles in a platoon are driving close together, it is not always possible to obtain an accurate measurement of lane markings (Solyom et al. (2013)). Secondly, the lane markings also may be of bad quality, obstructed by dirt/snow, or even not present (e.g., on intersections or rural areas), upon which vehicle following can serve as a fall-back.

In the situation when the lane-markings are not available, a more reliable approach is to track the preceding vehicle's lateral position based on the preceding vehicle's position and orientation (measured by the radar), and the preceding vehicle's velocity and acceleration (communicated through V2V). Thus, a vehicle-following controller based on the look-ahead approach is introduced (Ploeg et al. (2014)). However, the application of this look-ahead approach for lateral behavior has some drawbacks in the event of a cornering maneuver. The look-ahead control can command the follower vehicle to turn when it senses the difference between the orientation of the preceding and the follower vehicle, causing the follower to turn too early, thus cutting the corner. The deviation in the corner radius escalates with the distance to the preceding vehicle (Gehrig and Stein (1998)). To address the cutting corner behavior, several approaches have been proposed. The CUT (Control Using Trajectory) algorithm, introduced in Gehrig and Stein (1998), makes use of the time history associated with the preceding vehicle. The position coordinates of the preceding vehicle and the motion parameters of the follower vehicle are stored to determine the previous trajectory of the preceding vehicle. In Petrov (2008), Pham and Wang (2006), the cutting-corner behavior is compensated by shifting the reference point from the rear of the preceding vehicle to a static point behind it. For a platoon consisting of two vehicles, the results shows that the cutting-corner behavior has been compensated for a constant velocity scenario. Most of the controllers designed in the existing research (e.g., Petrov (2008), Rajamani et al. (2000), Solyom et al. (2013)) heavily depend on the assumption of constant or positive velocity for all vehicles in a platoon, which results in a linear state-space model that is controlled with pole placement, or optimal state feedback.

The main contribution of this chapter consists of the design of an extended look-ahead approach that can compensate cutting-corner behavior in vehicle platooning, with emphasis on the cornering maneuver, while maintaining a safe inter-vehicle distance. This extended look-ahead approach uses the velocity and heading direction information of the preceding vehicle (which are already available from radar and V2V), to create the "virtual" vehicle as a new tracking objective. A formal stability analysis of the resulting closed-loop model is provided using a Lyapunov-based method. To guarantee the asymptotic stability and the nonzero velocity of all vehicles, the maximum bounds of lateral and longitudinal accelerations are defined. Compared to the existing results of other vehicle-following controllers, the designed controllers do not depend on the assumption of constant velocity, and take the motion constraints of lateral and longitudinal accelerations into account.

The remaining part of this chapter is composed as follows: Section 3.2 describes the vehicle model and the look-ahead based controller design. In Section 3.3, the extended look-ahead approach is proposed. The system is simulated in MATLAB and the results are presented in Section 3.4. For further validation, the designed controller is also implemented in a unicycle mobile robot platform, as presented in Section 3.5. The last section summarizes the conclusions.

3.2   Vehicle modeling and look-ahead based controller design

The vehicle in a platoon is modeled as a unicycle on a Cartesian coordinate system. Consider a platoon of $m \in \mathbb{N}$ vehicles, with $S_m = \{i \in \mathbb{N} | 1 \leq i \leq m\}$ denoting the set of all vehicles in the platoon. The unicycle kinematic model is described by the following differential equations

$$\dot{x}_i = v_i \cos \theta_i \tag{3.1a}$$

$$\dot{y}_i = v_i \sin \theta_i \tag{3.1b}$$

$$\dot{v}_i = a_i \tag{3.1c}$$

$$\dot{\theta}_i = \omega_i, \tag{3.1d}$$

where (x_i, y_i) are the Cartesian coordinates of the unicycle, θ_i is the orientation of the unicycle with respect to the x axis, v_i is the longitudinal velocity, a_i is the longitudinal acceleration input, ω_i is the angular velocity input, and $i \in S_m$ is the vehicle index, increasing in upstream direction.

The main objective of vehicle i in a platoon is to follow the preceding vehicle $i-1$ at a desired distance, $d_{r,i}$. The desired distance between vehicles can be chosen as: (1) a constant spacing policy; or (2) a constant time gap spacing policy, in which the spacing policy is velocity dependent. The constant time gap spacing policy is adapted from Ploeg et al. (2011, 2014), which in this chapter is formulated as

$$d_{r,i} = \begin{bmatrix} d_{rx,i} \\ d_{ry,i} \end{bmatrix} = (r_i + h_i v_i) \begin{bmatrix} \cos \theta_i \\ \sin \theta_i \end{bmatrix}, \tag{3.2}$$

where $d_{r,i}$ is the desired distance vector between vehicle i and vehicle $i-1$, $r_i > 0$ is the standstill distance, $h_i > 0$ is the time gap, v_i is the velocity of vehicle i, and θ_i is the heading angle of vehicle i with respect to the x axis. It should be noted that in contrast to Ploeg et al. (2011, 2014), in this formulation the standstill distance is defined as a vector with angle θ_i, and can be understood as a look-ahead in the same direction as the vehicle's orientation (see Figure 3.1). The time gap h_i can be considered as the time needed by vehicle i to reach the current position of its preceding vehicle when traveling at constant velocity v_i.

It is assumed that each vehicle in the platoon can communicate and sense the movement of the neighboring vehicle, as depicted in Figure 3.1. Let $p_i := [x_i, y_i]^T$ be the position of vehicle i. Since the main focus of vehicle platooning is to maintain the inter-vehicle distance, it makes sense to derive the error dynamics based on the difference between the desired distance $d_{r,i}$ and the actual inter-vehicle distance. The spacing error vector is defined as

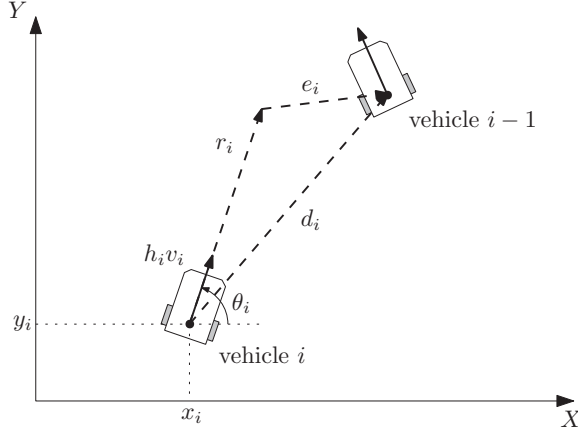$$e_i = d_i - d_{r,i} = (p_{i-1} - p_i) - d_{r,i}, \tag{3.3}$$

Figure 3.1: Error definition in vector term for follower vehicles, where e_i is the spacing error, and d_i is the actual distance between vehicle i and $i-1$.

with $d_{r,i}$ as in (3.2), and $d_i = (d_{x,i}, d_{y,i})^T$ is the actual distance between vehicle i and vehicle $i-1$. The spacing error (3.3) is decomposed in a global Cartesian coordinate system as follows

$$e_{x,i} = x_{i-1} - x_i - (r_i + h_i v_i) \cos \theta_i \tag{3.4a}$$

$$e_{y,i} = y_{i-1} - y_i - (r_i + h_i v_i) \sin \theta_i. \tag{3.4b}$$

To proceed, the following state components are defined

$$z_{1,i} = x_{i-1} - x_i - (r_i + h_i v_i) \cos \theta_i \tag{3.5a}$$

$$z_{2,i} = y_{i-1} - y_i - (r_i + h_i v_i) \sin \theta_i \tag{3.5b}$$

$$z_{3,i} = v_{i-1} \cos \theta_{i-1} - v_i \cos \theta_i \tag{3.5c}$$

$$z_{4,i} = v_{i-1} \sin \theta_{i-1} - v_i \sin \theta_i. \tag{3.5d}$$

It can be observed that the first and second component of (3.5) are identical to the position errors (3.4a, 3.4b), while the third and fourth component represent the velocity error in x and y direction, respectively. The inter-vehicle dynamics is obtained by differentiating (3.5) with respect to time, resulting in

$$\begin{bmatrix} \dot{z}_{1,i} \\ \dot{z}_{2,i} \end{bmatrix} = \begin{bmatrix} z_{3,i} \\ z_{4,i} \end{bmatrix} - F_i \begin{bmatrix} a_i \\ \omega_i \end{bmatrix} \tag{3.6a}$$

$$\begin{bmatrix} \dot{z}_{3,i} \\ \dot{z}_{4,i} \end{bmatrix} = H_{i-1} \begin{bmatrix} a_{i-1} \\ \omega_{i-1} \end{bmatrix} - H_i \begin{bmatrix} a_i \\ \omega_i \end{bmatrix}, \tag{3.6b}$$

with

$$F_i := \begin{bmatrix} h_i \cos \theta_i & -(r_i + h_i v_i) \sin \theta_i \\ h_i \sin \theta_i & (r_i + h_i v_i) \cos \theta_i \end{bmatrix} \tag{3.7a}$$

$$H_j := \begin{bmatrix} \cos \theta_j & -v_j \sin \theta_j \\ \sin \theta_j & v_j \cos \theta_j \end{bmatrix}, \quad j \in \{i-1, i\}. \tag{3.7b}$$

The system (3.6) represents the dynamics of the inter-vehicle error between vehicle $i-1$ and i. The objective is now to design a control input $[a_i, \omega_i]^T$ which asymptotically stabilizes the system (3.6) at zero. Let $r_i > 0$ and $h > 0$. By choosing the control input as

$$
\begin{bmatrix} a_i \\ \omega_i \end{bmatrix} = F_i^{-1} \begin{bmatrix} z_{3,i} + k_{1,i} z_{1,i} \\ z_{4,i} + k_{2,i} z_{2,i} \end{bmatrix}
$$
$$
= \begin{bmatrix} \frac{1}{h_i} \cos \theta_i & \frac{1}{h_i} \sin \theta_i \\ -\frac{\sin \theta_i}{r_i + h_i v_i} & \frac{\cos \theta_i}{r_i + h_i v_i} \end{bmatrix} \begin{bmatrix} z_{3,i} + k_{1,i} z_{1,i} \\ z_{4,i} + k_{2,i} z_{2,i} \end{bmatrix}, \tag{3.8}
$$

where $r_i + h_i v_i > 0$, the closed-loop error dynamics is obtained by substituting (3.8) into (3.6), eventually resulting in

$$
\begin{bmatrix} \dot{z}_{1,i} \\ \dot{z}_{2,i} \end{bmatrix} = - \begin{bmatrix} k_{1,i} & 0 \\ 0 & k_{2,i} \end{bmatrix} \begin{bmatrix} z_{1,i} \\ z_{2,i} \end{bmatrix} \tag{3.9a}
$$

$$
\begin{bmatrix} \dot{z}_{3,i} \\ \dot{z}_{4,i} \end{bmatrix} = -G_i \begin{bmatrix} z_{3,i} \\ z_{4,i} \end{bmatrix} + \begin{bmatrix} \xi_{1,i} \\ \xi_{2,i} \end{bmatrix}, \tag{3.9b}
$$

with

$$
\begin{bmatrix} \xi_{1,i} \\ \xi_{2,i} \end{bmatrix} := H_{i-1} \begin{bmatrix} a_{i-1} \\ \omega_{i-1} \end{bmatrix} - G_i \begin{bmatrix} k_{1,i} z_{1,i} \\ k_{2,i} z_{2,i} \end{bmatrix} \tag{3.10}
$$

$$
G_i := \begin{bmatrix} \frac{h_i v_i + r_i \cos^2 \theta_i}{h_i(r_i + h_i v_i)} & \frac{r_i \sin \theta_i \cos \theta_i}{h_i(r_i + h_i v_i)} \\ \frac{r_i \sin \theta_i \cos \theta_i}{h_i(r_i + h_i v_i)} & \frac{h_i v_i + r_i \sin^2 \theta_i}{h_i(r_i + h_i v_i)} \end{bmatrix}, \tag{3.11}
$$

and H_{i-1} as in (3.7b). With the controller (3.8), a linear system (3.9a), of which the poles can be place anywhere, is obtained. Since the identical behavior for x and y direction is desired, the same value for $k_{1,i} = k_1$ and $k_{2,i} = k_2$ can be chosen for all vehicles. Note that the input (3.8) requires the distance error $(z_{1,i}, z_{2,i})$ that can be obtained using a radar, and also the preceding vehicle velocity v_{i-1} and heading angle θ_{i-1}, which can be obtained through wireless communication. By choosing $k_1, k_2 > 0$, the first subsystem (3.9a) is globally asymptotically stable. Consequently, $(z_{1,i}, z_{2,i})$ converges to zero. It should also be noted that the condition of $r_i + h_i v_i > 0$, which is sufficiently fulfilled by $v_i > 0$ (forward driving), is necessary to determine the input (3.8). Thus, the stability of the overall system (3.9) and the condition of $v_i > 0$ are established by the following result.

Proposition 3.1. *Let $z_i = [z_{1,i}, z_{2,i}, z_{3,i}, z_{4,i}]^T$, $z_{12,i} = [z_{1,i}, z_{2,i}]^T$, and $z_{34,i} = [z_{3,i}, z_{4,i}]^T$. Consider the system (3.6) in closed loop with the control input (3.8). Assume that $0 < v_{i-1}^{\min} \leq v_{i-1}(t) \leq v_{i-1}^{\max}$ and let some $\varepsilon > 0$ be given satisfying $\varepsilon < v_{i-1}^{\min}$. If*

$$
\left\| H_{i-1} \begin{bmatrix} a_{i-1} \\ \omega_{i-1} \end{bmatrix} \right\|_2 = \left\| \begin{bmatrix} \ddot{x}_{i-1} \\ \ddot{y}_{i-1} \end{bmatrix} \right\|_2 < \frac{v_{i-1}^{\min} - \varepsilon}{\frac{r_i}{\varepsilon} + h_i}, \tag{3.12}
$$

then for sufficiently small initial conditions $z_i(0)$, $v_i(t) > 0$ and the input (3.8) is well defined. Furthermore, $\lim_{t \to \infty} \|z_{12,i}(t)\| = 0$, and $z_{34,i}(t)$ remains bounded.

Additionally, if

$$\lim_{t \to \infty} H_{i-1} \begin{bmatrix} a_{i-1} \\ \omega_{i-1} \end{bmatrix} = \lim_{t \to \infty} \begin{bmatrix} \ddot{x}_{i-1}(t) \\ \ddot{y}_{i-1}(t) \end{bmatrix} = 0, \quad (3.13)$$

then $\lim_{t \to \infty} \|z_{34,i}(t)\| = 0$, *i.e., the closed-loop system (3.6,3.8) is asymptotically stable.*

Proof. See Appendix A.1. □

Note that the conditions (3.12) and (3.13) are related to the constraints of accelerations in x and y, which can also be translated as constraints of longitudinal and lateral accelerations of the preceding vehicle in the platoon.

3.3 Extended look-ahead controller design

From (3.3), it can observed that the look-ahead design is based on the spacing policy as commonly used for CACC. From a platooning perspective, the disadvantage of this look-ahead strategy is that the follower vehicle's lateral position is only without error on a straight line. At a cornering maneuver this disadvantage leads to a common problem, known as cutting-corner behavior (Bayuwindra et al. (2016)). Without prior knowledge of the reference trajectory, the position controller in the conventional look-ahead design can make the follower vehicles turn too early at a cornering maneuver. In the event of cornering, vehicle i senses a position error due to the spacing policy in the conventional look-ahead approach and will turn sooner to correct errors, rather than wait until it arrives at the point of cornering. In order to make the vehicle i turn at the point of the corner, the look-ahead point of the vehicle i has to be extended, thus creating a "virtual" vehicle as the new tracking point for vehicle i. The purpose of this extension vector is to compensate the unintended lateral error due to the desired spacing distance. By using this extension vector, vehicle i tracks the virtual point on vehicle $i-1$, thus allowing it to turn at the point of cornering.

Let $s_{i-1} = [s_{x,i-1}, s_{y,i-1}]^T$ denote the look-ahead point extending from the base of vehicle $i-1$ (Figure 3.2), that can be viewed as a virtual vehicle acting as a position tracking point objective for vehicle i. In this approach, the look-ahead point is extended perpendicular to the heading direction of vehicle $i-1$. This extended look-ahead is applied during cornering maneuvers, i.e., when $\omega_{i-1} \neq 0$. Using the new tracking point objective, the spacing error for the extended look-ahead CACC is defined as

$$e_i = (p_{i-1} + s_{i-1}) - (p_i + r_i + h_i v_i). \quad (3.14)$$

The components of s_{i-1} in Cartesian coordinates are derived as follows

$$s_{x,i-1} = \bar{s}_{i-1} \sin \theta_{i-1} \quad (3.15)$$

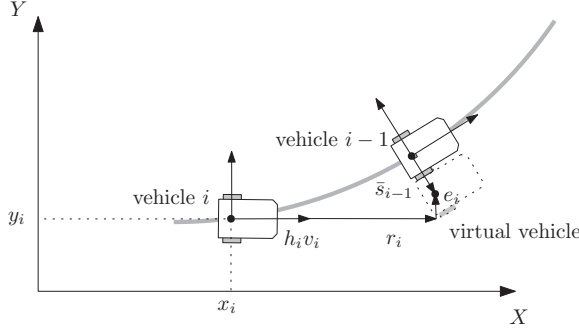$$s_{y,i-1} = -\bar{s}_{i-1} \cos \theta_{i-1}, \quad (3.16)$$

Figure 3.2: Error definition for the extended look-ahead approach, where e_i is the spacing error.

where $\bar{s}_{i-1}$ is the magnitude of the extension vector s_{i-1}. To prevent cutting corners, our aim is to formulate the extension vector s_{i-1} such that the vehicle i has the same turning radius as its preceding vehicle $i-1$. Since the direction of s_{i-1} is always perpendicular to the heading direction of vehicle $i-1$, only the magnitude (denoted by $\bar{s}_{i-1}$) needs to be determined (Bayuwindra et al. (2016)). The definition of $\bar{s}_{i-1}$ can be made by analyzing the steady-state behavior of the platoon on the circular movement, i.e., when errors $e_{x,i}$ and $e_{y,i}$ equal zero. In this approach, it is assumed that the heading angle difference between the preceding and follower vehicle is always smaller than $\pi/2$ such that the extension vector can always be defined. When vehicle $i-1$ turns to the positive y axis, it will have a turning radius R_{i-1} and the new tracking point of vehicle i is extended to the point S (see Figure 3.3). It therefore follows that

$$(R_{i-1} + \bar{s}_{i-1})^2 = R_{i-1}^2 + (r_i + h_i v_i)^2 , \tag{3.17}$$

with R_{i-1} as the turning radius of vehicle $i-1$, $\bar{s}_{i-1}$ as the magnitude of the extension vector, and $(r_i + h_i v_i)$ as the magnitude of the spacing policy. Let us define κ_{i-1} as the path curvature of vehicle $i-1$. By noting the fact that $\kappa_{i-1} = 1/R_{i-1} = \omega_{i-1}/v_{i-1}$ and by rearranging terms in (3.17), the magnitude of the extension vector $\bar{s}_{i-1}$ is defined as

$$\bar{s}_{i-1} = \begin{cases} 0 & \text{for } \kappa_{i-1} = 0 \\ \frac{-1+\sqrt{1+\kappa_{i-1}^2(r_i+h_i v_i)^2}}{\kappa_{i-1}} & \text{for } \kappa_{i-1} \neq 0. \end{cases} \tag{3.18}$$

For the case of $\kappa_{i-1} = 0$, which implies that $\omega_{i-1} = 0$, the vehicle $i-1$ drives on a straight line. Thus, $\bar{s}_{i-1}$ is zero and the definition of spacing error in (3.14) will be identical to (3.1). To show that $\bar{s}_{i-1}$ is continuous at $\kappa_{i-1} = 0$, we can use a Taylor expansion and take the limit as $\kappa_{i-1} \to 0$, such that

$$\lim_{\kappa_{i-1} \to 0} \bar{s}_{i-1} = \lim_{\kappa_{i-1} \to 0} \left(\tfrac{1}{2}\kappa_{i-1} (r_i + h_i v_i)^2 + \cdots \right) = 0.$$

In the previous section, the new coordinates $z_{3,i}$ and $z_{4,i}$ can be regarded as differences between the velocity of the preceding and follower vehicle in x and y
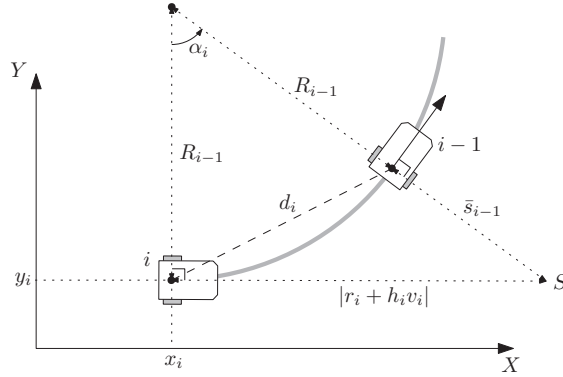
Figure 3.3: Magnitude of the extension vector, $\bar{s}_{i-1}$, where d_i is the actual distance between vehicle i and $i-1$.

direction, respectively, and it has been proven that the designed controller (3.8) asymptotically stabilizes the dynamics of $z_{3,i}$ and $z_{4,i}$. The convergence of $z_{3,i}$ and $z_{4,i}$ to zero has been shown in the previous section, under the condition that $[a_{i-1}, \omega_{i-1}]^T$ also converges to zero. However, if a platoon maneuvers on a curved path (i.e., ω_{i-1} is nonzero), $z_{3,i}$ and $z_{4,i}$ will not converge to zero according to (3.9b). Therefore, we redefine the coordinate transformation of $z_{3,i}$ and $z_{4,i}$ such that the convergence of $z_{3,i}$ and $z_{4,i}$ to zero on a curved path is also guaranteed, i.e., the velocity of the follower vehicle converges to the velocity of its preceding vehicle. To proceed, we define the new state components as

$$z_{1,i} = x_{i-1} + s_{x,i-1} - x_i - (r_i + h_i v_i)\cos\theta_i \tag{3.19a}$$

$$z_{2,i} = y_{i-1} + s_{y,i-1} - y_i - (r_i + h_i v_i)\sin\theta_i \tag{3.19b}$$

$$z_{3,i} = v_{i-1}\cos\theta_{i-1} - v_i\cos(\theta_i + \alpha_i) \tag{3.19c}$$

$$z_{4,i} = v_{i-1}\sin\theta_{i-1} - v_i\sin(\theta_i + \alpha_i). \tag{3.19d}$$

With this new choice of state components, the control objective can be formulated such that $[z_{1,i}, z_{2,i}]^T$ converges to zero. From Figure 3.3, we can define α_i, the angle of the arc between the vehicle i and vehicle $i-1$, as a function of κ_{i-1} and v_i satisfying

$$\alpha_i = \arctan[\kappa_{i-1}(r_i + h_i v_i)], \quad -\frac{\pi}{2} < \alpha_i < \frac{\pi}{2}. \tag{3.20}$$

Note that the definition of α_i only applies when $\alpha_i \in (-\pi/2, \pi/2)$, i.e., the orientation difference between the follower and its preceding vehicle has to be smaller than $\pi/2$. By noting that

$$\sin\alpha_i = \frac{\kappa_{i-1}(r_i + h_i v_i)}{\sqrt{1 + \kappa_{i-1}^2(r_i + h_i v_i)^2}} \tag{3.21}$$

$$\cos\alpha_i = \frac{1}{\sqrt{1 + \kappa_{i-1}^2(r_i + h_i v_i)^2}}, \tag{3.22}$$

derivatives of α_i and $\bar{s}_{i-1}$ with respect to time are given as

$$\dot{\alpha}_i = \alpha_{\kappa,i}\dot{\kappa}_{i-1} + \alpha_{a,i}a_i \tag{3.23}$$

$$\dot{\bar{s}}_{i-1} = s_{\kappa,i}\dot{\kappa}_{i-1} + s_{a,i}a_i, \tag{3.24}$$

with

$$\alpha_{\kappa,i} := (r_i + h_iv_i)\cos^2\alpha_i, \qquad \alpha_{a,i} := h_i\kappa_{i-1}\cos^2\alpha_i, \tag{3.25}$$

$$s_{\kappa,i} := \frac{1}{\kappa_{i-1}^2}(1 - \cos\alpha_i), \qquad s_{a,i} := h_i\sin\alpha_i. \tag{3.26}$$

To obtain the inter-vehicle dynamics, we first define a rotation matrix

$$R(\alpha_i) = \begin{bmatrix} \cos\alpha_i & -\sin\alpha_i \\ \sin\alpha_i & \cos\alpha_i \end{bmatrix}, \tag{3.27}$$

such that the term $[z_{3,i}, z_{4,i}]^T$ can be rewritten as

$$\begin{aligned}
\frac{1}{\cos\alpha_i}\begin{bmatrix} z_{3,i} \\ z_{4,i} \end{bmatrix} &= \begin{bmatrix} \cos\theta_{i-1} \\ \sin\theta_{i-1} \end{bmatrix}\frac{v_{i-1}}{\cos\alpha_i} - \frac{R(\alpha_i)}{\cos\alpha_i}\begin{bmatrix} \cos\theta_i \\ \sin\theta_i \end{bmatrix}v_i \\
&= \begin{bmatrix} \cos\theta_{i-1} \\ \sin\theta_{i-1} \end{bmatrix}\frac{v_{i-1}}{\cos\alpha_i} - \begin{bmatrix} \cos\theta_i \\ \sin\theta_i \end{bmatrix}v_i - \begin{bmatrix} -\sin\theta_i \\ \cos\theta_i \end{bmatrix}v_i\tan\alpha_i. \tag{3.28}
\end{aligned}$$

By differentiating (3.19) with respect to time and taking equations (3.23), (3.24), and (3.28) into account, we eventually obtain the inter-vehicle dynamics as follows

$$\begin{bmatrix} \dot{z}_{1,i} \\ \dot{z}_{2,i} \end{bmatrix} = \frac{1}{\cos\alpha_i}\begin{bmatrix} z_{3,i} \\ z_{4,i} \end{bmatrix} - \Gamma_{12,i}\begin{bmatrix} a_i \\ \omega_i \end{bmatrix} + \beta_{1,i} \tag{3.29a}$$

$$\begin{bmatrix} \dot{z}_{3,i} \\ \dot{z}_{4,i} \end{bmatrix} = H_{i-1}\begin{bmatrix} a_{i-1} \\ \omega_{i-1} \end{bmatrix} - \Gamma_{34,i}\begin{bmatrix} a_i \\ \omega_i \end{bmatrix} + \beta_{2,i}, \tag{3.29b}$$

with

$$\Gamma_{12,i} = \begin{bmatrix} h_i\cos\theta_i - s_{a,i}\sin\theta_{i-1} & -(r_i + h_iv_i)\sin\theta_i \\ h_i\sin\theta_i + s_{a,i}\cos\theta_{i-1} & (r_i + h_iv_i)\cos\theta_i \end{bmatrix} \tag{3.30}$$

$$\Gamma_{34.i} = \begin{bmatrix} \cos(\theta_i + \alpha_i) - \delta_i\sin(\theta_i + \alpha_i) & -v_i\sin(\theta_i + \alpha_i) \\ \sin(\theta_i + \alpha_i) + \delta_i\cos(\theta_i + \alpha_i) & v_i\cos(\theta_i + \alpha_i) \end{bmatrix} \tag{3.31}$$

$$\begin{aligned}
\beta_{1,i} &= \begin{bmatrix} -\sin\theta_i \\ \cos\theta_i \end{bmatrix}v_i\tan\alpha_i + R(\theta_{i-1})\begin{bmatrix} \bar{s}_{i-1}\omega_{i-1} \\ -s_{\kappa,i}\dot{\kappa}_{i-1} \end{bmatrix} \\
&\quad + \left(1 - \frac{1}{\cos\alpha_i}\right)\begin{bmatrix} \cos\theta_{i-1} \\ \sin\theta_{i-1} \end{bmatrix}v_{i-1} \tag{3.32}
\end{aligned}$$

$$\beta_{2,i} = v_i(r_i + h_iv_i)\cos^2\alpha_i\begin{bmatrix} \sin(\theta_i + \alpha_i) \\ -\cos(\theta_i + \alpha_i) \end{bmatrix}\dot{\kappa}_{i-1} \tag{3.33}$$

$$\delta_i = v_ih_i\kappa_{i-1}\cos^2\alpha_i, \tag{3.34}$$

$\bar{s}_{i-1}$ as in (3.18), and H_j, with $j \in \{i-1, i\}$, as in (3.7b). The objective is to design control inputs $[a_i, \omega_i]^T$ which asymptotically stabilize the states $[z_{1,i}, z_{2,i}, z_{3,i}, z_{4,i}]^T$ at zero. By taking the feedback as

$$\begin{bmatrix} a_i \\ \omega_i \end{bmatrix} = \Gamma_{12,i}^{-1} \left(\begin{bmatrix} k_1 z_{1,i} \\ k_2 z_{2,i} \end{bmatrix} + \frac{1}{\cos \alpha_i} \begin{bmatrix} z_{3,i} \\ z_{4,i} \end{bmatrix} + \beta_{1,i} \right) \tag{3.35}$$

$$\Gamma_{12,i}^{-1} = \frac{1}{\mu_i} \begin{bmatrix} (r_i + h_i v_i) \cos \theta_i & (r_i + h_i v_i) \sin \theta_i \\ -h_i \sin \theta_i - s_{a,i} \cos \theta_{i-1} & h_i \cos \theta_i - s_{a,i} \sin \theta_{i-1} \end{bmatrix} \tag{3.36}$$

$$\mu_i = h_i (r_i + h_i v_i) \left(1 - \sin \alpha_i \sin(\theta_{i-1} - \theta_i) \right), \tag{3.37}$$

where $r_i + h_i v_i > 0$, and substituting (3.35) into (3.29a) and (3.29b), we obtain the closed-loop system as follows

$$\begin{bmatrix} \dot{z}_{1,i} \\ \dot{z}_{2,i} \end{bmatrix} = - \begin{bmatrix} k_1 z_{1,i} \\ k_2 z_{2,i} \end{bmatrix} \tag{3.38a}$$

$$\begin{bmatrix} \dot{z}_{3,i} \\ \dot{z}_{4,i} \end{bmatrix} = H_{i-1} \begin{bmatrix} a_{i-1} \\ \omega_{i-1} \end{bmatrix} + \beta_{2,i} - \Gamma_{34,i} \Gamma_{12,i}^{-1} \begin{bmatrix} k_1 z_{1,i} \\ k_2 z_{2,i} \end{bmatrix}$$
$$- \Gamma_{34,i} \Gamma_{12,i}^{-1} \left(\frac{1}{\cos \alpha_i} \begin{bmatrix} z_{3,i} \\ z_{4,i} \end{bmatrix} + \beta_{1,i} \right). \tag{3.38b}$$

Using controller (3.35), we obtain a linear system (3.38a), of which the desired behavior can be obtained through pole placement and many other controller design methods. It can be observed that (3.38a) describes the controlled dynamics and (3.38b) represents the internal dynamics of the system. By the choice of $k_1, k_2 > 0$, the dynamics (3.38a) is exponentially stable. Thus, we establish the stability of the overall system (3.38) by the following proposition, which can be regarded as the main result of this chapter.

Proposition 3.2. *Consider the system (3.29) in closed loop with the control input (3.35). Assume that $0 < v_{i-1}^{\min} \leq v_{i-1}(t) \leq v_{i-1}^{\max}$ and let some $\varepsilon > 0$ be given such that $\varepsilon < v_{i-1}^{\min}$. If*

$$|\kappa_{i-1}| \leq \frac{1}{r_i + h_i \sqrt{2} \left(v_{i-1}^{\max} + v_{i-1}^{\min} - \varepsilon \right)} \tag{3.39}$$

and

$$h_{\kappa,i}^{\max} |\dot{\kappa}_{i-1}| + |a_{i-1}| \leq \frac{v_{i-1}^{\min} - \varepsilon}{2 \left(\frac{r_i}{\varepsilon} + h_i \right)}, \tag{3.40}$$

with $h_{\kappa,i}^{\max} = \frac{r_i^2}{h_i} + h_i \sqrt{2} \left(v_{i-1}^{\max} + v_{i-1}^{\min} - \varepsilon \right)$, then for sufficiently small initial conditions $z_i(0)$ we have that $v_i(t) > 0$ such that input (3.35) is well defined. Furthermore, we have $\lim_{t \to \infty} \|z_{12,i}(t)\| = 0$, and $z_{34,i}(t)$ remains bounded. Additionally, if $\lim_{t \to \infty} a_{i-1}(t) = 0$ and $\dot{\kappa}_{i-1}$ converges to zero as $t \to \infty$, then we have also $\lim_{t \to \infty} \|z_{34,i}(t)\| = 0$, i.e., the closed-loop system (3.29,3.35) is asymptotically stable.

Proof. See Appendix A.2. □

Therefore, we can conclude that the system (3.38) is internally stable as long as the curvature is not too large (bounded by (3.39)), and (3.40) is satisfied. It should be noted that condition (3.39) is related to the bound of longitudinal and lateral velocity of the preceding vehicle, while the condition (3.40) is related to the lateral jerk and longitudinal acceleration of the preceding vehicle.

3.4   Simulation results

To illustrate the effectiveness of the extended look-ahead controller, we conduct several simulations in MATLAB for a platoon of 4 vehicles under two scenarios: a circular path and an eight-shaped path. The spacing policy parameters are chosen as $r_i = 1$ m and $h_i = 0.2$ s, and the control parameters $k_1 = 3.5$ and $k_2 = 3.5$ are selected. The gains k_1 and k_2 for the controllers are determined by an iterative manner. High value gains result in a faster convergence towards a reference path, but a higher sensitivity to curvature changes. A trajectory tracking controller is applied in the first vehicle to track the predefined trajectory, while the extended look-ahead controller is applied in other vehicles to track their preceding vehicle. It is assumed that the position, velocity, and acceleration of the preceding vehicle can be obtained without any delay involved. Both the conventional and the extended look-ahead approach are simulated for comparison.

3.4.1   Circular path trajectory

In this scenario, the first vehicle drives on a straight path along the x axis with a constant initial velocity $v_1 = 5$ m/s. At time $t = 6$ s, it turns with yaw rate $\omega_1 = 0.5$ rad/s and moves in a circular motion. The initial positions $(x_i(0), y_i(0))$ are $(0,0)$, $(-2,2)$, $(-4,4)$, and $(-6,6)$ for vehicle 1, 2, 3, and 4, respectively, while the initial heading angle is $\theta_i(0) = 0$ for all i. As depicted in Figure 3.4, both look-ahead controllers perform well in the straight path, driving all follower vehicles to track their preceding vehicle without lateral error. However, the conventional look-ahead controller shows its shortcoming when the platoon enters a circular path. The vehicle with the conventional look-ahead cruises in a smaller radius than its preceding vehicle, as shown in Figure 3.4. This behavior occurs because at the moment the preceding vehicle turns, the controller senses a position error and then adjusts the position of follower instantaneously. As a result, the follower vehicle turns too early and cuts the corner. From Figure 3.4(left), which shows a close-up of the circular part of the track, it can be observed that vehicles 2-4 do not travel on the path with the same radii as vehicle 1. The difference of curvatures results in a lower longitudinal velocity of the follower vehicle than the one of the preceding vehicle, as depicted in Figure 3.5. This difference in velocity also affects the longitudinal spacing distance between vehicles (Figure 3.6). On the other hand, the extended look-ahead controllers successfully compensated the lateral deviation, thus keeping the follower vehicles to drive with the same radii as their preceding vehicle. By maintaining the same velocity for all vehicles, the extended look-ahead controllers manage to keep the same longitudinal spacing
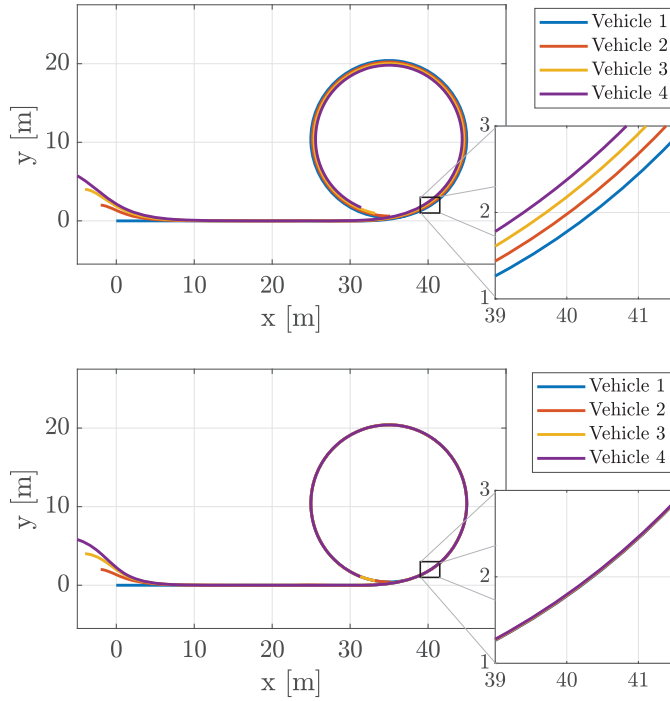
Figure 3.4: Trajectory of vehicles for the circular path scenario: conventional look-ahead (top) vs extended look-ahead (bottom).
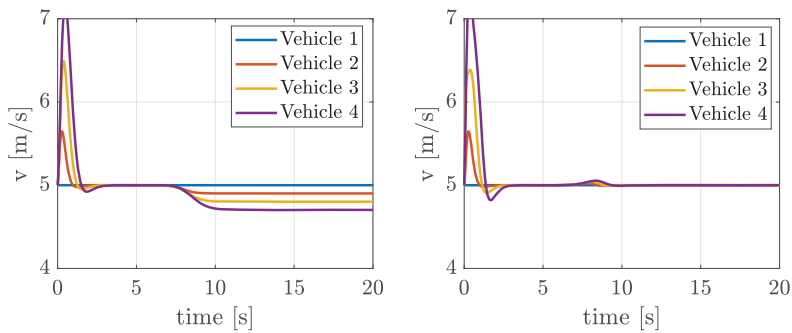

Figure 3.5: Velocity of vehicles for the circular path scenario: conventional look-ahead (left) vs extended look-ahead (right).
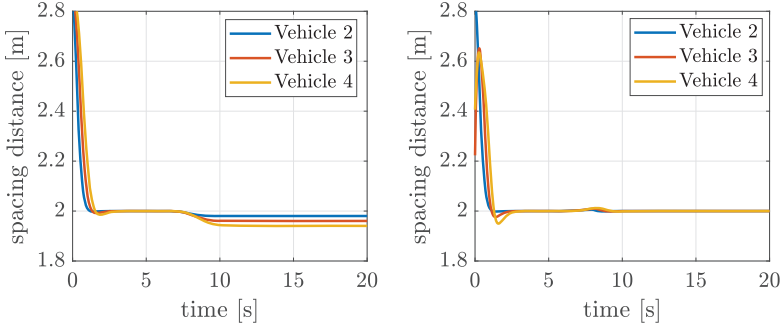
Figure 3.6: Longitudinal spacing distance of vehicles for the circular path scenario: conventional look-ahead (left) vs extended look-ahead (right).

distance between vehicles (Figure 3.6(right)). It is also worth noting that the velocity of all vehicles is always positive and never reaches zero for both look-ahead approaches, see Figure 3.5.

3.4.2   Eight-shaped path scenario

In this scenario, the robustness of the proposed controller against varying yaw rate ω is evaluated. The first vehicle starts at initial position $(30, 15)$, cruises along the eight-shaped path with a constant velocity $v_1 = 5$ m/s (equal to 18 km/h). The eight-shaped path is generated by half circles and quintic polynomial functions (see Figure 3.7). The initial positions of the other vehicles are $(28, 15)$, $(26, 15)$, and $(24, 15)$ for vehicle 2, 3, and 4, respectively. The initial heading angle is $\theta_i(0) = 0.7854$ rad for all i. It can be observed that the initial position errors are handled equally good by both types of look-ahead controllers. However, the difference in performance can be seen in a curve path. Analogously to the simulation results of the circular path, the extended look-ahead controller delivers better tracking performance than the conventional look-ahead controller, as shown by Figure 3.7. Vehicles with the conventional look-ahead drive with smaller radii than their preceding vehicle, while ones with the extended look-ahead drive with relatively equal radii with their preceding vehicle. It can also be observed from Figure 3.9(right) that the extended look-ahead controllers are capable to maintain the longitudinal spacing distance, and proven to be robust against varying yaw rate. From Figure 3.8, we can observe that velocities for all vehicles are always positive and never reach zero, which is a necessary condition for the designed controllers.
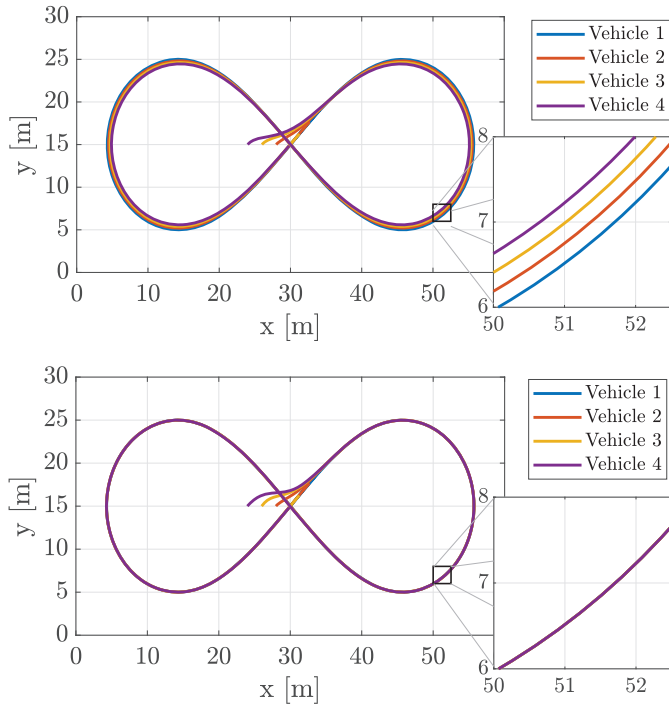
Figure 3.7: Trajectory of vehicles for the eight-shaped scenario: conventional look-ahead (top) vs extended look-ahead (bottom).
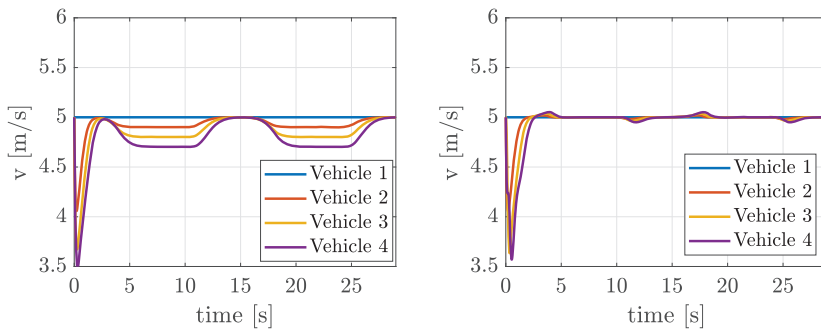

Figure 3.8: Velocity of vehicles for the eight-shaped path scenario: conventional look-ahead (left) vs extended look-ahead (right).
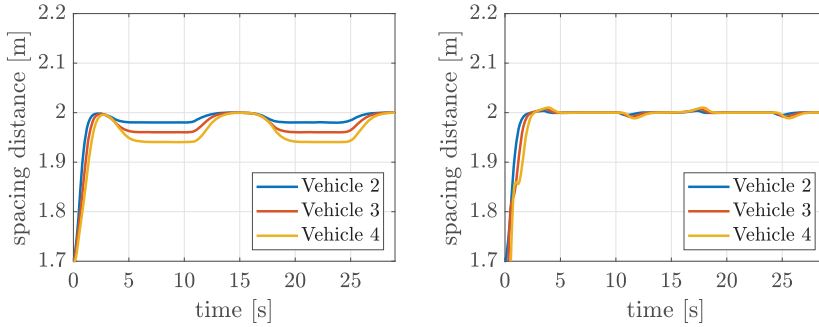
Figure 3.9: Longitudinal spacing distance of vehicles for the eight-shaped circular path scenario: conventional look-ahead (left) vs extended look-ahead (right).

3.5   Experiments

In this section, the error dynamics and the controllers that have been derived previously are implemented using the mobile robot E-puck. E-puck is used because the implementation is straightforward, using the camera localization system developed in Caarls (2009) that acquires the accurate position of unicycles. E-puck is a differential-wheeled non-holonomic mobile robot, designed by ASL laboratory at EPFL (École Polytechnique Fédérale de Lausanne, Switzerland) (Mondada and Bonani (2007)). The main specifications of the E-puck robot are given in Table 3.1.

3.5.1   Experimental setup

The experimental setup is shown in Figure 3.11. Each wheel of the E-puck robot is driven by a stepper motor, and the velocity control commands are sent to both stepper motors from an external PC through Bluetooth. To be able to communicate via Bluetooth, the E-puck has to be flashed through the Bluetooth Serial Communication (SerCom) protocol that allows it to read and parse commands that are sent from the external PC. Since an E-puck is equipped with an open Bluetooth protocol, a variety of programming languages can be used to control the robot, such as through the hyperterminal of Windows, MATLAB, or Python. An external PC is used to generate a reference trajectory and to determine the absolute coordinates and orientations of the robots from a measurement device (a Firewire camera AVT Guppy F-080b b/w combined with reacTIVision software) placed above the arena of 175 cm×128 cm. The position and orientation accuracy of these position measurements are ±0.0019 m for x and y position and ±0.0524 rad in θ direction, with a sample rate of 25 Hz (van den Broek et al. (2009)). The PC then uses the obtained information to implement the control algorithm for each E-puck. Each E-puck is attached with a unique marker (2D-barcode) consisting of 3×3 blocks. The color of the blocks in the corners is chosen

Figure 3.10: The E-puck mobile robot (left), and markers used for identification (right).
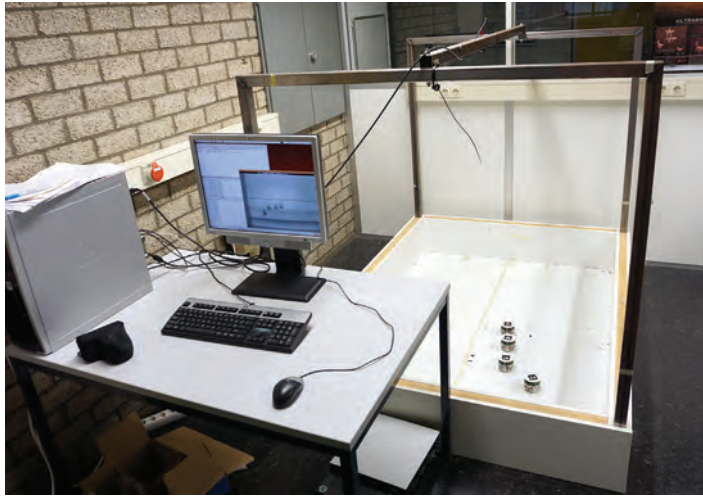

Figure 3.11: The experimental setup.

such that the orientation of the marker (thus, the orientation of the E-puck) can be determined (Caarls (2009), Morales and Nijmeijer (2016)). An example of the barcode used in the E-puck is shown in Figure 3.10(right). In our approach, we need to be able to measure the position of the preceding vehicle with respect to the coordinate frame of the ego vehicle. In the E-puck setup, all measurement regarding the position and orientation are done by a central camera placed above the arena. However, this central camera would not be available for the practical implementation in a real vehicle platooning. To address this issue, we could replace the central camera by a radar (to measure the longitudinal position of the preceding vehicle), and a forward-looking camera (to measure the lateral position), both attached on every vehicle in the platoon.

Since an E-puck is a differential-drive mobile robot, the direction of motion is

Table 3.1: E-puck specification

Specification	Values
Robot radius	37 mm
Wheel radius (r)	20.5 mm
Axle length (L)	52 mm
Speed unit	0.00628 rad/s
Encoder resolution	159.23
Maximum angular speed	1000 units
Maximum velocity	13 cm/s
Maximum angular velocity	5 rad/s

controlled by separately controlling the speed of the left and right wheels, denoted by $v_{l,i}$ and $v_{r,i}$, respectively. The transformation of the individual wheels speed to the linear velocity v_i and angular velocity ω_i can be determined using the following relation

$$\omega_i = \frac{v_{r,i} - v_{l,i}}{L}, \quad v_i = \frac{v_{r,i} + v_{l,i}}{2}, \tag{3.41}$$

where L is the length between the left and right wheels.

In order to support the simulation results presented in the previous section, for this experiment we define two kinds of reference trajectories: a circular trajectory and an eight-shaped trajectory. Given the size of the arena, an appropriate selection of the radius of the circular path is 0.4 m with the center point at $(0.7, 0.5)$, so that the reference trajectory stays within the arena. The eight-shaped trajectory is composed of half circles with a radius of 0.3 m and straight sections. The reference linear velocity is chosen as 0.04 m/s, and the controlled velocities v_i and ω_i of all E-pucks are physically limited by their respective maximum value as in Table 3.1. First, the reference trajectory for the first E-puck is defined. Afterwards, the positions of all E-pucks are measured and recorded in the PC through the camera. The decentralized controllers then calculate the inputs needed for each E-puck simultaneously and send the input velocity commands via Bluetooth. It should be noted that the controllers are executed in the main PC, not in the E-pucks themselves. The control parameters are selected as $k_1 = 2$ and $k_2 = 2$ for all E-pucks, while the spacing policy parameters are selected as $r_i = 0.1$ m and $h_i = 0.05$ s. The gains are selected in an iterative manner. Identical to the simulations, higher gains result in a faster convergence to the reference path, but a higher sensitivity to curvature changes. In the experiment, this is undesirable since a slight change in measurements, due to noise and sensor inaccuracy, could result in overcompensation. Both systems with the conventional and extended look-ahead are implemented, and the experiment results are presented in the next section to verify the simulation results. Since the E-puck has a velocity limitation (13 cm/s), all experiments were performed at low velocity.

3.5.2 Circular path scenario

In this scenario, we define the initial position of the reference trajectory at $(0.5, 0.1)$. Four E-pucks that are already in a platoon order are placed behind that initial position to ensure that they move forward. The reference trajectory itself acts as a reference only for the first E-puck, while the others use their preceding E-puck as a reference, i.e., E-puck 2 follows E-puck 1, E-puck 3 follows E-puck 2, and so on. The reference vehicle cruises in a straight trajectory with the velocity of 0.04 m/s along global x axis until it reaches $x = 0.8$ m, and then maneuvers into a circular trajectory. The trajectories of all E-pucks with the conventional and extended look-ahead controllers are shown in Figure 3.12 and Figure 3.13, respectively. As observed in both figures, on the straight trajectory all robots directly move to their desired position, subject to the spacing distance between robots. However, on the circular trajectory, the platoon with the conventional look-ahead approach suffers from the cutting-corner behavior, indicated by a smaller turning radius for each robot upstream. In contrast, the extended look-ahead controller shows satisfactory results, with all E-pucks driving closely to the reference trajectory. Moreover, the extended look-ahead controller also successfully maintains the longitudinal spacing distance between each E-puck at 0.1 m (see Figure 3.14). It can be observed from Figure 3.15 that the velocities of all E-pucks are nonzero. It should be noted that the differences between simulations and experiment regarding spacing distances and velocities at the start of the simulation and the experiment exist due to the different initial condition in simulation versus experiment. Moreover, there are also several factors that can affect the variation in the errors in experiment results: the stick-slip effects in the E-puck drive line, actuator delay, and the non-deterministic delay in the Bluetooth communication. In spite of these differences, it can be observed that our approach performs equally well in both simulations and experiments.

3.5.3 Eight-shaped path scenario

For the second experiment, an eight-shaped path is used to confirm the robustness of the controller against a varying yaw rate. The reference trajectory starts at $(0.7, 0.5)$ and the E-pucks are placed behind the reference's initial position to ensure that they move forward, i.e., $v_i > 0$ for all i. The platoon moves with the same topology as the previous experiment. The first E-puck tracks the reference trajectory, while the others follow their preceding robot. As expected, the platoon with the conventional look-ahead controller tends to cut the corner, and the deviation in radius with the reference escalates in upstream direction (Figure 3.16). The effectiveness of the extended look-ahead controller for the eight-shaped trajectory can be observed directly from Figure 3.17. The radius deviation has been successfully compensated, thus resulting in a better tracking performance than the conventional look-ahead. Due to the additional terms $\beta_{1,i}$ and $s_{a,i}$ in the extended look-ahead controller (3.35), the variation in the errors for the extended look-ahead is larger than the variation for the conventional look-ahead (see Figure 3.18). Nevertheless, the measurement noise in the extended look-ahead is

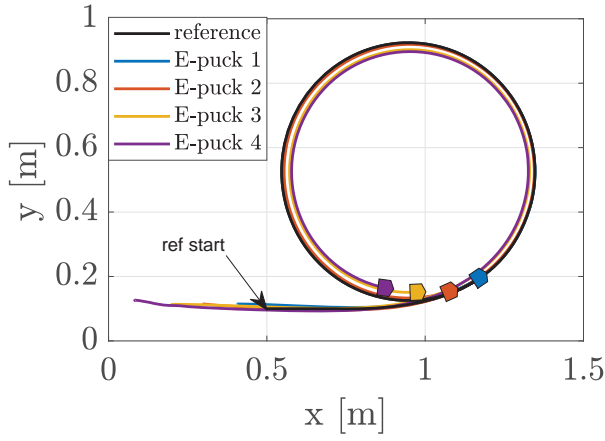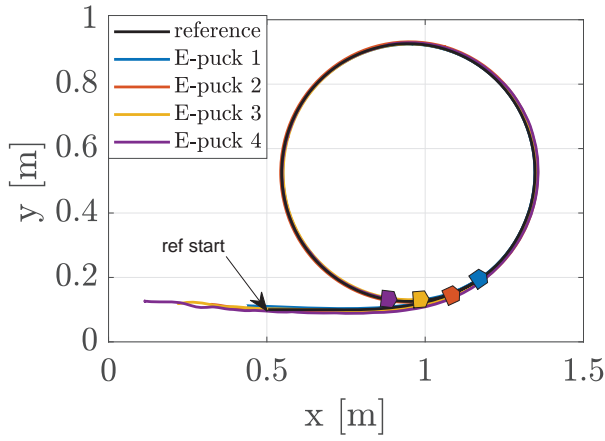Figure 3.12: Trajectory of E-pucks on a circular path with conventional look-ahead.

Figure 3.13: Trajectory of E-pucks on a circular path with extended look-ahead.

still small enough (less than 0.02 m) such that the longitudinal spacing distance between each E-puck can still be maintained at 0.1 m. It can also be observed that velocities of all E-pucks in this scenario are nonzero (Figure 3.19).

Figure 3.14: Longitudinal spacing distance for the circular path scenario: conventional look-ahead (left) vs extended look-ahead (right).

Figure 3.15: Velocities of E-pucks for circular path scenario: conventional look-ahead (left) vs extended look-ahead (right).

Figure 3.16: Trajectory of E-pucks on an eight-shaped path with conventional look-ahead.

Figure 3.17: Trajectory of E-pucks on an eight-shaped path with extended look-ahead.
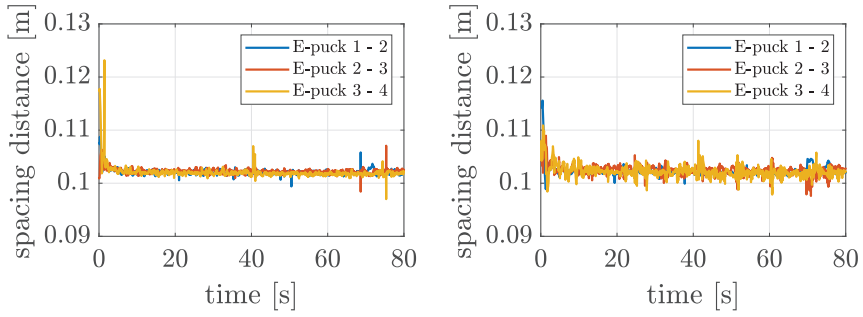
Figure 3.18: Longitudinal spacing distance for the circular path scenario: conventional look-ahead (left) vs extended look-ahead (right).
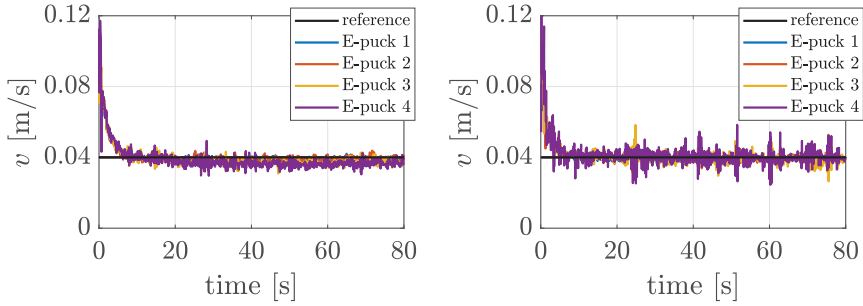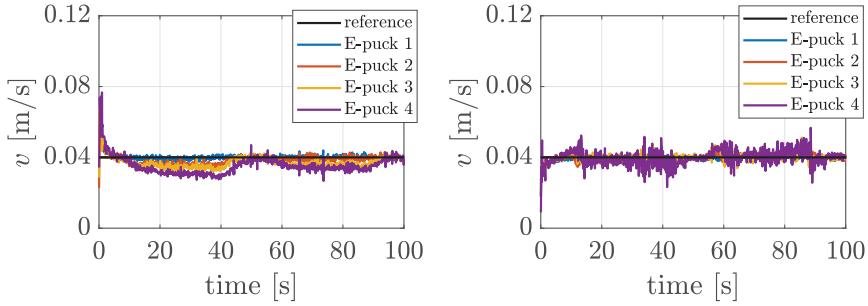

Figure 3.19: Velocities of E-pucks for eight-shaped path: conventional look-ahead (left) vs extended look-ahead (right).
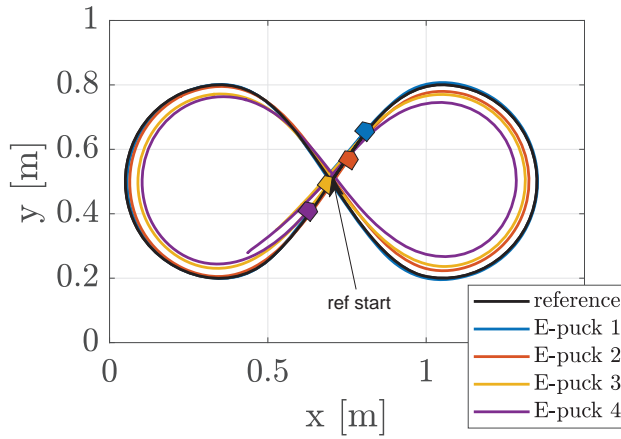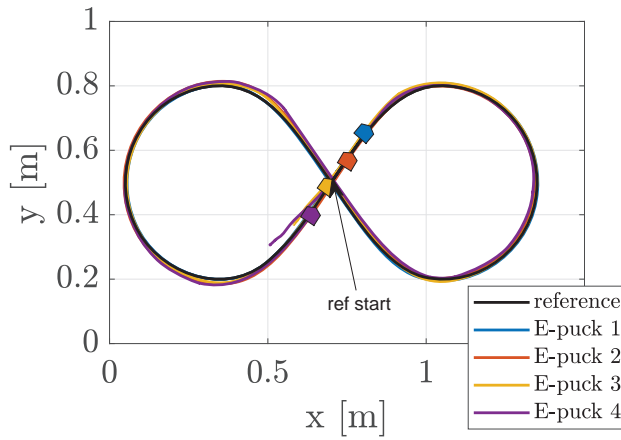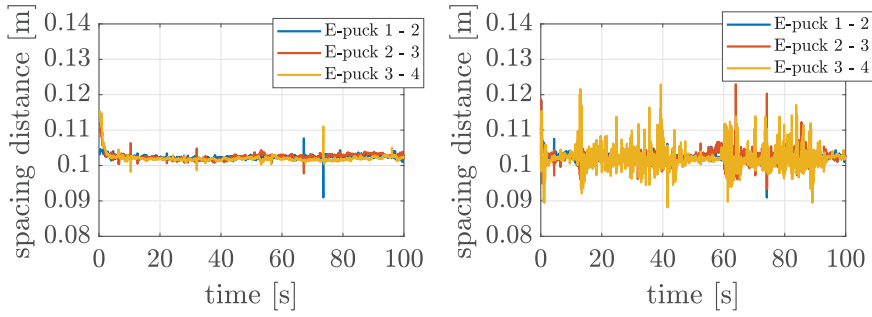
3.6 Conclusions

Cooperative driving for a platoon of unicycles has been studied with the emphasis on cornering maneuvers. By using only the current position information of the preceding vehicle, the platoon suffers from a cutting-corner behavior, in which the follower vehicle has a smaller radius than the preceding vehicle. The difference in radius with respect to the first vehicle escalates upstream, thus affecting the tracking performance at cornering. To ensure a better performance, the error dynamics at cornering have been redefined. The redefined error dynamics involve the follower vehicle tracking the end of a vector extending from the preceding vehicle. This point can be viewed as a virtual vehicle which acts as the tracking objective for the follower vehicle. The effectiveness of the proposed approach has been successfully demonstrated in simulation, and validated by an experiment with a platoon consisting of four E-pucks. In this experiment, a vehicle following maneuver has been demonstrated on a circular path and an eight-shaped path. The designed extended look-ahead approach has been proven to compensate the cutting-corner behavior, while satisfying the spacing policy requirement between vehicles.

Longitudinal and lateral extended look-ahead control with orientation-error observer in a local coordinate system

Abstract[1] - This chapter presents a novel extended look-ahead concept of an integrated lateral and longitudinal vehicle following controller with an orientation-error observer. The control law is based on input-output feedback to address a local tracking problem. It is known that due to the position control in the look-ahead approach, the follower vehicle may cut corners. To address this problem, a reference-induced extended look-ahead tracking point is introduced such that the cutting-corner is compensated. Moreover, the stability of the internal dynamics is analyzed. To address the situation where the orientation tracking error is not measurable or corrupted by noise, an orientation-error observer, constructed from the position tracking error, is designed. The performance of the extended look-ahead controller and the orientation-error observer is investigated by means of a simulation study, and validated with experiments on a mobile robot platform.

4.1 Introduction

In recent years, the increasing needs for mobility has caused a high need of transportation. One solution to compensate for the increasing number of vehicles is to develop more infrastructure or to increase the capacity of existing infrastructure. Since the development of the infrastructure is time consuming, costly, and infeasible in some situations, increasing highway capacity is seen as the most effective solution. One of the methods to increase the highway capacity is vehicle platooning. With the concept of automated vehicles, platooning allows a vehicle to drive

---

[1]This chapter is based on Bayuwindra et al. (2019a)

closer to its preceding vehicle by eliminating the reaction time of human driver. The concept of vehicle platooning in longitudinal movement is realized through Cooperative Adaptive Cruise Control (CACC). CACC, as an extension of ACC, utilizes wireless communication between vehicles (V2V communication) so that acceleration information of the preceding vehicle can be used as a feed-forward term to attenuate disturbances along the platoon (Ploeg et al. (2011)). This is an advantage of CACC over ACC, whereas the disturbance in ACC may be amplified in the upstream direction (Sheikholeslam and Desoer (1992a)). For lateral movement, vehicle platooning control can be designed by two main approaches, i.e., a path following approach and a trajectory tracking approach. In path following, the control objective is to drive the vehicle over a desired path without any time constraint, i.e., there is no requirement of when the vehicle should arrive at a certain point. Since there is no time requirement, the vehicle's longitudinal velocity can be freely regulated, independent of the position on the spatial path (Morin and Samson (2008)). On the other hand, in the trajectory tracking approach, the desired path is parameterized with respect to time, i.e., the vehicle is required to be at a specific position along the path at a specific time.

In Rajamani et al. (2000), a lane keeping controller based on the path following approach, is designed such that the vehicle follows a reference path, e.g., the path composed of lane markings (either road surface or embedded magnetic markings) using a camera or magnetic sensor, known as a "look-down" technique. It should be noted that the term "look-down" is rather loose since the vehicle also requires to look for the lane markings in front of it. The control objective of a lane keeping is to design a steering input that brings the lateral error, i.e., distance from the vehicle's position to the path, to zero. Most path following methods address the control problem by assigning the motion along a path in a single coordinate. The single intrinsic coordinate system used in the path following itself is known as a Serret-Frenet reference frame, where the origin is determined by the projection of the vehicle (Morin and Samson (2008)). The projection of the vehicle's position onto the path is then used as reference for the control problem. The research in Plaskonka (2015) has shown that the orthogonal projection with respect to the path has a local character in the sense that the vehicle has at first to get to the desired path orthogonally before it can project itself on the path. Since in the Serret-Frenet frame the longitudinal distance has been transformed into a curvilinear distance, the longitudinal control then can be realized through CACC. The combination of a lane keeping controller and CACC becomes a trajectory control problem, since there is a time requirement to be fulfilled. With this combined approach, the follower vehicles in a platoon drive in the exact same path as the leader vehicle, and the spacing distance objective can be fulfilled with the CACC controller (Lefeber et al. (2017)). However, the lane keeping performance in this approach relies heavily on the reference markers and V2I (vehicle-to-infrastructure) communication to provide the platoon with information about road structure. From the viewpoint of vehicle platooning, the major disadvantage of the path following approach is when the inter-vehicle distance is getting small, the look-down system is unable to track the lane markings accurately as they are

obstructed by the preceding vehicle (Solyom et al. (2013)).

As an alternative to lane keeping, a direct vehicle-following control is designed. A direct vehicle-following control uses the current preceding vehicle's position as a reference while keeping a desired distance. The vehicle-following control of vehicle platoons was developed from CACC and was first designed for a longitudinal control (see, e.g., Rajamani and Shladover (2001), Shladover et al. (1991), Swaroop et al. (2001)). In this approach, the follower vehicle tracks the current position of the preceding vehicle by using a camera (or lidar) and determines the relative distance with respect to the follower vehicle, commonly known as a "look-ahead" technique. The vehicle-following control was then extended to both longitudinal and lateral control in (Canudas de Wit (1998), Morales and Nijmeijer (2016), Petrov (2009)). The objective of this longitudinal and lateral vehicle-following control is to minimize the error between the measured relative distance and the desired distance (e.g., spacing policy in CACC), and to minimize the lateral error with respect to the preceding vehicle's path. One of the main challenges in this approach is to determine the path of the preceding vehicle. Since the follower vehicle can only measure the distance as a straight line (as opposed to the curvilinear distance in the Serret-Frenet frame), the follower vehicle can deviate from the path of the preceding vehicle during cornering, known as corner cutting. In Petrov (2009), a reference virtual point, which is positioned at a desired known distance behind the lead vehicle, is proposed to compensate the corner cutting. The results shows that the proposed solution was able to compensate the corner cutting for the path with small curvatures, but was ineffective for the path with large curvatures. In Bayuwindra et al. (2016), an extended look-ahead approach has been designed, based on dynamic feedback linearization, to compensate for the corner cutting. The extended look-ahead uses the velocity and heading information of the preceding vehicle (which are available from radar and V2V communication) to create a virtual reference-induced look-ahead point as a new tracking objective for the follower vehicle. The results are then elaborated in Bayuwindra et al. (2019b) with the formal stability analysis, where the stability of the internal dynamics is guaranteed under bounded curvatures, lateral jerk, and acceleration of the preceding vehicle. The error dynamics in Bayuwindra et al. (2016, 2019b) are defined as a global tracking problem, in which the position and orientation of each vehicle is assumed to be measurable with respect to a global (i.e., fixed) coordinate frame. The shortcoming of this method is that the global position and orientation of vehicles are commonly not available in practical situations.

The main contribution of this chapter is the design of the extended look-ahead controller as a local tracking problem, where the error dynamics are defined with respect to the target position of the follower vehicle. The advantage of our proposed controller to the path-following control (e.g., Morin and Samson (2008), Plaskonka (2015)) is that it does not need lane markings and utilizes the already available information from CACC setup, thus providing benefits for a practical implementation and cost-efficiency. To study the internal dynamics of the resulting system, a formal stability analysis is provided. Moreover, the control strategy is

then further extended with an orientation-error observer, addressing the situation where the relative orientation between vehicles is not measurable, or corrupted by noise. The effectiveness of the extended look-ahead controller against corner-cutting is demonstrated by a simulation case study, and further validated by an experiment with mobile robots.

The organization of this chapter is as follows: Section 4.2 presents the concept of trajectory tracking control of vehicle platoons with extended look-ahead, starting with the problem formulation. The extended look-ahead controller is proposed, and a stability analysis is subsequently provided. Section 4.3 presents the design of the orientation-error observer. The results of the simulation study are presented in Section 4.4. For further validation, the extended look-ahead controller and the orientation-error observer are implemented in a mobile robot platform in Section 4.5. Finally, the concluding remarks are discussed in Section 4.6.

4.2 Control of vehicle platooning with extended look-ahead

4.2.1 Problem formulation

Consider a unicycle-type vehicle with the posture $[x(t), y(t), \theta(t)]^T$ (see Figure 4.1) that can be described by following differential equations

$$\dot{x} = v \cos \theta \tag{4.1a}$$

$$\dot{y} = v \sin \theta \tag{4.1b}$$

$$\dot{\theta} = \omega, \tag{4.1c}$$

where $P_v = (x, y)$ are the Cartesian coordinates of the axle center of the vehicle, θ is the orientation of the vehicle with respect to the global X axis, v is the linear velocity input and ω is the angular velocity input of the vehicle.

Consider a reference vehicle with the posture $[x_r(t), y_r(t), \theta_r(t)]^T$ and the kinematics given by

$$\dot{x}_r = v_r \cos \theta_r \tag{4.2a}$$

$$\dot{y}_r = v_r \sin \theta_r \tag{4.2b}$$

$$\dot{\theta}_r = \omega_r, \tag{4.2c}$$

where (x_r, y_r) are the Cartesian coordinates of the axle center of the reference vehicle, θ_r is the orientation of the reference vehicle with respect to the global X axis, v_r and ω_r are the reference velocity and angular velocity input, respectively. The trajectory tracking problem is typically solved by stabilizing the position of P_v with respect to the reference P_r and orientation of θ with respect to the reference orientation θ_r. The relative kinematics between these points can be determined with respect to the follower vehicle frame (see, e.g., Jiang and Nijmeijer (1997),
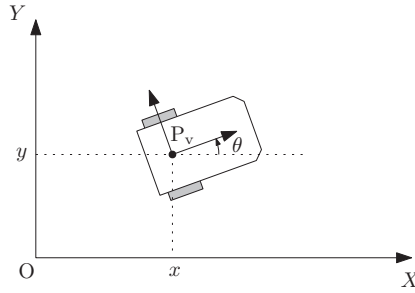
Figure 4.1: A unicycle mobile robot in Cartesian coordinates.

Kanayama et al. (1990), Loría and Panteley (2005), Panteley et al. (1998)), the reference vehicle frame (see, e.g., Morin and Samson (2008), Petrov (2009)), or any moving frame, which results in different error dynamics. In our approach, we choose the relative kinematics with respect to the frame of the desired posture of the follower vehicle. This choice makes the mathematical development easier than other frame choices, as explained in the next section.

Now consider a trajectory tracking problem with a look-ahead distance (referred as a vehicle-following control problem), in which the objective of the follower vehicle is to follow the reference vehicle at a desired distance d. We define P_0 as a target point of the follower vehicle, and P_{la} as a look-ahead point attached to the follower vehicle. The coordinates of P_{la} are defined as

$$x_{la} = x + d\cos\theta \tag{4.3a}$$

$$y_{la} = y + d\sin\theta, \tag{4.3b}$$

where (x, y) are the Cartesian coordinates of the follower vehicle, $|P_0 P_r| = d$, and the distance $d \in \mathbb{R}_+$ (see Figure 4.2). With this look-ahead point, the control objective of the vehicle following problem could then be to stabilize at zero the tracking errors $(x_{la} - x_r, y_{la} - y_r)$ of that point P_{la} with respect to the reference point P_r. However, in a curve, the leader-follower vehicle system has a unique instantaneous center of rotation (ICR), such that the line through the axle of each unicycle goes through this ICR. Consequently, when (x_{la}, y_{la}) have converged to (x_r, y_r), the follower vehicle will drive at a shorter distance to the ICR, i.e., it will cut corners (Bayuwindra et al. (2016), Petrov (2009)). It is interesting to remark that this problem is analogous to a truck-trailer combination, see Figure 4.3. On cornering maneuvers, a trailer coupled to the truck will also have the cutting-corner problem and human drivers solve this problem by letting the truck turn at the point in front of the cornering point, denoted by $\tilde{P}_c$, such that the trailer will travel on the desired arc, see Figure 4.4(left).

Based on the same approach, we extend the look-ahead point in our error dynamics, thus creating a "reference-induced look-ahead point" as the new tracking point objective (denoted by P_s) for the follower vehicle such that cutting corner can be compensated. The position of P_s in the Cartesian coordinate system is
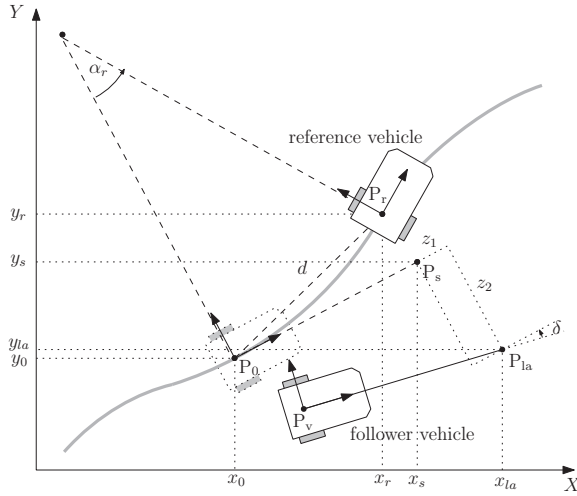
Figure 4.2: Trajectory tracking problem with extended look-ahead, where $|\mathrm{P_0P_r}| = |\mathrm{P_0P_s}| = d$.
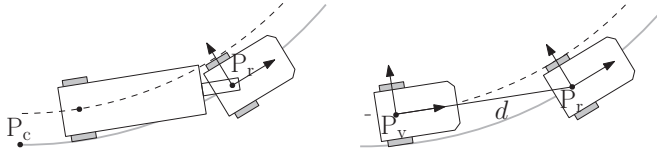
Figure 4.3: Analogy of cutting corner in a truck with trailer (left) and in a vehicle platooning (right). The solid gray line is a path traveled by the leader vehicle/truck, while the dashed black line is a path traveled by the follower vehicle/container.

Figure 4.4: Compensation of the cutting corner problem in a truck with container (left), and in a vehicle platooning (right).

defined by (x_s, y_s) and formulated such that the distance of $|P_v P_s|$ equals the look-ahead distance d (Figure 4.4(right)). In other words, the "reference-induced look-ahead point" P_s can be regarded as the position of where the look-ahead point P_{la} should be. With this new look-ahead point P_s, our control objective is then to stabili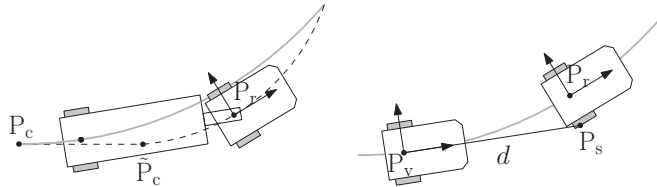ze at zero the tracking errors $(x_{la} - x_s, \, y_{la} - y_s)$, see Figure 4.2. Before we define the tracking error, first we shall derive the position of P_s geometrically based on the position of reference vehicle P_r.

4.2.2 Derivation of the reference-induced look-ahead point P_s

To derive the position of P_s, let us first denote P_0 as a moving origin point, where (x_0, y_0) is the position of P_0 in the Cartesian coordinate system, θ_0 is the angle with respect to the global X axis, and $|P_0 P_r| = d$. This point P_0 can also be considered as the position of where the follower vehicle P_v should be. Define α_r as the angle of the circular arc formed by P_0 and P_r, see Figure 4.5. To derive the angle α_r, let us denote κ_r as the curvature of the reference vehicle, which is defined as

$$\kappa_r := \frac{d\theta_r}{ds_r} = \left(\frac{d\theta_r}{dt}\right) / \left(\frac{ds_r}{dt}\right) = \frac{\omega_r}{v_r}, \tag{4.4}$$

where $v_r \neq 0$, θ_r is the orientation of the reference vehicle (which can also be considered as the angle of the tangent to the curve or path), and s_r is the curvilinear coordinate.

On a curved path, it can be observed that d characterizes the chord length of a circular segment formed by P_0 and P_r, and the angle α_r can be defined as

$$\alpha_r = 2 \arcsin\left(\frac{1}{2} d\kappa_r\right), \tag{4.5}$$

where $|\kappa_r| \leq \kappa^{\max} < 1/d$, and $\kappa^{\max}$ is a constant, maximum value of the curvature of the reference vehicle. It should be noted that α_r is defined as a function of the curvature κ_r of the reference vehicle, which fully determines the circular arc. Thus, it is not a circular arc through any two arbitrary points, but it is an arc through the position of P_r with a known curvature. By noting that (see Figure (4.5))

$$\sin\frac{\alpha_r}{2} = \frac{1}{2} d\kappa_r, \quad \cos\frac{\alpha_r}{2} = \frac{\sqrt{4 - d^2\kappa_r^2}}{2}, \tag{4.6}$$

the derivative of α_r with respect to time is obtained as

$$\dot{\alpha}_r = \frac{2d}{\sqrt{4 - d^2\kappa_r^2}} \dot{\kappa}_r. \tag{4.7}$$

Since the length of $P_0 P_r$ equals the desired inter-vehicle distance d, the position
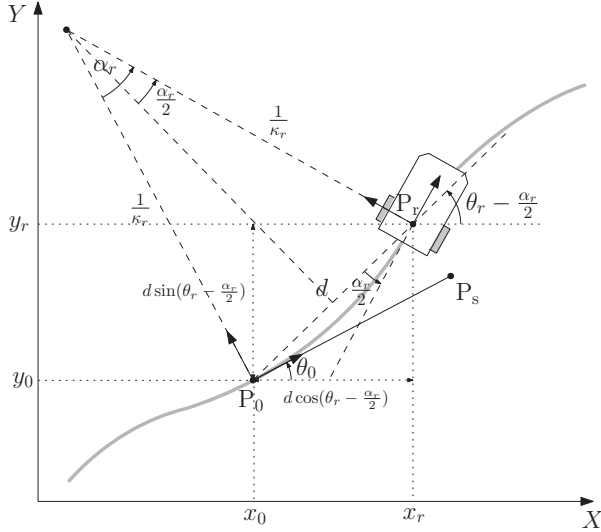
Figure 4.5: Projection of the reference-induced look-ahead point P_s.

of P_0 in a global Cartesian coordinate system can be defined as

$$x_0 = x_r - d \cos\left(\theta_r - \frac{\alpha_r}{2}\right) \tag{4.8a}$$

$$y_0 = y_r - d \sin\left(\theta_r - \frac{\alpha_r}{2}\right). \tag{4.8b}$$

First we define the rotation matrix as

$$R(\theta) = \begin{bmatrix} \cos\theta & -\sin\theta \\ \sin\theta & \cos\theta \end{bmatrix}. \tag{4.9}$$

From Figure 4.5, it can be observed that the coordinate of P_s can be obtained by a rotation of $-\frac{\alpha_r}{2}$ from the coordinate P_r around (x_0, y_0) as

$$\begin{bmatrix} x_s \\ y_s \end{bmatrix} = \begin{bmatrix} x_0 \\ y_0 \end{bmatrix} + R^T\left(\frac{\alpha_r}{2}\right)\begin{bmatrix} x_r - x_0 \\ y_r - y_0 \end{bmatrix}. \tag{4.10}$$

By substituting (4.8) into (4.10), applying the angle sum formula, and noting that $R(\theta_r - \alpha_r) = R(\theta_r)R^T(\alpha_r)$, we can eventually rewrite (4.10) as

$$\begin{bmatrix} x_s \\ y_s \end{bmatrix} = \begin{bmatrix} x_r \\ y_r \end{bmatrix} + d\begin{bmatrix} \cos\left(\theta_r - \alpha_r\right) - \cos\left(\theta_r - \frac{\alpha_r}{2}\right) \\ \sin\left(\theta_r - \alpha_r\right) - \sin\left(\theta_r - \frac{\alpha_r}{2}\right) \end{bmatrix}$$

$$\begin{bmatrix} x_s \\ y_s \end{bmatrix} = \begin{bmatrix} x_r \\ y_r \end{bmatrix} + dR\left(\theta_r - \alpha_r\right)\begin{bmatrix} 1 - \cos\frac{\alpha_r}{2} \\ -\sin\frac{\alpha_r}{2} \end{bmatrix}, \tag{4.11}$$

where $R(\theta_r - \alpha_r)$ as the rotation matrix through an angle $\theta_r - \alpha_r$. It can be observed that the position of the reference-induced look-ahead point P_s depends

on the position of the reference vehicle P_r, the angle α_r, and the angle $\theta_r - \alpha_r$, which in fact, is the desired orientation of the follower vehicle. On a straight path, $\alpha_r = 0$, thus P_s will be equal to P_r. In the following section, we define the error dynamics with the extended look-ahead approach.

4.2.3 Error dynamics and controller design of the extended look-ahead

We consider the trajectory tracking problem between P_{la} and P_s, expressed in the frame of the desired posture of the follower vehicle, with origin P_0. It should be noted that we define the relative kinematics with respect to this particular frame because we want to cancel the rotation matrix $R(\theta_r - \alpha_r)$ factor in (4.11). Hence, the error state components are defined as

$$\begin{bmatrix} z_1 \\ z_2 \end{bmatrix} = R^T (\theta_r - \alpha_r) \begin{bmatrix} x_{la} - x_s \\ y_{la} - y_s \end{bmatrix}, \tag{4.12}$$

with $x_{la} = x + d\cos\theta$, $y_{la} = y + d\sin\theta$, and $[x_s, y_s]^T$ as described in (4.11). It can be seen directly that $[z_1, z_2]^T$ denotes the relative position error. To obtain the error dynamics, we start first by differentiating $[z_1, z_2]^T$ with respect to time and taking (4.11) and (4.5) into account, resulting in

$$\begin{bmatrix} \dot{z}_1 \\ \dot{z}_2 \end{bmatrix} = (\omega_r - \dot{\alpha}_r) \begin{bmatrix} z_2 \\ -z_1 \end{bmatrix} + \begin{bmatrix} \cos\delta & -d\sin\delta \\ \sin\delta & d\cos\delta \end{bmatrix} \begin{bmatrix} v \\ \omega \end{bmatrix}$$
$$- \begin{bmatrix} \cos\alpha_r \\ \sin\alpha_r \end{bmatrix} v_r - \begin{bmatrix} \sin\frac{\alpha_r}{2} \\ 1 - \cos\frac{\alpha_r}{2} \end{bmatrix} d\omega_r + d\dot{\alpha}_r \begin{bmatrix} \frac{1}{2}\sin\frac{\alpha_r}{2} \\ 1 - \frac{1}{2}\cos\frac{\alpha_r}{2} \end{bmatrix}, \tag{4.13}$$

where

$$\delta = \theta - \theta_r + \alpha_r. \tag{4.14}$$

By applying the double angle formula on $\sin\alpha_r$ and $\cos\alpha_r$, substituting (4.6) and (4.4) into (4.13), we eventually obtain the error dynamics as

$$\begin{bmatrix} \dot{z}_1 \\ \dot{z}_2 \end{bmatrix} = (\omega_r - \dot{\alpha}_r) \begin{bmatrix} 0 & 1 \\ -1 & 0 \end{bmatrix} \begin{bmatrix} z_1 \\ z_2 \end{bmatrix} - \begin{bmatrix} v_r \\ d\omega_r \end{bmatrix}$$
$$+ \begin{bmatrix} \cos\delta & -d\sin\delta \\ \sin\delta & d\cos\delta \end{bmatrix} \begin{bmatrix} v \\ \omega \end{bmatrix} + \begin{bmatrix} h_{\kappa,1} \\ h_{\kappa,2} \end{bmatrix} \dot{\kappa}_r \tag{4.15}$$

with

$$h_{\kappa,1} = \frac{d^3\kappa_r}{2\sqrt{4 - d^2\kappa_r^2}}, \qquad h_{\kappa,2} = \frac{4d^2 - d^2\sqrt{4 - d^2\kappa_r^2}}{2\sqrt{4 - d^2\kappa_r^2}}. \tag{4.16}$$

If the follower vehicle converges to its desired position, θ converges to $\theta_r - \alpha_r$. Hence, δ in (4.14) is, in fact, the angular error of the follower vehicle. It can be observed that the error dynamics (4.15) consist of: a linear time-varying term multiplying $[z_1, z_2]^T$, since since ω_r and $\dot{\alpha}_r$ are external time-varying parameters;

and a nonlinear term multiplying inputs $[v, \omega]^T$, since δ is a state of the system. The objective now is to design control laws $[v, \omega]^T$ that asymptotically stabilize the system (4.15) at the origin, based on input-output feedback linearization in Khalil (2002, Chapter 13), Nijmeijer and van der Schaft (1990). Since the matrix multiplying $[v, \omega]^T$ is invertible, by choosing the control inputs

$$\begin{bmatrix} v \\ \omega \end{bmatrix} = \begin{bmatrix} \cos \delta & \sin \delta \\ -\frac{1}{d} \sin \delta & \frac{1}{d} \cos \delta \end{bmatrix} \begin{bmatrix} -k_1 z_1 + v_r - h_{\kappa,1} \dot{\kappa}_r \\ -k_2 z_2 + d\omega_r - h_{\kappa,2} \dot{\kappa}_r \end{bmatrix}, \tag{4.17}$$

where $d > 0$, we obtain the closed-loop system as follows

$$\begin{bmatrix} \dot{z}_1 \\ \dot{z}_2 \end{bmatrix} = \begin{bmatrix} -k_1 & \omega_r - \dot{\alpha}_r \\ -\omega_r + \dot{\alpha}_r & -k_2 \end{bmatrix} \begin{bmatrix} z_1 \\ z_2 \end{bmatrix}. \tag{4.18}$$

Noted that by the input-output feedback linearization, we obtain a closed-loop system which is a linear time-varying (LTV) system. Hence, the Lyapunov stability criterion is used to prove the stability of the closed-loop system. By the choice of $k_1, k_2 > 0$, it can be directly verified that the origin of subsystem $[z_1, z_2]^T$ is exponentially stable by the Lyapunov function $V_{12}(z_1, z_2) = \frac{1}{2} z_1^2 + \frac{1}{2} z_2^2$ such that

$$\dot{V}_{12}(z_1, z_2) = -k_1 z_1^2 - k_2 z_2^2 < 0, \tag{4.19}$$

for $(z_1, z_2) \neq 0$, which means that $\dot{V}_{12}$ is negative definite in (z_1, z_2). Since, however, the model (4.1) is of third order and the error dynamics (4.15) are of second order, first-order internal dynamics are present. The internal dynamics are the unobservable part of the system dynamics that comply with the desired output, while the zero dynamics is the internal dynamics of the system when the system output is kept at zero by the input (Khalil (2002)). It should be noted that analyzing the (global) stability of the internal dynamics has a more generic meaning than only analyzing the stability of the zero dynamics. Therefore, in the next section we analyze the stability of the internal dynamics.

4.2.4   Stability analysis of the internal dynamics

From Section 4.2.3, it has been shown that the control law (4.17) exponentially stabilizes the second-order error dynamics, which leaves us with the first-order internal dynamics since the original model (4.1) is of third order. The first obvious choice for the internal state would be δ, since δ resembles the orientation error between the actual and the desired orientation of the follower vehicle. However, in a steady state condition, which implies that $z_1 = z_2 = 0$ and $\dot{\kappa}_r = 0$, this choice leads to two equilibrium points $\delta = 0$ and $\delta = \arctan[(-2d\kappa_r)/(d^2\kappa_r^2 - 1)]$, where the physical interpretation of these points is depicted in Figure 4.6 (see Appendix B.1 for the derivation). The posture (x_1, y_1, θ_1) is the stable equilibrium point, and can be considered as the correct posture of where the follower vehicle should be. On the other hand, (x_2, y_2, θ_2) is the unstable equilibrium point, and depends on the curvature of the preceding vehicle. Due to the curvature-dependence of this unstable equilibrium point, we define z_3 such that the stable
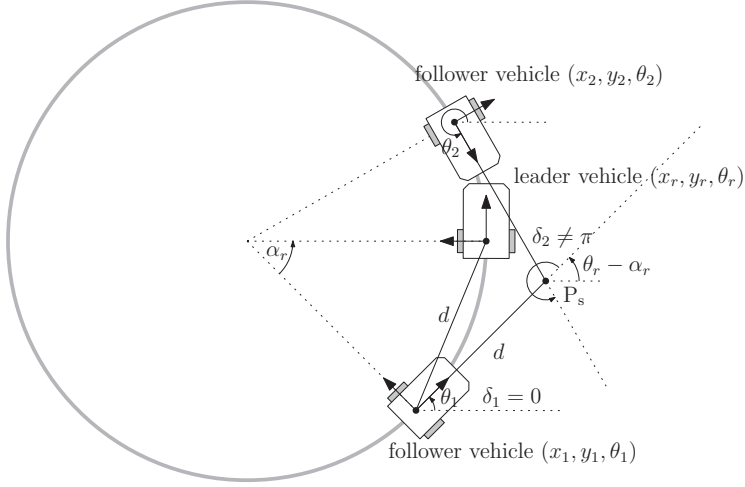
Figure 4.6: Posture of the follower vehicle, (x_1, y_1, θ_1) and (x_2, y_2, θ_2), on two equilibrium points. In the stable equilibrium point (x_1, y_1, θ_1), $\delta_1 = 0$; and in the unstable equilibrium point (x_2, y_2, θ_2), $\delta_2 \neq 0 \neq \pi$.
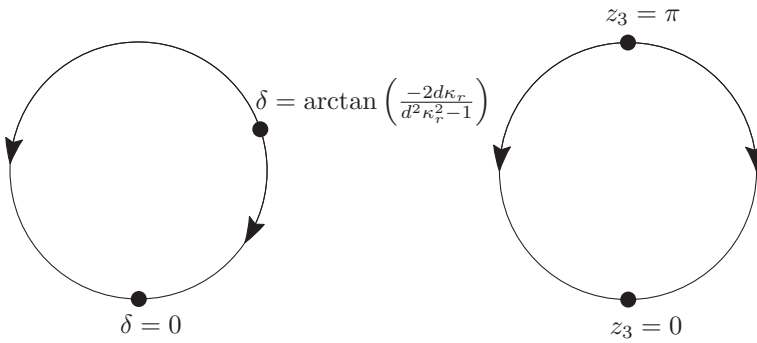
Figure 4.7: The mapping of the equilibrium points from δ (left) to z_3 (right). By this mapping, the stable equilibrium point is at $z_3 = 0$; and the unstable equilibrium point maps to $z_3 = \pi$.

equilibrium point corresponds with $z_3 = 0$ and the unstable equilibrium point with $z_3 = \pi$ (see Figure 4.7). To that end, we define

$$z_3 = \delta + \beta, \tag{4.20}$$

where the angle β is characterized by (see Appendix B.2 for the derivation)

$$\sin \beta = \frac{d\kappa_r \cos \delta - d\kappa_r}{\sqrt{d^2 \kappa_r^2 \left(1 - \cos \delta\right)^2 + \left(1 + d\kappa_r \sin \delta\right)^2}}, \tag{4.21a}$$

$$\cos \beta = \frac{1 + d\kappa_r \sin \delta}{\sqrt{d^2 \kappa_r^2 \left(1 - \cos \delta\right)^2 + \left(1 + d\kappa_r \sin \delta\right)^2}}. \tag{4.21b}$$

where $|\kappa_r| \leq \kappa_r^{\max} < 1/d$. Note that from (4.20) and straightforward application of the trigonometric rules for the sum of angles, we have

$$\sin z_3 = \frac{\sin \delta + d\kappa_r \left(1 - \cos \delta\right)}{\sqrt{d^2 \kappa_r^2 \left(1 - \cos \delta\right)^2 + \left(1 + d\kappa_r \sin \delta\right)^2}}, \tag{4.22a}$$

$$\cos z_3 = \frac{\cos \delta + d\kappa_r \sin \delta}{\sqrt{d^2 \kappa_r^2 \left(1 - \cos \delta\right)^2 + \left(1 + d\kappa_r \sin \delta\right)^2}}. \tag{4.22b}$$

Moreover, the derivative of β with respect to time follows from the inverse tangent function, derived from (4.21a) and (4.21b), yielding

$$\dot{\beta} = \frac{d\dot{\kappa}_r \cos \delta - d\dot{\kappa}_r}{d^2 \kappa_r^2 \left(1 - \cos \delta\right)^2 + \left(1 + d\kappa_r \sin \delta\right)^2}$$
$$- \left(\frac{d\kappa_r \sin \delta + d^2 \kappa_r^2 \left(1 - \cos \delta\right)}{d^2 \kappa_r^2 \left(1 - \cos \delta\right)^2 + \left(1 + d\kappa_r \sin \delta\right)^2} \right) \dot{\delta}. \tag{4.23}$$

Using (4.21), (4.22), (4.17), and noting the fact that $\dot{\delta} = \omega - \omega_r + \dot{\alpha}_r$, we obtain the derivative of z_3 with respect to time as

$$\dot{z}_3 = \frac{d\dot{\kappa}_r \cos \delta - d\dot{\kappa}_r}{d^2 \kappa_r^2 \left(1 - \cos \delta\right)^2 + \left(1 + d\kappa_r \sin \delta\right)^2}$$
$$+ \left(\frac{d^2 \kappa_r^2 \left(1 - \cos \delta\right) + d\kappa_r \sin \delta + 1}{d^2 \kappa_r^2 \left(1 - \cos \delta\right)^2 + \left(1 + d\kappa_r \sin \delta\right)^2} \right) \dot{\delta}$$
$$= f_3 \left(z \right), \tag{4.24}$$

where

$$f_3\left(z\right) = -\frac{\bar{v}_r}{d}\sin z_3 + \xi_r \tag{4.25}$$

$$\bar{v}_r = \frac{N}{\sqrt{\Delta}} v_r \tag{4.26}$$

$$\xi_r = \frac{N}{\Delta}\left(\frac{k_1\sin\delta}{d}z_1 - \frac{k_2\cos\delta}{d}z_2\right) + g_\kappa \dot{\kappa}_r \tag{4.27}$$

$$N = d^2\kappa_r^2\left(1 - \cos\delta\right) + d\kappa_r\sin\delta + 1 \tag{4.28}$$

$$\Delta = d^2\kappa_r^2\left(1 - \cos\delta\right)^2 + \left(1 + d\kappa_r\sin\delta\right)^2 \tag{4.29}$$

$$g_\kappa = \frac{N}{\Delta}f_r\left(\delta, d, \kappa_r\right) - \frac{d\left(1 - \cos\delta\right)}{\Delta} \tag{4.30}$$

$$f_r\left(\delta, d, \kappa_r\right) = \frac{4d}{2\sqrt{4 - d^2\kappa_r^2}} + \frac{d^2\kappa_r}{2\sqrt{4 - d^2\kappa_r^2}}\sin\delta$$
$$- \frac{4d - d\sqrt{4 - d^2\kappa_r^2}}{2\sqrt{4 - d^2\kappa_r^2}}\cos\delta, \tag{4.31}$$

$z = (z_1, z_2, z_3)$, $(N, \Delta) > 0$ (see (B.14) and (B.15) in Appendix B.3), and δ as in (4.14). It should be noted that (4.24) is a closed-loop system since the inputs (v, ω) have been taken into account. Thus, the overall closed-loop system is composed of (4.18) and (4.24), which is a third order system.

Remark 4.1. Note that since $|\kappa_r| \leq \kappa_r^{\max} < 1/d$, $\bar{v}_r$ is lower- and upper-bounded by

$$|v_r| \leq |\bar{v}_r| < \sqrt{2}\,|v_r|\,, \tag{4.32}$$

and $|\xi_r|$ is bounded by

$$|\xi_r| \leq \tfrac{2+\sqrt{2}}{d}k_1\,|z_1| + \tfrac{2+\sqrt{2}}{d}k_2\,|z_2| + \tfrac{7d}{9}\,|\dot{\kappa}_r|\,. \tag{4.33}$$

Proof of (4.32) and (4.33). See Appendix B.3. □

Using these bounds on $|\bar{v}_r|$ and $|\xi_r|$, asymptotic stability of the internal dynamics (4.24) can be concluded by the following proposition.

Proposition 4.1. *Consider the dynamics (4.24) where $\bar{v}_r$ and ξ_r are given in (4.26) and (4.27), respectively. Let $z_{12} = [z_1, z_2]^T$, and assume for all $t \geq 0$ that $0 < v_r^{\min} \leq v_r(t)$, $|\kappa_r(t)| \leq \kappa_r^{\max} < 1/d$, and $|\dot{\kappa}_r(t)| \leq K$, where $d, K \in \mathbb{R}^+$.*

1. For $\varepsilon > 0$, if

$$\|z_{12}(0)\| \leq \frac{v_r^{\min}\varepsilon}{\left(2 + \sqrt{2}\right)\sqrt{k_1^2 + k_2^2}}, \tag{4.34}$$

where $k_1, k_2 > 0$, then there exists t^* such that for $t \geq t^*$,

$$|\sin z_3(t)| \leq \tfrac{7d^2}{9v_r^{\min}}K + \varepsilon. \tag{4.35}$$

2. *Moreover, if additionally*

$$\lim_{t \to \infty} \dot{\kappa}_r(t) = 0, \tag{4.36}$$

   then $\lim_{t \to \infty} \sin z_3(t) = 0$.

3. *Finally, for* $0 < \varepsilon < \frac{3}{10}$, *if (4.34) holds,*

$$\cos z_3(0) \geq \sqrt{1 - \left(\frac{7}{18} - \frac{8}{27}\varepsilon\right)^2}, \tag{4.37}$$

   and

$$|\dot{\kappa}_r(t)| \leq K = \frac{v_r^{\min}}{d^2}\left(\frac{1}{2} - \frac{5}{3}\varepsilon\right), \tag{4.38}$$

   we have $v(t) \geq \varepsilon v_r^{\min} > 0$ *and* $\lim_{t \to \infty} z_3(t) = 0$, *rendering the internal dynamics (4.24) stable.*

Proof. See Appendix B.4.   □

Therefore, we can conclude that the internal dynamics (which correspond to the orientation of the vehicle) are stable under these conditions: the initial position error is not too large (bounded by (4.34)), the initial orientation error is bounded by (4.37), and the curvature derivative of the preceding vehicle is bounded by (4.38). Moreover, it is important to note that for a platoon with more than 2 vehicles, $v(t)$ will become the reference for the next vehicle. By Proposition 4.1(c), the requirement of $v(t) > 0$ is fulfilled for the initial condition $z_3(0)$ being bounded by (4.37) and $\dot{\kappa}_r(t)$ satisfying (4.38).

4.3   Orientation-error observer design

From the previous section, it has been proven that the proposed controller design (4.17) guarantees that all error states (z_1, z_2, z_3) converge to zero, under the assumption that all states of the kinematic model are available and measurable for control. Here, the relative position (z_1, z_2) can be obtained from the camera or lidar, the preceding vehicle states (v_r, ω_r) can be obtained through wireless communication with the preceding vehicle, κ_r can be determined from v_r and ω_r, $\dot{\kappa}_r$ can be approximated by the backward Euler method, and δ is determined from the relative orientation $\theta - \theta_r$ and α_r, which may be measured using the camera. It is assumed that the relative position (z_1, z_2) can be measured accurately, and there is no delay involved in the wireless communication. In practical situations, there is often a case where the orientation of vehicles (θ, θ_r, or both) are not available, or disturbed by noise due to inherent limitations of the vision system. To address this problem, a state feedback controller combined with an observer that estimates the orientation was designed in Jakubiak et al. (2002), Noijen et al. (2005). However, these approaches result in a combined observer-controller design which is different than the proposed tracking controller (4.17). Therefore, we adapt the observer designed in Jakubiak et al. (2002) by determining the orientation angle θ from the available states (z_1, z_2, v, ω) and design an observer such

that the estimated angle (denoted by $\hat{\theta}$) converges to the actual orientation angle θ.

Consider the kinematic model of the unicycle as given in (4.1), and the available outputs as $[x, y]^T$. We extend the dimension of the system (4.1) by defining new variables s and c as

$$s = \sin\theta, \qquad\qquad c = \cos\theta, \qquad\qquad (4.39)$$

which replace the orientation angle θ. As a result, we obtain the extended model of the unicycle as

$$\dot{x} = vc, \qquad\qquad \dot{y} = vs, \qquad\qquad (4.40a)$$
$$\dot{s} = \omega c, \qquad\qquad \dot{c} = -\omega s, \qquad\qquad (4.40b)$$

where $[x, y]^T$ are the available outputs, $[v, \omega]^T$ are inputs, s and c as defined in (4.39). It should be noted that the transformation from the three-dimensional system (4.1) to four-dimensional system (4.40) introduces a constraint of the form $s^2 + c^2 = 1$.

Based on (4.40), an observer for x, y, c, and s can be defined as follows

$$\dot{\hat{x}} = v\hat{c} + l_1\zeta_x \qquad\qquad (4.41a)$$
$$\dot{\hat{y}} = v\hat{s} + l_2\zeta_y \qquad\qquad (4.41b)$$
$$\dot{\hat{c}} = -\omega\hat{s} + l_3v\zeta_x \qquad\qquad (4.41c)$$
$$\dot{\hat{s}} = \omega\hat{c} + l_4v\zeta_y, \qquad\qquad (4.41d)$$

where $l_1, l_2, l_3, l_4 > 0$, and $\zeta_x = x - \hat{x}$, $\zeta_y = y - \hat{y}$, $\zeta_c = c - \hat{c}$, and $\zeta_s = s - \hat{s}$ are the observer errors. Thus, we obtain the following observer error dynamics

$$\dot{\zeta}_x = \dot{x} - \dot{\hat{x}} = v\zeta_c - l_1\zeta_x \qquad\qquad (4.42a)$$
$$\dot{\zeta}_y = \dot{y} - \dot{\hat{y}} = v\zeta_s - l_2\zeta_y \qquad\qquad (4.42b)$$
$$\dot{\zeta}_c = \dot{c} - \dot{\hat{c}} = -\omega\zeta_s - l_3v\zeta_x \qquad\qquad (4.42c)$$
$$\dot{\zeta}_s = \dot{s} - \dot{\hat{s}} = \omega\zeta_c - l_4v\zeta_y. \qquad\qquad (4.42d)$$

It can be observed directly that if (4.42) converges to zero, then the estimated states $(\hat{x}, \hat{y}, \hat{c}, \hat{s})$ converge to (x, y, c, s). To prove stability of (4.42), the following proposition can be used.

Proposition 4.2 (Jakubiak et al. (1999), Beumer (2017))**.** *Consider the dynamics (4.42) with $l_1, l_2, l_3, l_4 > 0$. If v, ω are bounded differentiable functions, $\dot{v}$ is bounded, and $0 < v_{\min} \leq v(t)$, then (4.42) is uniformly globally asymptotically stable (UGAS) at the origin.*

Proof. See Appendix B.5. □

Using Proposition 4.2, we have that the origin of (4.42) is uniformly globally asymptotically stable (UGAS) and $\zeta_x(t)$, $\zeta_y(t)$, $\zeta_c(t)$, $\zeta_s(t)$ converge to zero as $t \to \infty$, subject to the necessary and sufficient condition of $v(t) > 0$ for all t [see Proposition 4.1(c)]. It remains to prove the convergence of the estimated orientation angle to the actual orientation angle θ. Define the estimated orientation angle $\hat{\theta}$ as

$$\hat{\theta} := \operatorname{atan2}(\hat{s}, \hat{c}), \tag{4.43}$$

where $\hat{c}$ and $\hat{s}$ are generated by the observer (4.41). Note also that

$$\sin\hat{\theta} = \frac{\hat{s}}{\sqrt{\hat{c}^2 + \hat{s}^2}}, \qquad \cos\hat{\theta} = \frac{\hat{c}}{\sqrt{\hat{c}^2 + \hat{s}^2}}, \qquad \tan\hat{\theta} = \frac{\hat{s}}{\hat{c}}. \tag{4.44}$$

Let us define $\zeta_\theta = \tan(\theta - \hat{\theta})$. By noting that $\zeta_c = c - \hat{c}$, $\zeta_s = s - \hat{s}$, and using the fact that $\tan\theta = \sin\theta/\cos\theta$, we have

$$\begin{aligned}
\zeta_\theta &= \frac{\tan\theta - \tan\hat{\theta}}{1 + \tan\theta\tan\hat{\theta}} = \frac{\hat{c}\sin\theta - \hat{s}\cos\theta}{\hat{c}\cos\theta + \hat{s}\sin\theta} \\
&= \frac{(c - \zeta_c)\sin\theta - (s - \zeta_s)\cos\theta}{(c - \zeta_c)\cos\theta + (s - \zeta_s)\sin\theta} \\
&= \frac{\zeta_s\cos\theta - \zeta_c\sin\theta}{1 - \zeta_c\cos\theta - \zeta_s\sin\theta}.
\end{aligned} \tag{4.45}$$

Since $\zeta_c(t)$ and $\zeta_s(t)$ converge to zero, we have $\zeta_\theta(t)$ converge to zero as $t \to \infty$, which directly implies the convergence of $\hat{\theta}$ to θ for the initial estimated orientation error satisfying $|\theta(0) - \hat{\theta}(0)| < \pi/2$.

4.4 Simulations

In order to illustrate the effectiveness of the extended look-ahead controller and the observer, a number of simulations are performed. Additionally, the purpose of this simulation is to properly determine the control parameters for the experimental setup. First, we consider a scenario of 4 vehicles platoon, where all states (position and orientation) can be measured accurately and are not disturbed by noise. This allows us to investigate the optimal gains k_1 and k_2 and the effectiveness of the extended look-ahead controller against corner-cutting. Second, we consider a scenario of a 2 vehicles platoon where the second vehicle is controlled by extended look-ahead controller with the orientation-observer, in the presence and absence of noise. In this scenario, the performance of the observer is evaluated.

We consider a platoon of 4 vehicles, with the first vehicle controlled by the tracking controller of Jiang and Nijmeijer (1997) to track a predefined eight-shaped trajectory, while the other vehicles controlled by the extended look-ahead controller to track their respective preceding vehicle. It should be noted that the first vehicle can also be directly controlled (simulating a driving scenario where the first vehicle is driven by a human), or controlled by other trajectory-tracking (e.g.,
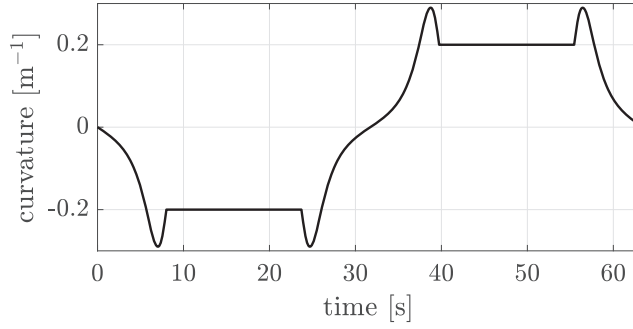
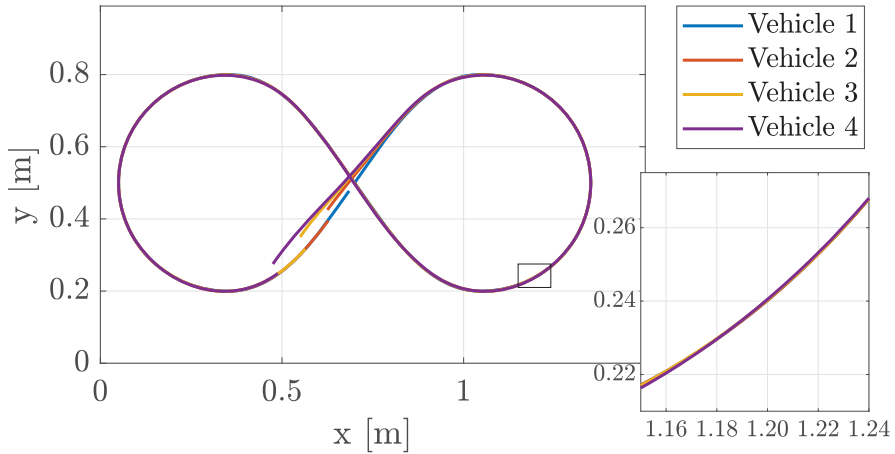Figure 4.8: Reference curvature for an eight-shaped path with $v = 0.06$ m/s.

Figure 4.9: Trajectory of 4-vehicles platoon tracking an eight-shaped path, with $k_1 = k_2 = 0.75$.
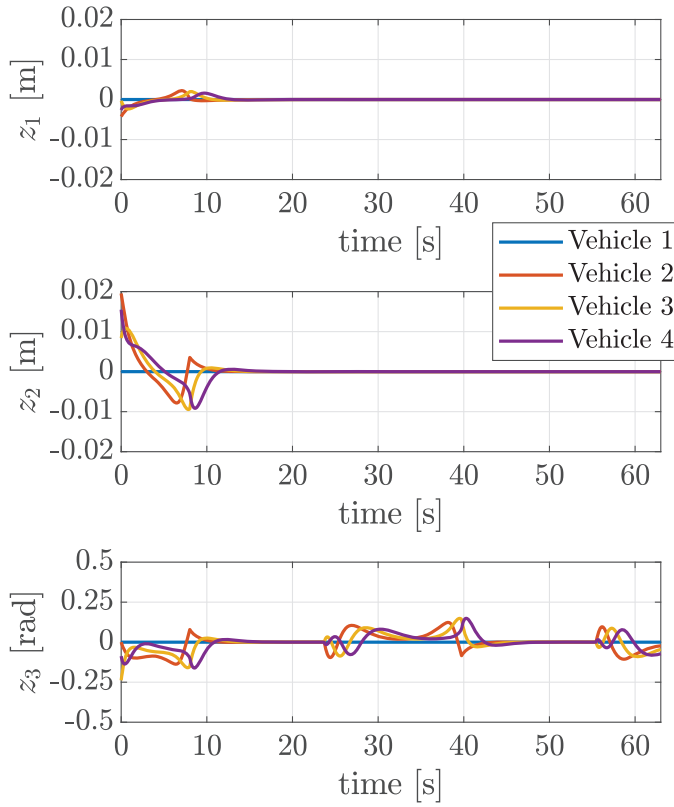
Figure 4.10: Errors of a platoon with the extended look-ahead controller on an eight-shaped path.

Kanayama et al. (1990)) or path-following controllers (e.g., Plaskonka (2015)). The eight-shaped trajectory is generated by two-half circles with the radius 0.3 m and quintic polynomial functions. The controller performance to track a circular trajectory (constant curvature) as in Bayuwindra et al. (2019b) is also performed, but the eight-shaped trajectory is chosen since it also represents a combination of constant and varying curvatures. The reference curvature of the eight-shaped path is given in Figure 4.8. The dimensions of the track are chosen in accordance with the experimental setup, which is presented in the next section. The first vehicle starts at initial position $(x, y) = (0.7, 0.5)$ m, maneuvering along the eight-shaped path. The other vehicles start at $(0.625, 0.425)$, $(0.55, 0.35)$, and $(0.475, 0.275)$ for vehicle 2, 3, and 4, respectively. All vehicles are initiated with $v = 0.06$ m/s and $\theta = 0.9707$ rad/s, and $d = 0.1$ m is chosen. The extended look-ahead controller gain is determined by an iterative manner and is equal for vehicle 2, 3, and 4. It should be noted that the choice for the proper gain is also determined by the available experimental arena and the reference trajectory. It is also worth noting that the higher gain value results in a faster convergence towards the desired path. However, the higher gain value also results in a more sensitive response to the curvature change. In practical situation, this is undesirable since a slight change in states measurement (e.g., due to noise, sensor inaccuracy) could result in an over compensation. The trajectory of all vehicles with $k_1 = k_2 = 0.75$ is shown in Figure 4.9. It can be observed that all vehicles in the platoon converges to the reference path and corners are not cut. This shows the advantage of our controller in comparison to the controller in Petrov (2009), where corners with $\dot{\kappa}_r \neq 0$ are still cut. From Figure 4.10, it can be observed that z_1 and z_2 converge to zero. On the other hand, the orientation error z_3 converges to zero if $\dot{\kappa}_r = 0$, which can be seen from $t = 11$ s until $t = 22$ s and from $t = 42$ s until $t = 55$ s. On the transition state when $\dot{\kappa}_r \neq 0$, z_3 is bounded given the condition that $\dot{\kappa}_r$ is small enough.

In the second scenario, we consider a platoon of 2 vehicles, with identical parameters as vehicle 1 and vehicle 2 in the previous simulation. A two-vehicles setting is used since we want to study the convergence of the estimated orientation to the true orientation of the follower vehicle. The first vehicle is controlled by the tracking controller of Jiang and Nijmeijer (1997), while the second vehicle is controlled by the extended look-ahead controller (4.17) with the observer (4.41). The initial condition of the observer states are set as $\hat{x}(0) = 0.625$, $\hat{y}(0) = 0.425$, and $\hat{\theta} = 0.8$ rad/s. It is assumed that the position can be measured accurately without any noise, while the orientation measurement is disturbed by a noise. The noise of the orientation sensor is simulated as a white noise with a power spectral density of 5×10^{-5}. For the observer gains, we select $l_1 = 10$, $l_2 = 10$, $l_3 = 1000$, and $l_4 = 1000$. First, we simulate the system without the observer, i.e., the control laws (4.17) are calculated using the orientation measured from the sensor with noise. Second, we simulate the system with the orientation-error observer, where the orientation is estimated based on the position sensor. We denote θ as the true orientation, $\hat{\theta}$ as the estimated orientation, and $\bar{\theta}$ as the orientation obtained from the sensor. The error plots of $\theta - \bar{\theta}$ (for the scenario without the observer)
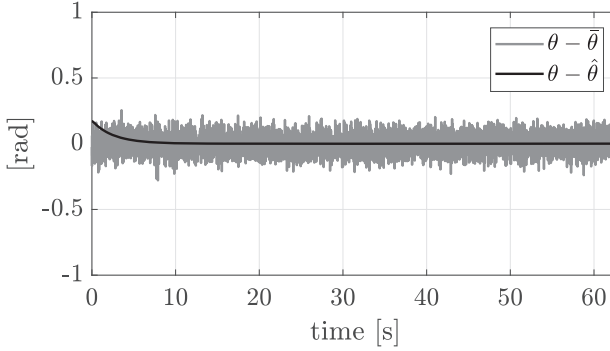
Figure 4.11: Errors of $\theta - \hat{\theta}$ and $\theta - \bar{\theta}$, where θ is the true orientation, $\hat{\theta}$ is the estimated orientation, and $\bar{\theta}$ is the orientation obtained from the sensor with noise.

and $\theta - \hat{\theta}$ (for the scenario with the observer) are depicted in Figure 4.11. It can be observed that for the scenario without the observer, the measured orientation (shown in gray line) is heavily disturbed by noise. On the other hand, the error $\theta - \hat{\theta}$ (shown in black line) is not disturbed by noise and converges to zero, which means that the estimated orientation $\hat{\theta}$ converges to the true orientation θ.

4.5   Experiments

In this section, we conduct an experiment to confirm the theoretical analyses and subsequent to the simulation results. This practical experiment is conducted also to provide an insight in how the parameters for our controller can be chosen to accommodate the slave controller in mobile robots. Furthermore, the purpose of this experiment is to verify the performance of the orientation-error observer in an experimental environment, where the orientation measurement is disturbed by noise due to inherent limitation of the sensor/vision system. The main components of this experimental setup are four E-pucks (Mondada and Bonani (2007)) a PC, and a camera, with identical setup as in Chapter 3.

In order to support comparison of the simulation results presented in the previous section, for this experiment we use the identical eight-shaped reference trajectory as in the simulation. In the first experiment, we use the extended look-ahead controller without the observer, thus, the orientation of the mobile robots are obtained directly from the camera. The objectives of the first experiment are to study the effectiveness of the extended look-ahead controller, compared to the theoretical results presented in the previous section, to verify the suitable gain for the experiment, and to study the behavior of the system under the presence of measurement noises. In the second experiment, we apply the observer to estimate the orientation of the mobile robots. The objective of this second experiment is to
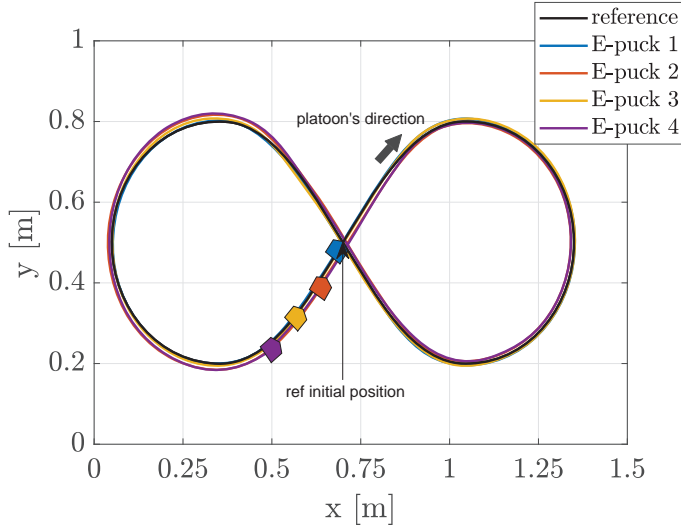
Figure 4.12: Trajectory of E-pucks with extended look-ahead controller, where the orientation is measured directly from the camera.

Figure 4.13: 2-norm of the position error from experiments incorporating extended look-ahead controller without observer.

study the effectiveness of the observer in practice, and to confirm the simulation results. All E-pucks are initiated with $v = 0.06$ m/s, with the controller gains $k_1 = k_2 = 0.75$ for both experiments, and with the observer gains $l_1 = 10$, $l_2 = 10$, $l_3 = 1000$, and $l_4 = 1000$ for the second experiment.

Figure 4.12 shows the trajectory of robots with the extended look-ahead controller. It can be observed that the trajectory of all follower robots converge to the reference trajectory. Clearly, this experiment shows that the extended look-ahead controller effectively avoids corner-cutting. However, it can be seen that

Figure 4.14: Trajectory of E-pucks with extended look-ahead controller and an orientation observer. The orientation of each E-puck is estimated from the position.
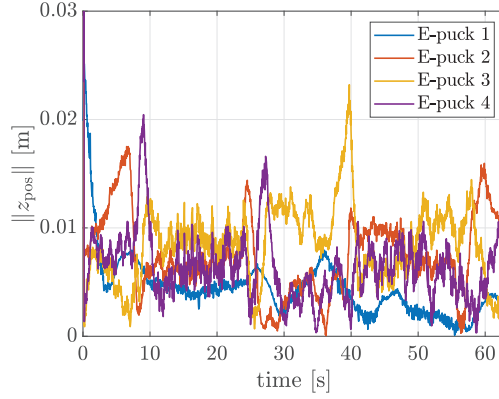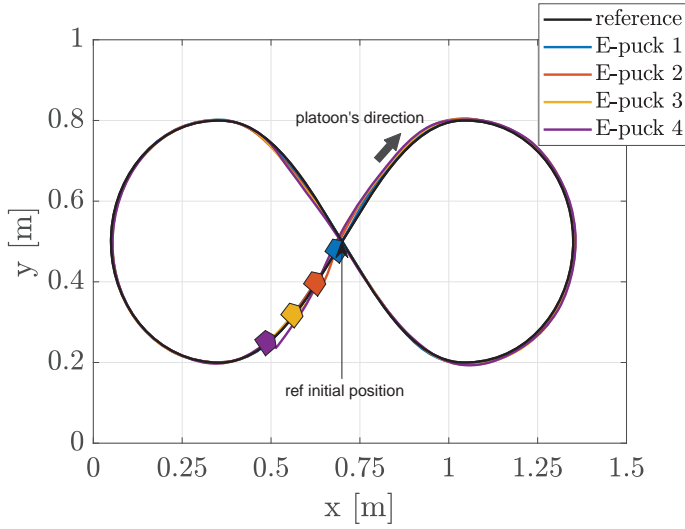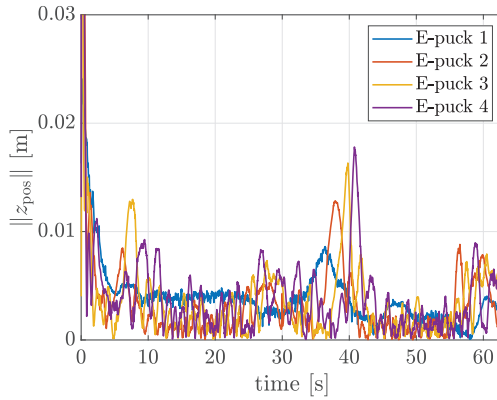

Figure 4.15: 2-norm of the position error from experiments incorporating extended look-ahead controller with observer.

the follower vehicles start to deviate on the left side of the eight-shaped path, due to the inaccuracy (due to noise, or displacement of the 2D marker) in the orientation measurement. The 2-norm of the position error, define as $\sqrt{z_1^2 + z_2^2}$, is depicted in Figure 4.13. It can be observed from this plot that E-puck 3 has the largest deviation, peaking at $t = 40$ s. To address this problem, the orientation-error observer is integrated to the extended-look-ahead controller in the second experiment. In Figure 4.14, the trajectory of all robots with the extended look-ahead controller and orientation-error observer is shown. It can be seen directly that the tracking accuracy of all follower robots is improved, thus showing the effectiveness of the orientation-error observer. From Figure 4.15, where the 2-norm of the position error is depicted, it can also be verified that the observer reduces the deviation caused by the inaccuracy of the orientation measurement. We may also notice some measurement noises on the position measurement, but they are small enough (less than 0.02 m) and can be safely neglected.

4.6   Conclusions

This chapter presents a novel extended look-ahead controller in vehicle platooning. The look-ahead target point is extended to a virtual point induced from the position and the curvature of the reference vehicle, thus ensuring a better tracking performance at cornering, preventing corner-cutting behavior. A stability result on the internal dynamics is presented, showing that the closed-loop system is stable under the given bound of the reference curvature and the initial relative position and orientation of the vehicles. The simulation results show that the proposed approach improves the tracking performance at cornering, ensuring that the corners are not cut. To address the orientation measurement noise in the experiment, an orientation-error observer is also designed. The effectiveness of the integrated extended look-ahead controller and orientation-error observer is further validated by means of experiment with a platoon consisting of four E-pucks. The experimental results confirm that the application of the extended look-ahead controller in vehicle platooning compensates for corner-cutting, and also confirm that the observer reduces the noise presents in the orientation measurement. The continuation of this chapter is to extend the approach to the single-track model, as an important step towards the application of our controller in a real vehicle. To adapt our controller to a single-track dynamic model with tire forces, we can design a slave controller that controls acceleration or speed, internally compensating for the vehicle mass. The stability of the real vehicle can be guaranteed by other controllers (Electronic Stability Control (ESC), or Anti-Lock Braking System (ABS), for instance), and our controller can be used in conjunction with those other controllers. In conclusion, the application of our controller to the real vehicle may poses additional conditions, but is feasible.

Application of the extended look-ahead controller to a single-track vehicle platoon

5.1 Introduction

In the previous chapters, the corner-cutting problem in a unicycle platoon is solved by the extended look-ahead controllers, where a "reference-induced" virtual vehicle is used as a look-ahead target for the following vehicle. Chapter 3 explored the problem by decomposing the inter-vehicle distance error in global coordinates, and the extended look-ahead controller (hereafter referred to as the global extended look-ahead controller) is designed to regulate that inter-vehicle distance error to zero. Although the global extended look-ahead controller solves the corner-cutting problem, it needs an accurate global position measurement of each vehicle, which is not always available in a commercial vehicle. To this end, Chapter 4 extended the exploration to a case where the relative kinematics are defined with respect to a vehicle-fixed frame, and the controller (hereafter referred to as the local extended look-ahead controller) is designed to regulate the inter-vehicle distance error to zero, while also compensating the corner-cutting. However, for a vehicle with a large acceleration, the kinematic model is no longer valid since the lateral forces generated by the tires affect the longitudinal and lateral motion of a vehicle (Rajamani (2012)). Therefore, in this chapter, the lateral and longitudinal motion of a vehicle is described using a dynamic single-track model, where the lateral forces generated by tires are taken into account.

Due to the effect of lateral forces generated by the tires in a dynamic single-track model (hereafter referred to as the single-track model), the extended look-ahead controllers developed for a unicycle platoon in the previous chapters cannot directly be applied to a platoon of vehicles modeled by a single-track model. To

be able to adapt the extended look-ahead controllers, first a control point of a single-track model, i.e., the point to which the unicycle controller outputs apply, is chosen. Secondly, the unicycle controller outputs have to be transformed to the inputs of the single-track model. The transformation is implemented using input inversion, which was investigated first in Silverman (1969), and later extended to a certain class of nonlinear systems in Khalil (2002) and Isidori (1995). Due to the nonlinearity of the single-track vehicle model, the inverse cannot be obtained analytically. Consequently, several other methods are taken into account, being a numerical approach, a first-, and a second-order Taylor approximation.

The outline of this chapter is as follows. Section 5.2 first provides an overview of the single-track vehicle model. Section 5.3 derives the input inversion for the center of gravity as a control point. In this section, the tracking performance and the computation time of a numerical approach, first-, and second-order Taylor approximation are also compared. Section 5.4 and Section 5.5 derive the input inversion for the rear axle center and front axle center, respectively, as control points. These control points are chosen to demonstrate the flexibility of the adopted approach. Finally, Section 5.6 summarizes the main conclusions.

5.2 Dynamic single-track vehicle model

Consider the single-track vehicle model (Attia et al. (2012), Rajamani (2012)), which is commonly used to model the lateral and longitudinal dynamics of a vehicle under normal driving conditions. The dynamic single-track model is given by

$$\dot{v}_x = \frac{1}{m} \left(F_{lf} \cos \delta - F_{cf} \sin \delta + F_{lr} \right) + v_y \dot{\psi} \tag{5.1a}$$

$$\dot{v}_y = \frac{1}{m} \left(F_{lf} \sin \delta + F_{cf} \cos \delta + F_{cr} \right) - v_x \dot{\psi} \tag{5.1b}$$

$$\ddot{\psi} = \frac{1}{I} \left(l_f F_{lf} \sin \delta + l_f F_{cf} \cos \delta - l_r F_{cr} \right), \tag{5.1c}$$

where v_x, v_y, and $\dot{\psi}$ denote the longitudinal, lateral, and yaw velocity, respectively. Furthermore, m is the mass of the vehicle, I is the moment of inertia, l_f is the distance between the front tires and the center of gravity, and l_r is the distance between the rear tires and the center of gravity. The longitudinal forces which act on the tire direction are F_{lf}, F_{lr}, and the cornering forces are F_{cf}, F_{cr}, at the front and rear tire, respectively. The steering angle of the front wheel is denoted by δ, which acts as the input to the system. The cornering forces F_{cf} and F_{cr} are generated by the tires, and depend on the lateral tire slip angle α_f and α_r of the respective tire. From Figure 5.1, the lateral slip angles at the front and rear tires
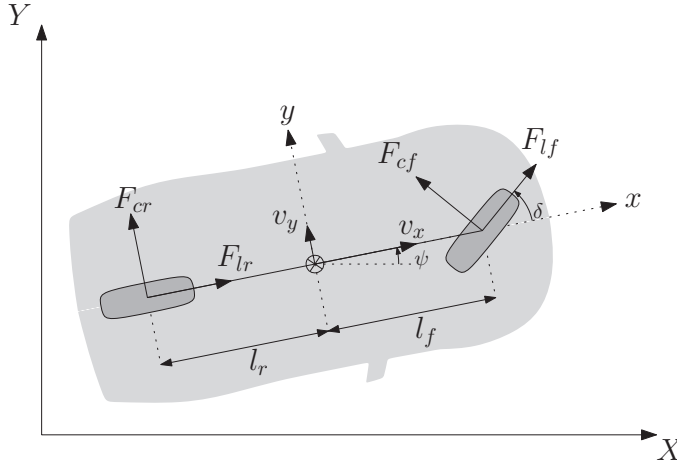
Figure 5.1: The single-track model.

are defined as

$$\alpha_f = \delta - \arctan\left(\frac{v_{yf}}{v_{xf}}\right) = \delta - \arctan\left(\frac{v_y + l_f\dot{\psi}}{v_x}\right) \tag{5.2a}$$

$$\alpha_r = -\arctan\left(\frac{v_{yr}}{v_{xr}}\right) = -\arctan\left(\frac{v_y - l_r\dot{\psi}}{v_x}\right), \tag{5.2b}$$

where v_{xj} and v_{yj}, $j \in \{f, r\}$, denote the longitudinal and lateral velocity components of either front or rear wheel, respectively. The mapping from α_j to F_{cj}, with $j \in \{f, r\}$, depends on the tire model and can vary in complexity depending on the road condition and required accuracy. In vehicle platooning, regular motorway driving conditions, a low longitudinal acceleration and small slip angles α_j, $j \in \{f, r\}$, are considered. Thus, the linear tire model, where the cornering forces depend proportionally on their respective slip angles, can be deployed (Rajamani and Zhu (2002)). In their linear regime, the cornering forces can be expressed as

$$F_{cf} = C_{\alpha f}\alpha_f \tag{5.3a}$$

$$F_{cr} = C_{\alpha r}\alpha_r, \tag{5.3b}$$

where $C_{\alpha j}$, $j \in \{f, r\}$, denote the cornering stiffness coefficient of the respective tire. The inputs of the single-track model are the longitudinal forces F_{lf}, F_{lr}, and the steering angle δ. A front-wheel drive vehicle is considered, where F_{lf} is the traction force of the engine and $F_{lr} = 0$. Thus, the objective of the vehicle platooning is to design the inputs (F_{lf}, δ) such that the vehicle follows its preceding vehicle at a desired distance.

In previous chapters, the objective of vehicle following is fulfilled by designing the inputs (a_u, ω_u) or (v_u, ω_u) for the unicycle system, where a_u is the longitudinal acceleration input, v_u is the longitudinal velocity input, and ω_u is the yaw rate

input, such that a desired inter-vehicle distance is achieved. The spacing errors (for both longitudinal and lateral distances) between the preceding and the following vehicle are defined as a difference between the actual inter-vehicle distance and a desired distance. In two-dimensional space, the spacing errors can either be decomposed in global Cartesian coordinates (see Chapter 3), or in local coordinates, where the relative kinematics can be defined with respect to a particular frame, e.g., a moving vehicle-fixed frame (see Chapter 4). The results of these controller outputs for a unicycle can be viewed as the desired motion for a control point, that regulates the velocity and orientation of that point. By choosing any control point of the single-track model, the controller outputs for a unicycle can in fact be extended/adapted as desired values for that particular control point. This control point can be chosen arbitrarily, for instance as: (1) the center of gravity, (2) the rear axle center, or (3) the front axle center. The actual inputs of the single-track model (F_{lf}, δ) then can be computed based on the outputs generated by the unicycle controller through the input inversion, which also depends on the chosen control point. It should be noted that obtaining the inverse of a nonlinear model is generally not straightforward, and a numerical approach or an approximation may have to be adopted. Therefore, in the next sections, the input inversions of the three above mentioned control points of the single-track model are studied.

5.3 Center of gravity as a control point

In this section, the center of gravity of a single-track model (5.1) is chosen as a control point, after which the outputs in the form of longitudinal acceleration and yaw rate are defined. It is then shown that due to the choice of these outputs, the algebraic model is obtained and the input inversion can be applied.

5.3.1 Input inversion

The chassis kinematic model at the center of gravity of a single-track model in a Cartesian coordinate frame is given by

$$\dot{X} = v_x \cos\psi - v_y \sin\psi \tag{5.4a}$$

$$\dot{Y} = v_x \sin\psi + v_y \cos\psi, \tag{5.4b}$$

where (X, Y) are the Cartesian coordinates of the center of gravity (see Figure 5.2), and (x, y, ψ) dynamics are as described in (5.1). Let v be the velocity of the center of gravity, based on $\dot{X}$ and $\dot{Y}$, and θ be the angle between the direction of v and the Cartesian X-axis, given by

$$v = \sqrt{\dot{X}^2 + \dot{Y}^2} = \sqrt{v_x^2 + v_y^2} \tag{5.5}$$

$$\theta = \arctan\left(\frac{\dot{Y}}{\dot{X}}\right) = \arctan\left(\frac{v_x \sin\psi + v_y \cos\psi}{v_x \cos\psi - v_y \sin\psi}\right), \tag{5.6}$$
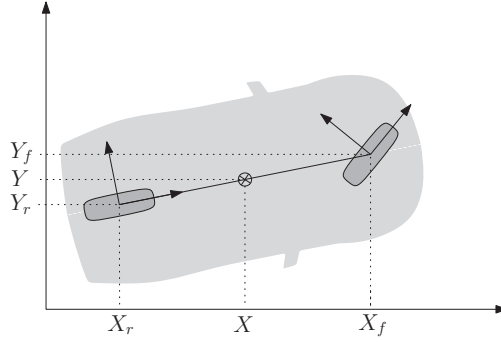
Figure 5.2: The single-track model with different control points: the center of gravity (X, Y), the rear axle center (X_r, Y_r), and the front axle center (X_f, Y_f).

where (5.4) is used. The longitudinal acceleration and the yaw rate of this point can be obtained by differentiating (5.5) and (5.6) with respect to time, resulting in

$$\dot{v} = \frac{v_x \dot{v}_x + v_y \dot{v}_y}{\sqrt{v_x^2 + v_y^2}} = a, \qquad\qquad \dot{\theta} = \frac{v_x \dot{v}_y - \dot{v}_x v_y}{v_x^2 + v_y^2} + \dot{\psi} = \omega, \qquad (5.7)$$

where it is assumed that $\sqrt{v_x^2 + v_y^2} = v \neq 0$, and the outputs are defined as (a, ω). With these derivations, the center of gravity of the single-track model is viewed as a unicycle with a velocity v and an orientation θ with respect to the global X-axis. The Cartesian coordinates of this point are given by (X, Y) and the inputs are given as the longitudinal acceleration a and the yaw rate ω. Therefore, any control inputs of longitudinal acceleration and yaw rate that are designed for a unicycle can be applied directly to (5.7).

Setting $(a, \omega) = (a_u, \omega_u)$, where (a_u, ω_u) can be any arbitrary control law developed for a unicycle, and applying it to (5.7) yields

$$\begin{bmatrix} a_u \\ \omega_u \end{bmatrix} = \frac{1}{v} \begin{bmatrix} v_x & v_y \\ -\frac{1}{v} v_y & \frac{1}{v} v_x \end{bmatrix} \begin{bmatrix} \dot{v}_x \\ \dot{v}_y \end{bmatrix} + \begin{bmatrix} 0 \\ \dot{\psi} \end{bmatrix}, \qquad (5.8)$$

with v as in (5.5). The actual inputs (F_{lf}, δ) of a front-wheel drive single-track model can be obtained by substituting (5.1a), (5.1b) into (5.8), and taking (5.2), (5.3) into account, eventually resulting in the inverse as

$$\begin{bmatrix} \cos\delta & -\sin\delta \\ \sin\delta & \cos\delta \end{bmatrix} \begin{bmatrix} F_{lf} \\ C_{\alpha f}\left(\delta - \sigma_f\right) \end{bmatrix} = \begin{bmatrix} \zeta_1 \\ \zeta_2 \end{bmatrix}, \qquad (5.9)$$

where

$$\zeta_1 := \frac{m}{v}v_x a_u - m v_y \omega_u \tag{5.10a}$$

$$\zeta_2 := \frac{m}{v}v_y a_u + m v_x \omega_u + C_{\alpha r}\arctan\left(\frac{v_y - l_r\dot{\psi}}{v_x}\right) \tag{5.10b}$$

$$\sigma_f := \arctan\left(\frac{v_y + l_f\dot{\psi}}{v_x}\right). \tag{5.10c}$$

Due to the multiplication terms $\delta\sin\delta$ and $\delta\cos\delta$, the solution (F_{lf}, δ) can not be determined analytically, but it can be determined numerically or by approximations, e.g., using Taylor series. The Taylor series is obtained by first multiplying both sides of (5.9) with the inverse of the first matrix on the left hand side resulting in

$$\begin{bmatrix} F_{lf} \\ C_{\alpha f}(\delta - \sigma_f) \end{bmatrix} = \begin{bmatrix} \cos\delta & \sin\delta \\ -\sin\delta & \cos\delta \end{bmatrix}\begin{bmatrix} \zeta_1 \\ \zeta_2 \end{bmatrix}. \tag{5.11}$$

From the first row of (5.11), the longitudinal force input F_{lf} of the single-track model is obtained as

$$F_{lf} = \zeta_1\cos\delta + \zeta_2\sin\delta, \tag{5.12}$$

where δ is the steering angle input and is yet to be determined. To determine δ, let $f(\delta, v_x, v_y, \dot{\psi}, a_u, \omega_u)$ be the difference between the left and right hand side of the second row of (5.11), as follows

$$f\left(\delta, v_x, v_y, \dot{\psi}, a_u, \omega_u\right) = C_{\alpha f}\delta - C_{\alpha f}\sigma_f + \zeta_1\sin\delta - \zeta_2\cos\delta, \tag{5.13}$$

and the solution of $f(\delta, \cdot) = 0$ for δ can be approximately determined by Taylor series approximation of (5.13) around $\delta = 0$. It should be noted that due to the physical limitation of a vehicle, the steering angle δ is relatively small and always bounded. At higher speed maneuvers, the steering angle is smaller when compared to lower speed maneuvers. Moreover, normal driving conditions and moderate speed are always assumed in vehicle platooning, with no special maneuvers (e.g., parking, stopping, or turning back) involved. Therefore, the steering angle δ is relatively small and the first- or the second-order Taylor expansion is expected to be sufficiently accurate to approximate the function $f(\delta, \cdot)$. The accuracy of both Taylor approximations against varying yaw rate (thus, the trajectory radius) are further investigated in the next part of this section.

The first-order Taylor series of $f(\delta, \cdot)$ around $\delta = 0$ is given by

$$f(\delta, \cdot) \approx \delta\left(C_{\alpha f} + \zeta_1\right) - C_{\alpha f}\sigma_f - \zeta_2, \tag{5.14}$$

thus, $f(\delta, \cdot) = 0$ yields

$$\delta_1 = \frac{C_{\alpha f}\sigma_f + \zeta_2}{C_{\alpha f} + \zeta_1}. \tag{5.15}$$

Table 5.1: Vehicle's parameters

Parameter	Value	Parameter	Value
$l_{f,i}$	1.2 m	I_i	2875 mN/s^2
$l_{r,i}$	1.6 m	$C_{\alpha f,i}$	20,000 N/rad
m_i	1575 kg	$C_{\alpha r,i}$	33,000 N/rad

It should be noted that (5.15) equals the first iteration step of the Newton-Raphson method of the function (5.13) for $f(\delta, \cdot) = 0$ with an initial guess of $\delta_0 = 0$, which is obtained as follows:

$$\delta_1 = \delta_0 - \frac{f(\delta_0)}{f'(\delta_0)} = \frac{C_{\alpha f}\sigma_f + \zeta_2}{C_{\alpha f} + \zeta_1}. \tag{5.16}$$

On the other hand, the second-order Taylor series of $f(\delta, \cdot)$ around $\delta = 0$ is given by

$$f(\delta, \cdot) \approx \delta\left(C_{\alpha f} + \zeta_1\right) - C_{\alpha f}\sigma_f - \zeta_2 + \frac{1}{2}\zeta_2\delta^2. \tag{5.17}$$

Thus, $f(\delta, \cdot) = 0$ yields

$$\delta_2 = \frac{-\left(C_{\alpha f} + \zeta_1\right) \pm \sqrt{\left(C_{\alpha f} + \zeta_1\right)^2 + 2\zeta_2\left(C_{\alpha f}\sigma_f + \zeta_2\right)}}{\zeta_2}. \tag{5.18}$$

For a case where the yaw rate ω_u and the acceleration a_u are zero, i.e., the vehicle drives on a straight path with constant velocity, it is desirable to have a steering angle equal to zero. By substituting $\omega_u = 0$ and $a_u = 0$ to (5.18), the condition of $\delta_2 = 0$ is fulfilled by the root with positive sign. Hence, the root with a positive sign is chosen.

To illustrate how well the first- and second-order Taylor approximation fit the real value of δ obtained using a numerical approach, a numerical study is conducted. An arbitrary time instance $t = \tau$, where $v_x(\tau) = 10$ m/s, $v_y(\tau) = 0$ m/s, $\dot{\psi}(\tau) = 0$ is chosen, with the vehicle's parameters as in Table 5.1. The iterations are performed for varying ω_u and a_u, where ω_u is given in the interval $[-3, 3]$ with 0.05 increment and $a_u = \{-5, 0, 5\}$. To find the solution of $f(\delta, \cdot) = 0$ numerically, the function `fzero` in MATLAB® is used. This function is based on Dekker's algorithm, which uses a combination of bisection, secant and inverse quadratic interpolation methods (Brent (1973)). The result of this iteration is then compared with the approximated δ_1 and δ_2, which are obtained using first and second-order Taylor series, respectively.

A comparison between the numerical approach, the first- and the second-order Taylor series, for several values of ω_u and a_u is presented in Figure 5.3. For a small yaw rate, the first-order Taylor series provide an adequate approximation of the steering angle δ. The accuracy of the first-order Taylor approximation depends on the desired yaw rate of the vehicle. Under a constant speed of 10 m/s
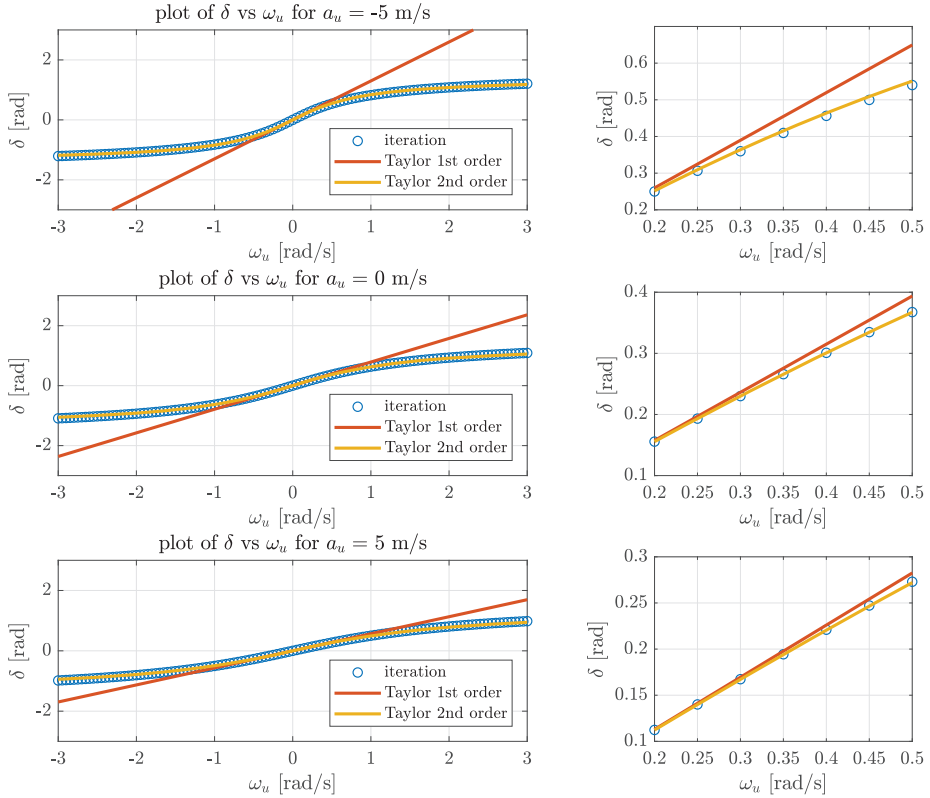
Figure 5.3: Plots of δ against varying yaw rate ω_u and longitudinal acceleration a_u (left). Zooming in to $\omega_u = [0.2, 0.5]$ shows the accuracy of the both first- and second-order Taylor approximations.

(=36 km/h), the first-order Taylor approximation is accurate for the yaw rate $|\omega_u| \leq 0.25$ rad/s (as shown in Figure 5.3(right)), which corresponds to a circular trajectory with a diameter bigger than or equal to 80 m. Thus, it can be concluded that the first-order Taylor is good enough to track a circular trajectory with a minimum diameter of 80 m when driving with a speed of 36 km/h. It should be noted that by using the relation between the velocity and yaw rate of the vehicle, the minimum diameter of the trajectory of which the first-order Taylor approximation is good enough can be roughly estimated for any arbitrary constant speed. On the other hand, it is clearly shown that the second-order Taylor series yields a better approximation to the real value of δ for varying yaw rate than the first-order Taylor series. Although the numerical approach gives the exact solution of δ, it should be noted that its computation time can be relatively slow, and can result in a delayed steering response in a vehicle platooning. Therefore, in the next section, the computation time of the numerical approach, the first- and second-order Taylor series, using the extended look-ahead controller (3.35) that is designed in Chapter 3, are studied.

5.3.2 Global extended look-ahead controller

Using the input inversion as described in the previous section, the control point of the single-track model is now viewed as a unicycle. Thus, controllers that were previously designed for the unicycle can be adapted for the center of gravity control point of a single-track model. Consider a platoon of $m \in \mathbb{N}$ vehicles, with $S_m = \{i \in \mathbb{N} \mid 1 \leq i \leq m\}$ denoting the set of all vehicles in the platoon, and denote (X_i, Y_i) as the Cartesian coordinates and θ_i as the orientation of the center of gravity of vehicle i. The actual inputs, longitudinal force $F_{lf,i}$ and the steering angle δ_i, can be obtained through the input inversion explained in the previous section. To prevent corner-cutting, the extended look-ahead controller in a global coordinate frame (see Chapter 3) with a velocity-dependent desired distance, is considered. In this approach, a look-ahead point attached to the follower vehicle is defined as P_i^{la} and a "reference-induced" look-ahead point P_{i-1}^s is defined as the new tracking point objective, and the control objective is to regulate the acceleration and the yaw rate (a_i, ω_i) to stabilize the position error between P_i^{la} and P_{i-1}^s, see Figure 5.4. To this extent, the controller (3.35) that has been designed in Chapter 3 is used, and the inverse is applied to (a_i, ω_i) such that the actual inputs of the single-track model $(F_{lf,i}, \delta_i)$ are obtained. It should be noted that by using this global extended look-ahead controller, the assumption of the nonzero velocity that was made for the inverse in (5.7) is fulfilled by Proposition 3.2.

Due to the nonlinearity of the single-track model, the input inversion can be obtained by a numerical approach, first-order Taylor, or second-order Taylor approximation. The simulation for a platoon of four vehicles is performed such that the performance and the computation time of each method can be compared. To depict a real platooning condition, a path combination of a straight road and a roundabout is chosen. The dimensions for a two-lane roundabout in the Nether-

Figure 5.4: Trajectory tracking problem with extended look-ahead for the center of gravity control point.

Table 5.2: Dimension for two-lane roundabout in the Netherlands (Royal Haskoning (2009)) and the United States (Federal Highway Administration (2000))

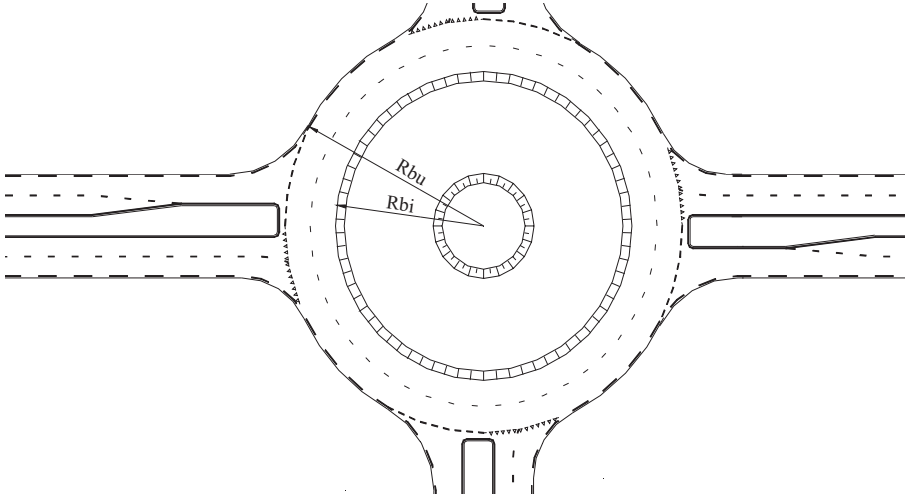| Design element	Netherlands		United States	
	Minimum	Maximum	Minimum	Maximum
Outer circle radius (Rbu)	20 m	38 m	22.5 m	30 m
Inner circle radius (Rbi)	10 m	30 m	12.7 m	26.3 m

Figure 5.5: Design parameters of a two-lane roundabout (source Royal Haskoning (2009)).

lands and the United States are given in Table. 5.2. The recommended speed of the vehicle entering the roundabout is approximately 38 km/h in the Netherlands (Royal Haskoning (2009)), and less than 50 km/h in the United States (Federal Highway Administration (2000)).

The first vehicle in the platoon is directly controlled (simulating a driving scenario when the first vehicle is driven by a human), maneuvering on a straight path along the X-axis with a constant initial velocity $10\,\text{m/s} = 36\,\text{km/h}$. It should be noted that the first vehicle is also modeled as a single-track model (5.1), where the inputs are given in (F_{lf}, δ). The first vehicle follows a straight line for 4 s, after which it maneuvers into a circular trajectory with a curvature of $0.04\,\text{m}^{-1}$ (which is equal to a roundabout with a 50 m diameter), compliant with the standards in the Netherlands or the United States. Hence, the nominal yaw rate on the circular trajectory equals 0.4 rad/s. The initial global positions $(X_i(0), Y_i(0))$ are chosen as $(0,0)$, $(-8,2)$, $(-16,4)$, and $(-24,6)$ for vehicle 1, 2, 3, and 4, respectively. The initial heading angle $\psi_i(0) = 0$ is chosen for all vehicles. Parameters for all vehicles are given in Table 5.3, and simulations are conducted for three methods of inversion: first-order Taylor, second-order Taylor, and the numerical approach.

Table 5.3: Parameters for vehicle

Parameter	Value	Parameter	Value
$l_{f,i}$	1.2 m	I_i	2875 mN/s^2
$l_{r,i}$	1.6 m	r_i	6.8 m
m_i	1575 kg	h_i	0.1 s
$C_{\alpha f,i}$	20,000 N/rad	$k_{1,i}$	2
$C_{\alpha r,i}$	33,000 N/rad	$k_{2,i}$	2

Table 5.4: Performance time results

	Total process time (2301 samples)	Average process time per sample
First-order Taylor expansion	2.4477 s	1.1 ms
Second-order Taylor expansion	2.6756 s	1.2 ms
Numerical approach, $\delta_{\text{init}}(k) = 0$	4.1472 s	1.8 ms
Numerical approach, $\delta_{\text{init}}(k) = \delta_1(k)$	2.8266 s	1.2 ms
Numerical approach, $\delta_{\text{init}}(k) = \delta(k-1)$	2.8395 s	1.2 ms

For the numerical approach, three different initial conditions δ_{init} for the `fzero` function are used. First, the initial condition of $\delta_{\text{init}}(k) = 0$ for every k-th iteration is used; secondly, the initial condition of $\delta_{\text{init}}(k) = \delta_1(k)$ for each iteration, where $\delta_1(k)$ is the result from the first-order Taylor approximation, is used; lastly, the solution of the previous step is chosen as initial value for the next step, i.e., $\delta_{\text{init}}(k) = \delta(k-1)$.

The simulation is performed with a fixed step time of 0.01 s, with a total simulation time of 23 s. The computation time of the iteration and controllers calculation process are presented in Table 5.4. The results confirm that the first-order Taylor approximation requires less process time than the other two methods, while the numerical method (for $\delta_{\text{init}}(k) = 0$) requires the longest process time. This is to be expected since the numerical method is executed by first finding an interval of δ_i where the root exists and iterating the process until the root is found. On the other hand, by using the initial condition of $\delta_{\text{init}}(k) = \delta_1(k)$, the total process time of the numerical method is improved to 2.8266 s, where the average process time per sample is equal to 1.2 ms. By using the initial condition of $\delta_{\text{init}}(k) = \delta(k-1)$, the computation time is comparable with the initial condition of $\delta_{\text{init}}(k) = \delta_1(k)$. Although the total process time of the numerical method with $\delta_{\text{init}}(k) = \delta_1(k)$ improved compared to the one with $\delta_{\text{init}}(k) = 0$, the second-order Taylor is still 5.64% faster than the numerical method with $\delta_{\text{init}}(k) = \delta_1(k)$.

Figure 5.6: Resulting trajectories of the center of gravity for platoon of four vehicles (top), and steering angles (bottom) using the global extended look-ahead controller and the first-order Taylor approximation.
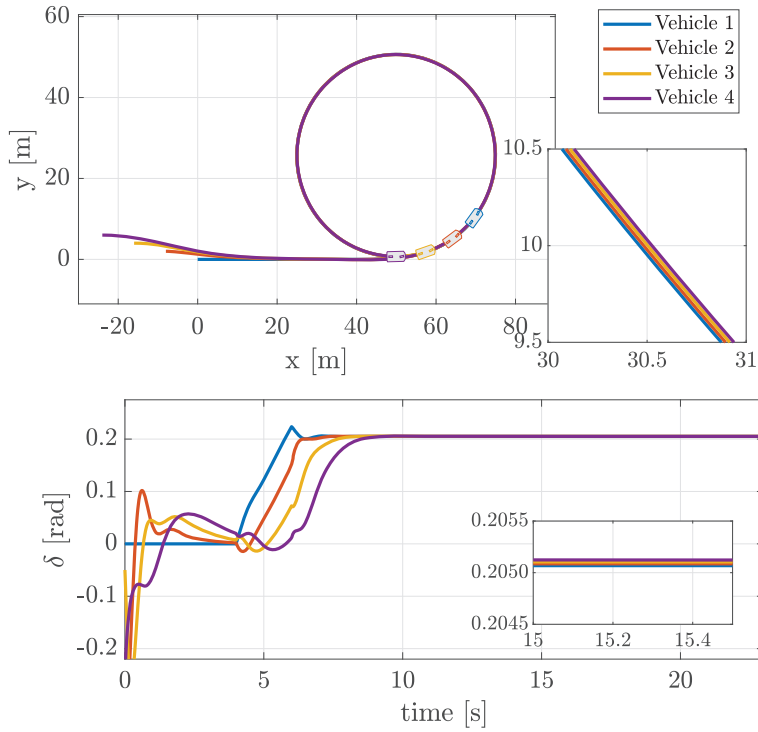
Figure 5.7: Resulting trajectories of the center of gravity for platoon of four vehicles (top), and steering angles (bottom) using the global extended look-ahead controller and the second-order Taylor approximation.
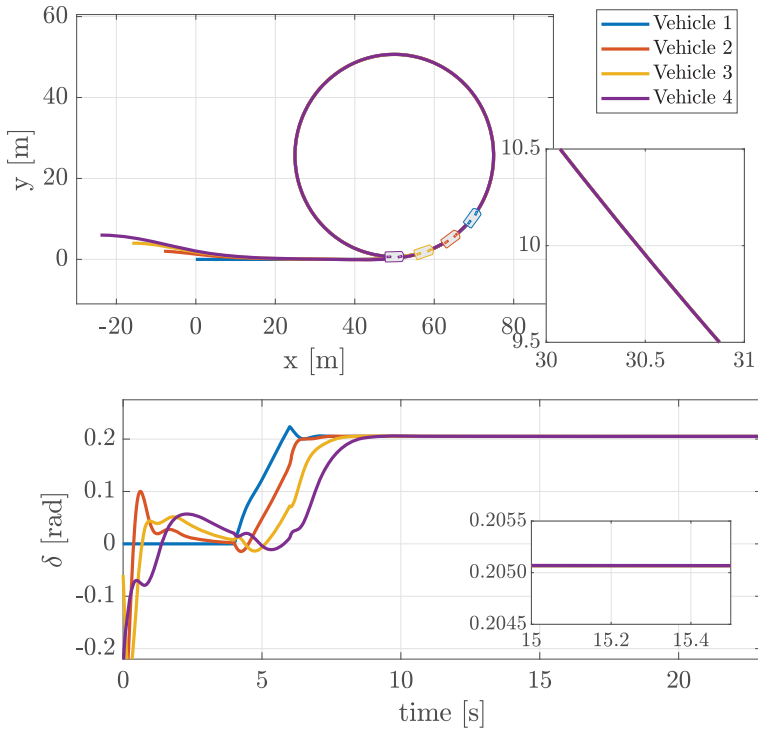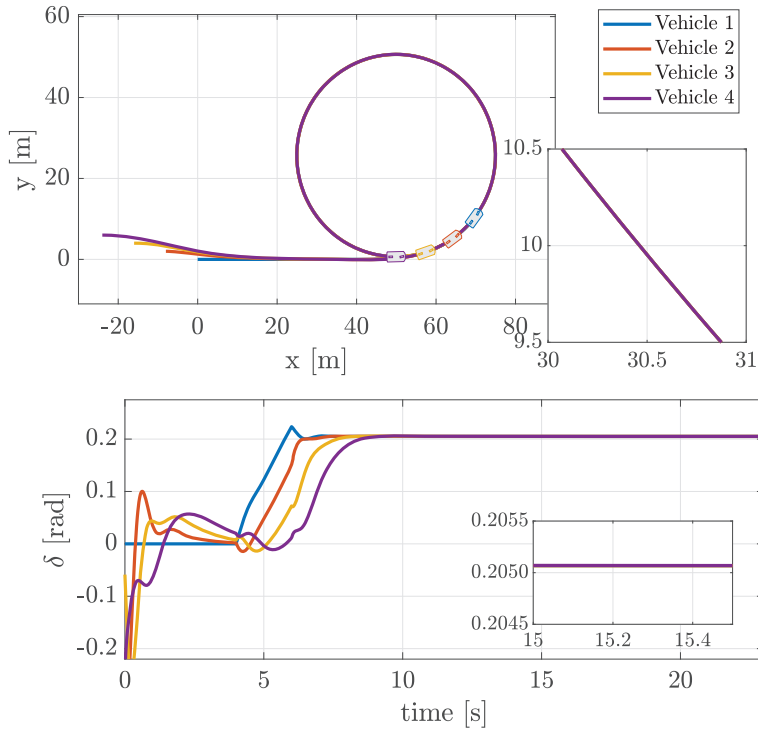
Figure 5.8: Resulting trajectories of the center of gravity for platoon of four vehicles (top), and steering angles (bottom) using the global extended look-ahead controller and the numerical approach.

Figure 5.6, Figure 5.7, and Figure 5.8 show the trajectories of the platoon and the time responses of the steering angle for the first-order Taylor, second-order Taylor approximation, and the numerical method, respectively. The plots show that the steering angle responses of the second-order Taylor approximation and the numerical method are identical, which then confirm the results in the previous section. Moreover, the steering angle of all vehicles converges to the same value, which means that all vehicles have identical curvature. On the other hand, the steering angle plot of the first-order Taylor (Figure 5.6(bottom)) shows that the steering angle of the follower vehicle deviates from its preceding vehicle. As a result, all vehicles in the platoon do not have the same curvature, as depicted in Figure 5.6(top). The simulation results indicate that the higher-level controller that was designed in Chapter 3 is not very robust against model uncertainties, thus, an integral action is needed to compensate for the uncertainties. For standard-size roundabouts, normal driving conditions and moderate speed, the accuracy of the first-order Taylor approximation is acceptable, with a steering angle deviation less than 0.0001 rad (Figure 5.6(bottom)).

This simulation also confirms the result in the previous section (Figure 5.3(middle, right)), which shows a deviation of the steering angle of the first-order Taylor approximation with respect to the numerical method, when the vehicle drives with a constant velocity of 10 m/s and a yaw rate of 0.4 rad/s. With a constant velocity of 10 m/s, the first-order Taylor approximation is accurate in approximating the steering angle if the yaw rate is smaller than 0.25 rad/s, which is equal to maneuvering on a roundabout with a minimum diameter of 80 m.

Therefore, it can be concluded that the second-order Taylor approximation yields a good trade-off between accuracy and computation time. For a high yaw rate and dynamic driving conditions (for example, a tight cornering and frequent accelerating and braking), the solution of the second-order Taylor approximation provides a better approximation of δ than the first-order Taylor approximation, while also providing a faster computation time than the numerical method.

5.3.3　Local extended look-ahead controller

The simulation results presented in the previous section have shown that the global extended look-ahead controller (3.35) can be directly applied to the single-track model through an inverse to the control inputs (a, ω) of the center of gravity control point, since the outputs of the global extended look-ahead controller in Chapter 3 are also given in the form of a longitudinal acceleration a_u and yaw rate ω_u. Now consider the local extended look-ahead controller, where the controller outputs are given as

$$
\begin{bmatrix} v_u \\ \omega_u \end{bmatrix} = \begin{bmatrix} \cos\left(\theta - \theta_r + \alpha_r\right) & \sin\left(\theta - \theta_r + \alpha_r\right) \\ -\frac{1}{d}\sin\left(\theta - \theta_r + \alpha_r\right) & \frac{1}{d}\cos\left(\theta - \theta_r + \alpha_r\right) \end{bmatrix} \begin{bmatrix} -k_1 z_1 + v_r - h_{\kappa,1}\dot{\kappa}_r \\ -k_2 z_2 + d\omega_r - h_{\kappa,2}\dot{\kappa}_r \end{bmatrix},
$$
$$(5.19)$$

where d is the desired inter-vehicle distance, (v_r, ω_r) are the longitudinal velocity
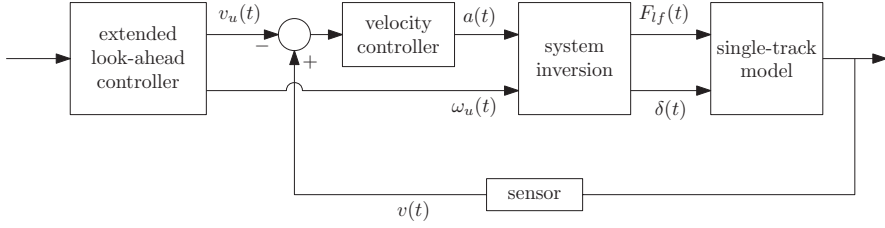
Figure 5.9: Block diagram of the local extended look-ahead controller with the feedback velocity controller.

and yaw rate of the preceding vehicle, κ_r is the curvature of the preceding vehicle, θ and θ_r are the orientation of the following vehicle and the preceding vehicle, respectively. It can be observed that the application of the local extended look-ahead controller (5.19) to the single-track model is not straightforward since the outputs of the controller are in the form of longitudinal velocity v_u and yaw rate ω_u. The desired longitudinal acceleration a_u for the control point must now be obtained from (5.19) by differentiation of v_u with respect to time. However, the differentiation results in a one-dimensional dynamic extension, where v_u is considered as an extra state. By setting the actual acceleration of the single-track model as $a = a_u$, where $a = \dot{v}$ and $a_u = \dot{v}_u$, the convergence of the actual velocity of the single-track vehicle v to the desired velocity generated by the local extended look-ahead controller, v_u, cannot be guaranteed, since the convergence of $\dot{v} \rightarrow \dot{v}_u$ does not not guarantee the convergence of $v \rightarrow v_u$. To this end, a velocity error state is defined as

$$e_v = v - v_u, \tag{5.20}$$

where v is the actual longitudinal velocity of the single-track model on the center of gravity control point, and v_u is the desired longitudinal velocity generated by the unicycle controller (5.19). The convergence of this velocity error to zero can be guaranteed using a feedback controller, with the block diagram as shown in Figure 5.9.

The desired acceleration $\dot{v}_u$ is obtained by differentiating v_u in (4.17) with respect to time, resulting in

$$
\begin{aligned}
\dot{v}_u = &\left(-k_1 \dot{z}_1 + a_r - \dot{h}_{\kappa,1}\dot{\kappa}_r - h_{\kappa,1}\ddot{\kappa}_r\right) \cos\left(\theta - \theta_r + \alpha_r\right) \\
&- \left(-k_1 z_1 + v_r - h_{\kappa,1}\dot{\kappa}_r\right)\left(\omega - \omega_r + \dot{\alpha}_r\right) \sin\left(\theta - \theta_r + \alpha_r\right) \\
&+ \left(-k_2 \dot{z}_2 + d\dot{\omega}_r - \dot{h}_{\kappa,2}\dot{\kappa}_r - h_{\kappa,2}\ddot{\kappa}_r\right) \sin\left(\theta - \theta_r + \alpha_r\right) \\
&+ \left(-k_2 z_2 + d\omega_r - h_{\kappa,2}\dot{\kappa}_r\right)\left(\omega - \omega_r + \dot{\alpha}_r\right) \cos\left(\theta - \theta_r + \alpha_r\right),
\end{aligned} \tag{5.21}
$$

where $(\dot{z}_1, \dot{z}_2)$ are the position error dynamics as in (4.15), defined as

$$
\begin{bmatrix} \dot{z}_1 \\ \dot{z}_2 \end{bmatrix} = (\omega_r - \dot{\alpha}_r) \begin{bmatrix} 0 & 1 \\ -1 & 0 \end{bmatrix} \begin{bmatrix} z_1 \\ z_2 \end{bmatrix} - \begin{bmatrix} v_r \\ d\omega_r \end{bmatrix}
$$
$$
+ \begin{bmatrix} \cos\left(\theta - \theta_r + \alpha_r\right) & -d\sin\left(\theta - \theta_r + \alpha_r\right) \\ \sin\left(\theta - \theta_r + \alpha_r\right) & d\cos\left(\theta - \theta_r + \alpha_r\right) \end{bmatrix} \begin{bmatrix} v \\ \omega \end{bmatrix} + \begin{bmatrix} h_{\kappa,1} \\ h_{\kappa,2} \end{bmatrix} \dot{\kappa}_r, \tag{5.22}
$$

and α_r, $\dot{\alpha}_r$, $h_{\kappa,1}$, $h_{\kappa,2}$ as in (4.5), (4.7), (4.16):

$$\alpha_r = 2 \arcsin \left(\frac{1}{2} d \kappa_r \right), \qquad \dot{\alpha}_r = \frac{2d}{\sqrt{4 - d^2 \kappa_r^2}} \dot{\kappa}_r, \tag{5.23}$$

$$h_{\kappa,1} = \frac{d^3 \kappa_r}{2 \sqrt{4 - d^2 \kappa_r^2}}, \qquad h_{\kappa,2} = \frac{4d^2 - d^2 \sqrt{4 - d^2 \kappa_r^2}}{2 \sqrt{4 - d^2 \kappa_r^2}}. \tag{5.24}$$

Moreover, (a_r, ω_r) are the acceleration and the yaw rate of the preceding vehicle, κ_r is the curvature of the preceding vehicle, and ω is the yaw rate input to the following vehicle which is yet to be determined. It is now straightforward to design a globally exponentially stabilizing feedback as

$$a = -k_{pv} e_v + \dot{v}_u, \tag{5.25}$$

with $k_{pv} > 0$ and $\dot{v}_u$ as in (5.21). Using (5.25), the velocity of the single-track model v is guaranteed to converge to the desired velocity v_u. On the other hand, the desired yaw rate of the single-track model is obtained by setting $\omega = \omega_u$, as

$$\omega = \omega_u = -\frac{1}{d} \left(-k_1 z_1 + v_r - h_{\kappa,1} \dot{\kappa}_r \right) \sin \left(\theta - \theta_r + \alpha_r \right)$$
$$+ \frac{1}{d} \left(-k_2 z_2 + d \omega_r - h_{\kappa,2} \dot{\kappa}_r \right) \cos \left(\theta - \theta_r + \alpha_r \right). \tag{5.26}$$

Thus, (5.25) and (5.26) can be considered as a desired motion of the single-track model control point, which is regulated by the local extended look-ahead controller derived in Chapter 4. The inverse for the local extended look-ahead controller is then obtained by substituting (5.25) and (5.26) into (5.7), by taking (5.1a) and (5.1b) into account, as

$$\begin{bmatrix} F_{lf} \\ C_{\alpha f} \left(\delta - \sigma_f \right) \end{bmatrix} = \begin{bmatrix} \cos \delta & \sin \delta \\ -\sin \delta & \cos \delta \end{bmatrix} \begin{bmatrix} \bar{\zeta}_1 \\ \bar{\zeta}_2 \end{bmatrix}, \tag{5.27}$$

where

$$\bar{\zeta}_1 := \frac{m}{v} v_x \left(-k_{pv} e_v + \dot{v}_u \right) - m v_y \omega \tag{5.28a}$$

$$\bar{\zeta}_2 := \frac{m}{v} v_y \left(-k_{pv} e_v + \dot{v}_u \right) + m v_x \omega + C_{\alpha r} \arctan \left(\frac{v_y - l_r \dot{\psi}}{v_x} \right), \tag{5.28b}$$

ω as in (5.26), and σ_f as in (5.10c). Note that (5.28) is identical to (5.10), where a_u in (5.10) is replaced by $-k_{pv} e_v + \dot{v}_u$. Thus, the exact same inversion procedure can be applied, and the actual inputs (F_{lf}, δ) then can be obtained by following along the exact approach in the previous section.

It should be noted that the terms $\dot{z}_1$, $\dot{z}_2$, α_r, $\dot{\alpha}_r$ in (5.21) depend on the states from both follower and preceding vehicle, which are measurable. However, the terms $\dot{\omega}_r$ and $\ddot{\kappa}_r$ might not be available to be measured in practical situations. In
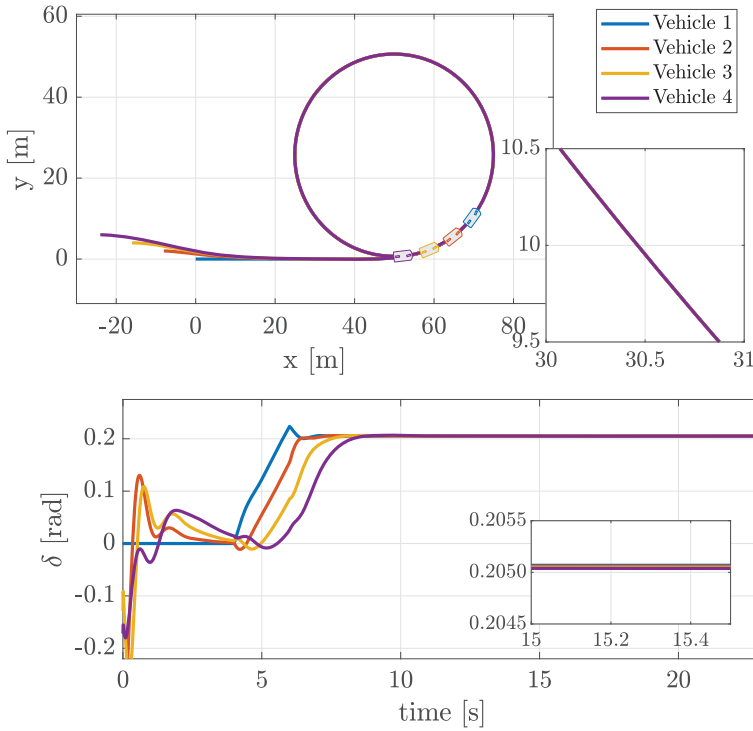
Figure 5.10: Resulting trajectories of the center of gravity for platoon of four vehicles (top), and steering angles (bottom) in a noiseless measurement scenario. The local extended look-ahead controller is used, with the approximation of $\dot{\omega}_r \approx 0$ and $\ddot{\kappa}_r \approx 0$.

a noiseless condition, one can obtain these terms by means of numerical differentiation (e.g., finite difference approximation). However, in a practical situation, measured signals are always disturbed by noise. In this case, numerical differentiation will amplify noise from these signals, which is undesirable. Therefore, the importance of $\dot{\omega}_r$ and $\ddot{\kappa}_r$ in both noiseless and noisy measurement is investigated in the following simulation.

To investigate the importance of $\dot{\omega}_r$ and $\ddot{\kappa}_r$, two cases are considered: (1) the case where the assumption of $\dot{\omega}_r \approx 0$ and $\ddot{\kappa}_r \approx 0$ are made; (2) the case where $\dot{\omega}_r$ and $\ddot{\kappa}_r$ are approximated by a numerical differentiation. Both conditions are simulated in two scenarios, a noiseless and a noisy measurement scenario. In a noisy measurement scenario, the orientation, yaw rate, and velocity sensors for all vehicles are disturbed by noise, where the noise is simulated as white noise with a constant power spectral density with height of 5×10^{-7}. On the other hand, the position sensors are assumed to be noiseless. The simulation for a platoon with the local extended look-ahead controller is performed using identical initial conditions, vehicle parameters, and control parameters as the previous simulation.
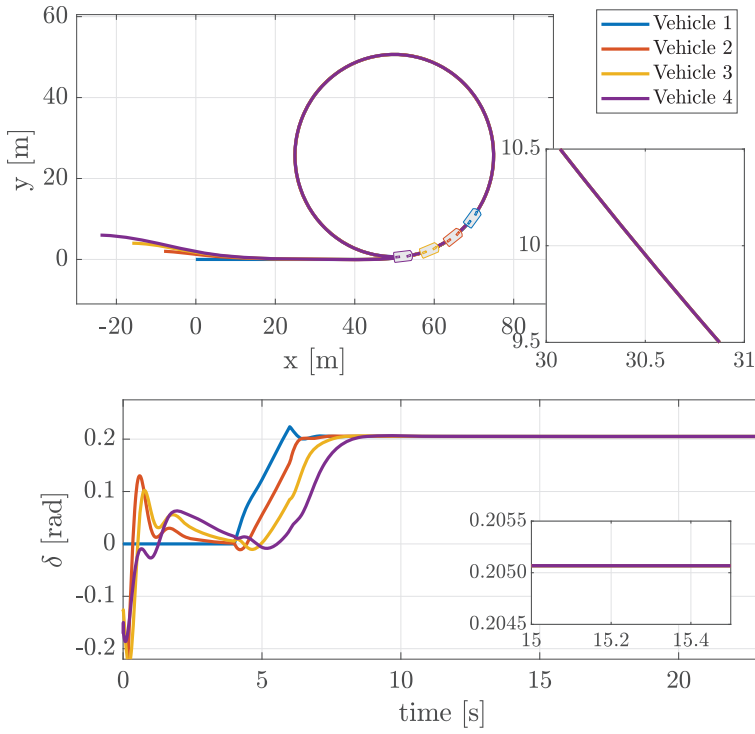
Figure 5.11: Resulting trajectories of the center of gravity for platoon of four vehicles (top), and steering angles (bottom) in a noiseless measurement scenario. The local extended look-ahead controller is used, where $\dot{\omega}_r$ and $\ddot{\kappa}_r$ are approximated by a numerical differentiation.
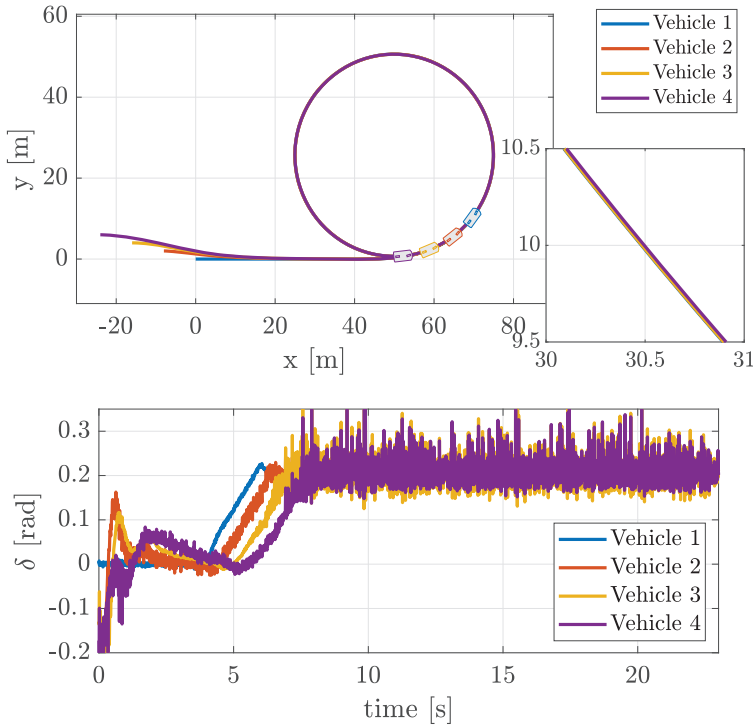
Figure 5.12: Resulting trajectories of the center of gravity for platoon of four vehicles (top), and steering angles (bottom) in a noisy measurement scenario. The local extended look-ahead controller is used, with the approximation of $\dot{\omega}_r \approx 0$ and $\ddot{\kappa}_r \approx 0$.

The inverse from (a, ω) to (F_{lf}, δ) is applied using the numerical approach.

The resulting trajectories of the center of gravity control point and steering angles in a noiseless scenario with the approximation of $\dot{\omega}_r \approx 0$ and $\ddot{\kappa}_r \approx 0$ are depicted in Figure 5.10. It can be observed that the resulting steering angles of vehicles do not exactly converge to the same value, due to the approximation of $\dot{\omega}_r \approx 0$ and $\ddot{\kappa}_r \approx 0$. Nevertheless, the deviation is very small (less than 0.0001 rad) and hardly affects the resulting paths, thus, the deviation can be safely neglected. On the other hand, the numerical differentiation of $\dot{\omega}_r$ and $\ddot{\kappa}_r$ in a noiseless scenario does not significantly improve the convergence of the steering angles, as depicted in Figure 5.11.

The resulting trajectories of the center of gravity control point and steering angles in a noisy measurement scenario for the zero approximation and the numerical differentiation are depicted in Figure 5.12 and Figure 5.13, respectively. It can be clearly seen that the steering angles of vehicles for both approximations are affected by noise. As a consequence, the following vehicle drives with a slightly
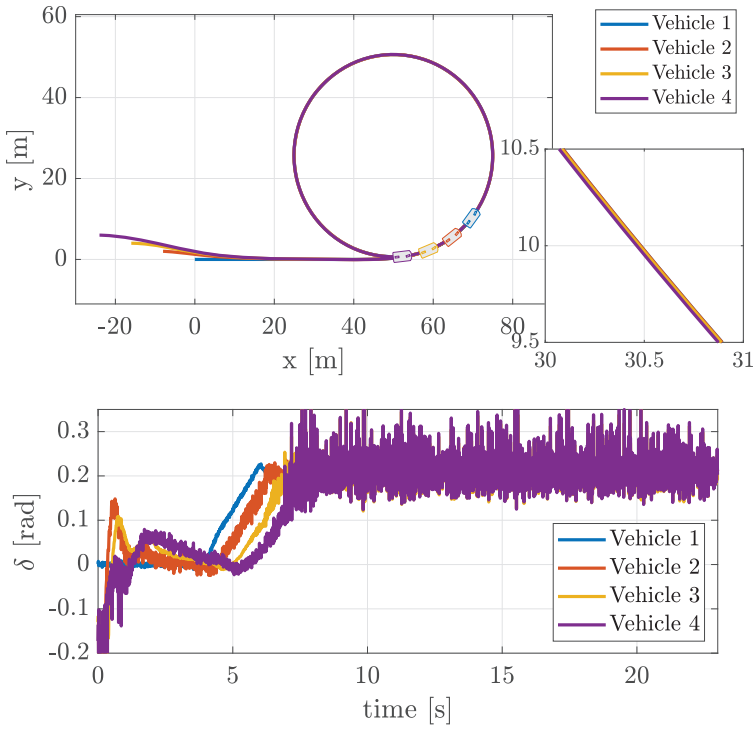
Figure 5.13: Resulting trajectories of the center of gravity for platoon of four vehicles (top), and steering angles (bottom) in a noisy measurement scenario. The local extended look-ahead controller is used, where $\dot{\omega}_r$ and $\ddot{\kappa}_r$ are approximated by a numerical differentiation.

different curvature than the preceding vehicle. For the case of zero approxima-
tion, the curvature deviation between vehicles is not significantly large (less than
$0.01\,\mathrm{m}^{-1}$). On the other hand, the curvature deviation for the case of numerical
differentiation is clearly visible, where vehicle 4 has the largest curvature devi-
ation (with respect to vehicle 1) due to the amplification of the noise from its
predecessors, see Figure 5.13(top).

Therefore, this simulation clearly shows that under a normal driving condition,
$\dot{\omega}_r$ and $\ddot{\kappa}_r$ can be safely approximated by zero, without any significant effect
on tracking performances. In a practical situation where the measurement is
corrupted by noise, the zero approximations of $\dot{\omega}_r$ and $\ddot{\kappa}_r$ give better tracking
performance than the approximation by numerical differentiation.

5.4 Rear axle center as a control point

Having derived the input inversion for the center of gravity as a control point, and
having applied the inverse to support both the global and the local extended look-
ahead controller, this section further studies the rear axle center as a control point.
To obtain the input inversion for the rear axle center, the Cartesian coordinates
of the rear axle center are defined first. Next, the longitudinal acceleration and
the yaw rate of that rear axle center point are formulated, which then allows the
formulation of the input inversion of the rear axle center as a control point. The
resulting inverse is then simulated for a platoon of four vehicles using both global
and local extended look-ahead controllers.

5.4.1 Input inversion

Consider the rear axle center of the single-track vehicle model with Cartesian
coordinates (X_r, Y_r), see Figure 5.2, where the chassis kinematic model can be
described by the following equations

$$\dot{X}_r = v_x \cos\psi - v_y \sin\psi + l_r \dot{\psi} \sin\psi \tag{5.29a}$$

$$\dot{Y}_r = v_x \sin\psi + v_y \cos\psi - l_r \dot{\psi} \cos\psi, \tag{5.29b}$$

where $(v_x, v_y, \dot{\psi})$ dynamics are as described in (5.1). Following the line of thought
of Section 5.3.1, the following equations are eventually obtained

$$\dot{v}_r = \frac{1}{v_r} \left\{ v_x \dot{v}_x + \left(v_y - l_r \dot{\psi}\right)\left(\dot{v}_y - l_r \ddot{\psi}\right) \right\} \tag{5.30}$$

$$\dot{\theta}_r = \frac{1}{v_r^2} \left\{ -\left(v_y - l_r \dot{\psi}\right)\dot{v}_x + v_x \dot{v}_y - l_r v_x \ddot{\psi} \right\} + \dot{\psi}, \tag{5.31}$$

where $(\dot{v}_r, \dot{\theta}_r) = (a_r, \omega_r)$ are the longitudinal acceleration and the yaw rate, de-
fined as new inputs. By substituting (5.1) into (5.30) and (5.31), the following

equations are obtained

$$\begin{bmatrix} a_r \\ \omega_r \end{bmatrix} = H \begin{bmatrix} \cos\delta & -\sin\delta \\ \sin\delta & \cos\delta \end{bmatrix} \begin{bmatrix} F_{lf} \\ F_{cf} \end{bmatrix} + \begin{bmatrix} h_1 \\ h_2 \end{bmatrix}, \tag{5.32}$$

where

$$H := \frac{1}{v_r} \begin{bmatrix} \frac{1}{m} v_x & \left(\frac{1}{m} - \frac{l_f l_r}{I}\right)\left(v_y - l_r \dot\psi\right) \\ -\frac{1}{m v_r}\left(v_y - l_r \dot\psi\right) & \frac{1}{v_r}\left(\frac{1}{m} - \frac{l_f l_r}{I}\right) v_x \end{bmatrix} \tag{5.33}$$

$$h_1 := \frac{1}{v_r}\left(\frac{1}{m} + \frac{l_r^2}{I}\right)\left(v_y - l_r \dot\psi\right) F_{cr} + \frac{l_r}{v_r} v_x \dot\psi^2 \tag{5.34}$$

$$h_2 := \frac{v_x}{v_r^2}\left(\frac{1}{m} + \frac{l_r^2}{I}\right) F_{cr} - \frac{l_r}{v_r^2}\left(v_y - l_r \dot\psi\right) \dot\psi^2. \tag{5.35}$$

The inverse is obtained by inverting the matrix H and the rotation matrix by δ, as

$$\begin{bmatrix} F_{lf} \\ F_{cf} \end{bmatrix} = \begin{bmatrix} \cos\delta & \sin\delta \\ -\sin\delta & \cos\delta \end{bmatrix} H^{-1} \begin{bmatrix} a_r - h_1 \\ \omega_r - h_2 \end{bmatrix}, \tag{5.36}$$

with

$$H^{-1} = \begin{bmatrix} \frac{m}{v_r} v_x & -m\left(v_y - l_r\dot\psi\right) \\ \frac{1}{v_r}\left(\frac{mI}{I - m l_f l_r}\right)\left(v_y - l_r\dot\psi\right) & \left(\frac{mI}{I - m l_f l_r}\right) v_x \end{bmatrix} \tag{5.37}$$

$$F_{cf} = C_{\alpha f}\left(\delta - \arctan\left(\frac{v_y + l_f\dot\psi}{v_x}\right)\right), \tag{5.38}$$

eventually resulting in

$$\begin{bmatrix} F_{lf} \\ C_{\alpha f}\left(\delta - \sigma_f\right) \end{bmatrix} = \begin{bmatrix} \cos\delta & \sin\delta \\ -\sin\delta & \cos\delta \end{bmatrix} \begin{bmatrix} \zeta_1 \\ \zeta_2 \end{bmatrix}, \tag{5.39}$$

with

$$\zeta_1 := \frac{m}{v_r} v_x a_r - m\left(v_y - l_r\dot\psi\right)\omega_r - m l_r \dot\psi^2 \tag{5.40}$$

$$\zeta_2 := \frac{1}{v_r}\left(\frac{mI}{I - m l_f l_r}\right)\left(v_y - l_r\dot\psi\right) a_r + \left(\frac{mI}{I - m l_f l_r}\right) v_x \omega_r$$

$$+ \left(\frac{I + m l_r^2}{I - m l_f l_r}\right) C_{\alpha r} \arctan\left(\frac{v_y - l_r\dot\psi}{v_x}\right) \tag{5.41}$$

$$\sigma_f := \arctan\left(\frac{v_y + l_f\dot\psi}{v_x}\right). \tag{5.42}$$

Following the same line of the approach for the center of gravity control point, the actual inputs of the single-track model (F_{lf}, δ) can be obtained as approximate solutions of (5.36) using either a first- or second-order Taylor approximation around $\delta = 0$, or a numerical approach.
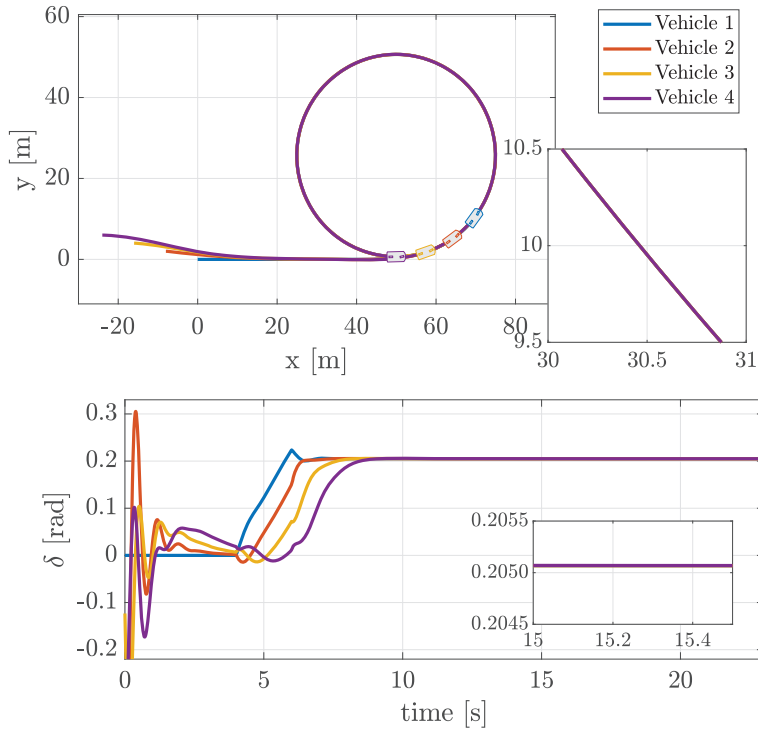
Figure 5.14: Resulting trajectories of the center of gravity for platoon of four vehicles (top), and steering angles (bottom) using the global extended look-ahead controller with the rear axle center as a control point.
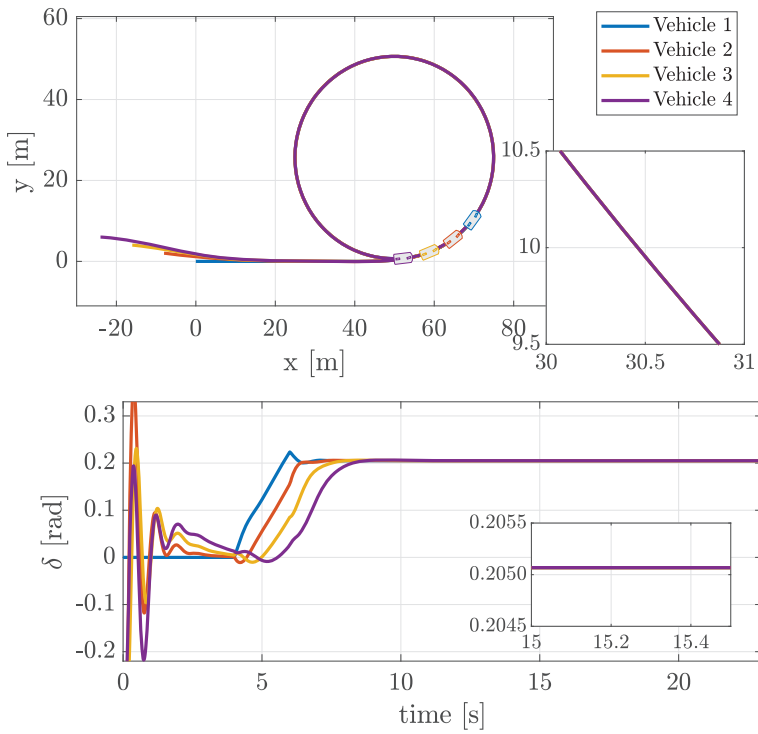
Figure 5.15: Resulting trajectories of the center of gravity for platoon of four vehicles (top), and steering angles (bottom) using the local extended look-ahead controller with the rear axle center as a control point.

5.4.2 Simulation results

To validate the input inversion for the rear axle center as a control point, two simulations of a platoon of four vehicles with both global and local extended look-ahead controller are conducted in this section. Like the simulation in the previous section, the first vehicle in the platoon is directly controlled and maneuvers on the same path as in the previous simulation, where the path is given as a combination of a straight and circular path. In other words, the first vehicle has an identical steering angle and curvature as the one in the previous simulation. The identical path of the first vehicle is chosen to study the effect of a different control point to the behavior of the follower vehicles. The rest of the vehicles are controlled by either the global extended look-ahead controller (3.35) or local extended look-ahead controller (5.25, 5.26). For both controllers, the rear center axle point of the follower vehicle tracks the corresponding point of the preceding vehicle. To investigate the effect of a different control point on the system response, identical initial conditions, vehicle parameters, and control parameters as in the previous simulation are used. The inverse from the unicycle outputs to the single-track inputs (F_{lf}, δ) is applied using the numerical approach.

The resulting trajectories of the center of gravity and steering angles of a platoon with the global extended look-ahead controller are depicted in Figure 5.14. In comparison to the steering angle response of the system with the center of gravity as a control point (Figure 5.8), it can be clearly seen that the steady-state steering angle response of the two control points, from $t = 5$ s until $t = 25$ s, are identical. However, it can also be observed that the initial steering angle response of the rear axle center as a control point has larger amplitudes than the one of the center of gravity as a control point. This is to be expected since the rear axle center has a larger distance from the steering point than the center of gravity, thus requires a larger steering response in order to compensate the inter-vehicle distance errors, when the identical control parameters and initial conditions are used. In spite of the difference in the initial steering response, all vehicles eventually drive with the same curvature, as depicted in Figure 5.14(top). The steering angle response of a platoon with the local extended look-ahead controller, as depicted in Figure 5.15(bottom), clearly shows the same behavior as the global extended look-ahead controller. Nevertheless, the curvature of all vehicles converges to the same value.

5.5 Front axle center as a control point

In this section, the inverse for the front axle center as a control point is formulated. The resulting inverse is then simulated for a platoon of four vehicles using both global and local extended look-ahead controllers.

5.5.1 Input inversion

Consider the front axle center of the single-track vehicle model with Cartesian coordinates (X_f, Y_f), see Figure 5.2. The kinematic model of this point can be described by the following equations

$$\dot{X}_f = v_x \cos\psi - v_y \sin\psi - l_f \dot{\psi} \sin\psi \tag{5.43a}$$

$$\dot{Y}_f = v_x \sin\psi + v_y \cos\psi + l_f \dot{\psi} \cos\psi, \tag{5.43b}$$

where $(v_x, v_y, \dot{\psi})$ dynamics are as described in (5.1). Following the line of thought of Section 5.3.1 and 5.4.1, the inverse is eventually obtained as

$$\begin{bmatrix} F_{lf} \\ C_{\alpha f}(\delta - \sigma_f) \end{bmatrix} = \begin{bmatrix} \cos\delta & \sin\delta \\ -\sin\delta & \cos\delta \end{bmatrix} \begin{bmatrix} \zeta_1 \\ \zeta_2 \end{bmatrix}, \tag{5.44}$$

with

$$\zeta_1 := \frac{m}{v_f} v_x a_f - m\left(v_y + l_f \dot{\psi}\right)\omega_f + m l_f \dot{\psi}^2 \tag{5.45}$$

$$\zeta_2 := \frac{1}{v_f}\left(\frac{mI}{I + ml_f^2}\right)\left(v_y + l_f\dot{\psi}\right)a_f + \left(\frac{mI}{I + ml_f^2}\right)v_x\omega_f$$

$$+ \left(\frac{I - ml_f l_r}{I + ml_f^2}\right)C_{\alpha r}\arctan\left(\frac{v_y - l_r\dot{\psi}}{v_x}\right) \tag{5.46}$$

$$\sigma_f := \arctan\left(\frac{v_y + l_f\dot{\psi}}{v_x}\right). \tag{5.47}$$

By setting $(a_f, \omega_f) = (a_u, \omega_u)$, where (a_u, ω_u) are the outputs of the global extended look-ahead or the local extended look-ahead controller, the actual inputs of the single track model (F_{lf}, δ) can be obtained as solutions of (5.44) by using the first- or second-order Taylor approximation around $\delta = 0$, or the numerical method.

5.5.2 Simulation results

In order to validate the input inversion for the front axle center as a control point, two simulations using both global and local extended look-ahead are conducted. To compare the results with the other two control points, identical initial conditions, vehicle parameters, and control parameters as the previous simulation are used. In this simulation, the first vehicle is also directly controlled by identical inputs as the one in previous simulations, i.e., it drives over the exact same path with the identical steering angle and curvature as the two previous simulations. Both global and local extended look-ahead controllers are applied to other vehicles, where the front axle center point of the follower vehicle tracks the corresponding point of its preceding vehicle. As expected, the steady-state steering angle responses of the front axle center as a control point using both controllers are identical to the responses of the other two control points, as depicted in
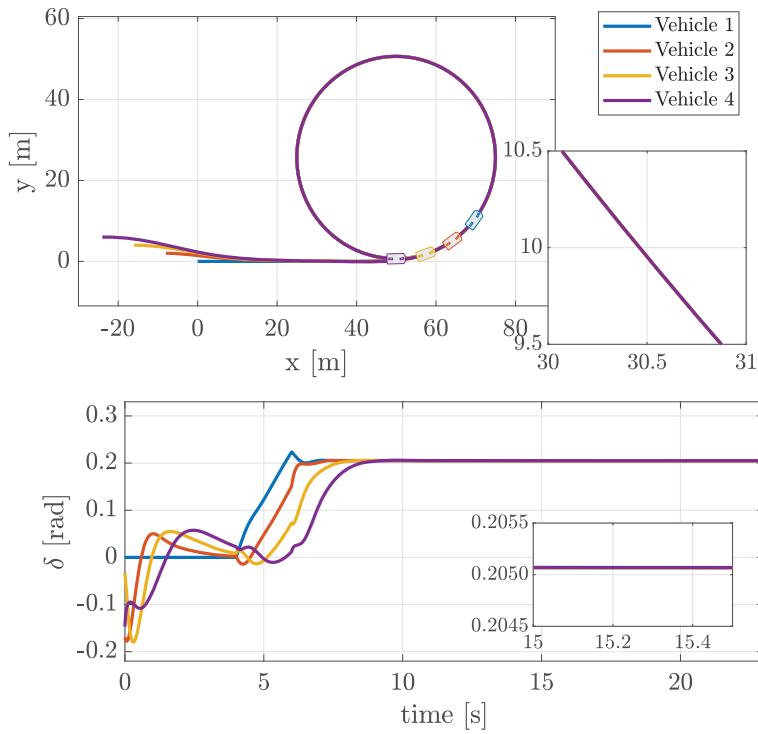
Figure 5.16: Resulting trajectories of the center of gravity for platoon of four vehicles (top), and steering angles (bottom) using the global extended look-ahead controller with the front axle center as a control point.
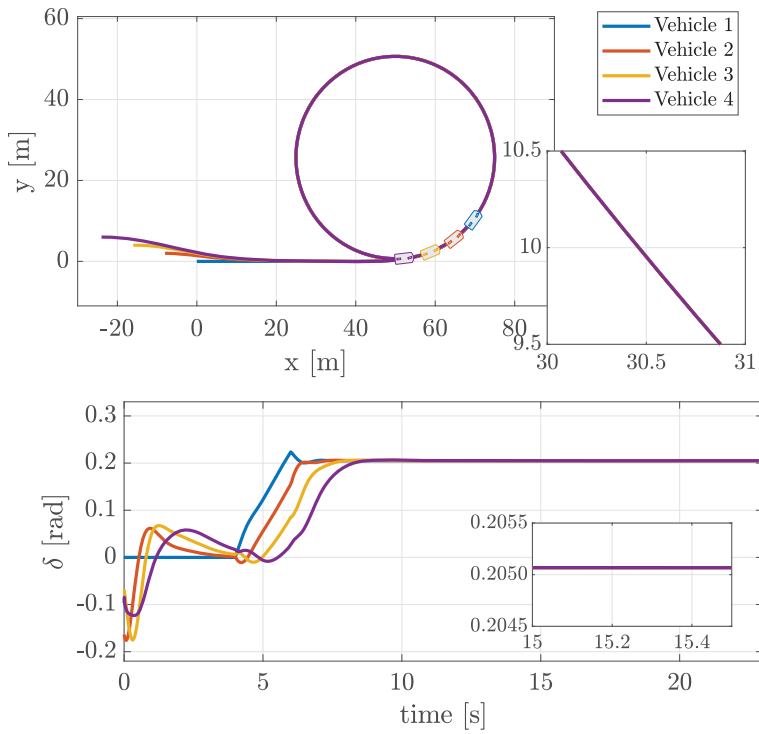
Figure 5.17: Resulting trajectories of the center of gravity for platoon of four vehicles (top), and steering angles (bottom) using the local extended look-ahead controller with the front axle center as a control point.

Figure 5.16(bottom) and Figure 5.17(bottom) for global and local extended look-ahead controller, respectively. A slight difference, in comparison to the other control points, can be observed in the initial steering angle responses. In contrast with the initial responses of the rear axle center as a control point, the initial steering responses of the front axle center as a control point have smaller amplitudes, which is to be expected since the front axle center also acts as a steering point.

5.6 Conclusions

In this chapter, the implementation of the global and local extended look-ahead controller to the platoon of vehicles, modeled by a single-track model, is presented. Due to the nonlinearity of the single-track model, the input inversion can only be approximated using the first-, second-order Taylor approximation, or a numerical approach. All approximations result in converging curvatures of vehicles in the platoon, with a trade-off between tracking performance and computation time performance. The first-order Taylor approximation yields the fastest computation time but is the least accurate among the three aforementioned approaches. The simulation results show that the accuracy of the first-order Taylor approximation depends on the yaw rate of the vehicle (thus, the curvature of the road). On the other hand, the numerical approach gives the most accurate but the slowest computation time. From the simulation results, it can be concluded that the second-order Taylor approximation yields a good trade-off between the accuracy of the steering angle approximation and the computation time.

To validate the results further, three control points of a single-track model are chosen: the center of gravity; the rear axle center; and the front axle center. Among the three control points, the most obvious choice is the center of gravity control point, since the single-track model is usually defined at the center of gravity. The rear axle center is not recommended due to its furthest distance from the steering point. The simulation results confirm that the extended look-ahead controller, both global and local, can be applied to the single-track vehicle platoon using the input inversions for the three aforementioned control points.

Conclusions and recommendations

This chapter summarizes the main conclusions of this thesis in Section 6.1. In Section 6.2, recommendations for future research are discussed.

6.1 Conclusions

In this thesis, we have focused on the extended look-ahead for longitudinal and lateral control of vehicles in a platoon. The primary objectives for the follower vehicle are to drive the same path as their preceding vehicle while keeping a desired distance. This implies that corner-cutting of the follower vehicle is undesired. One might think that the path following approach, as opposed to the direct vehicle following approach, does not suffer from corner cutting. However, the path following approach relies heavily on the path, which can be a drawback. As an illustration, consider a simple case of a platoon with two vehicles, where the leader vehicle is driven by a human and the follower vehicle is automated. From a practical point of view, there are several considerations that determine the control strategy for the follower vehicle: it is not always possible to obtain information about the lane or the path of the leader vehicle; lane markings are not always available; detours; and the inaccuracy of GPS in vehicles. Under those considerations, all the follower vehicle can do is to directly follow the leader vehicle. By implementing the extended look-ahead approach presented in this thesis, it appeared that the corner cutting problem in a direct vehicle following approach can be eliminated.

The extended look-ahead control is designed based on a vehicle following approach. Using the current position and orientation of the preceding vehicle, the follower vehicle steers towards its preceding vehicle. In contrast to the path-following approach, the main challenge in the vehicle following approach is that the follower vehicle does not have any information about the path (either road path or path history of the preceding vehicle). Consequently, the vehicle following

approach may be prone to corner-cutting. We approached the problem of vehicle platooning as a truck coupled to multiple trailers. By driving with a slightly smaller curvature than the road curvature, a truck can compensate corner-cutting for its trailers. Based on this approach, we were able to design the extended look-ahead approach for vehicle platooning. A reference-induced look-ahead point is designed as a function of the curvature of the preceding vehicle and the desired inter-vehicle distance, which is then used as a target point for the follower vehicle driving through corners. By tracking this reference-induced look-ahead point, the follower vehicle is then able to maneuver on the same path as its preceding vehicle. A more detailed explanation of the results presented in this thesis is given in the next paragraphs.

In Chapter 3, a look-ahead based controller designed for an integrated longitudinal and lateral vehicle platooning is introduced. The vehicle is modeled as a fourth-order kinematic unicycle, where the inputs are given as longitudinal acceleration and yaw rate. The desired inter-vehicle distance is formulated in a global coordinate system (Cartesian coordinate system) and is defined as a vector with two components. The extended look-ahead point is formulated in the global coordinates and defined as a function of the curvature of the preceding vehicle and the desired inter-vehicle distance. A stabilizing control law for the extended look-ahead approach is designed using input-output linearization and is well-defined if the velocity of the follower vehicle is nonzero. By using Lyapunov stability techniques, we are able to show the asymptotic stability of the overall system under bounds of curvature, rate of curvature, and longitudinal acceleration of the preceding vehicle. By these conditions, we are also able to guarantee a nonzero velocity of the follower vehicle. The signals that have to be considered for this controller are: the global positions of vehicles, which can be obtained by DGPS; the preceding vehicle states, which can be obtained through V2V communication; and relative orientation, which can be measured by a camera or an INS in conjunction with the V2V communication. The performance of the extended look-ahead approach is analyzed by simulation studies, involving a circular path (with constant curvature) and an eight-shaped path (with varying curvature). As a result, we can conclude that the extended look-ahead approach successfully compensates for corner-cutting on both paths without the need for path information. By the experiment with the E-puck mobile robots, we can conclude the advantages of our extended look-ahead approach: the real time implementation of this approach is relatively simple and does not require heavy computational processes; and the necessary signals for the controller can be easily measured. The potential application of this controller is not only limited to vehicle platooning, but also to warehouse robots in the situation when lane markings are unreliable.

Chapter 4 explores the design of the extended look-ahead approach in a local coordinate system. From the practical implementation point of view, there is a situation where the global position of vehicles is not available. Thus, the adaptation of the extended look-ahead approach in a local coordinate system is needed. The vehicle platoon is modeled as a platoon of unicycles, and the target look-

ahead point is defined as a function of the current position, the curvature of the preceding vehicle, and the desired inter-vehicle distance. A stabilizing control law is designed using input-output linearization, which results in a first-order internal dynamics. Using Lyapunov stability techniques, we are able to show that the overall system is asymptotically stable, under bounds on the curvature, curvature rate of the preceding vehicle, and the initial orientation error between the follower and the preceding vehicle. In addition, these bounds also guarantee the nonzero velocity of the follower vehicle, which is an important aspect that guarantee asymptotic stability for vehicle platoons with more than two vehicles. The signals needed for the extended look-ahead controller in a local coordinate system are: relative position, which can be obtained by lidar or a camera; the preceding vehicle states, which can be obtained through V2V communication; and relative orientation, which can be measured by a camera or an INS in conjunction with the V2V communication. It is assumed that all these signals can be obtained accurately and that there is no delay involved in V2V communication. To address a situation where the INS is not available or are disturbed by noise, we used an orientation-error observer. By using the observer, we are able to determine the orientation angle using the relative position, velocity, and yaw rate of the preceding vehicle. The performance of the extended look-ahead in a local coordinate system and the orientation-error observer is analyzed by both simulation and experiment studies. The results confirm the benefit of the extended look-ahead to eliminate corner-cutting and the benefit of the orientation-error observer to improve the tracking performance. By using the identical experimental setup as in Chapter 3, we can conclude that the extended look-ahead controller for the local coordinate system and the observer can be easily implemented with a relatively light computational processes. Moreover, by guaranteeing the nonzero velocity of the follower vehicle, we are able to show that the proposed approach is suitable for platoons of any length, thereby handling the scalability issue. Hence, it is concluded that the extended look-ahead approach and the observer have the potential to solve the cutting corner problem of vehicle platooning in confined spaces (e.g., tunnels, etc), addressing the situation where GPS and INS might be unreliable.

In Chapter 5, as an important step towards the application of the proposed controller to actual vehicles, the extended look-ahead controller is developed for a single-track vehicle platoon. The vehicle in this chapter is modeled as a dynamic single-track vehicle model, where the inputs are given as a longitudinal force and steering angle. The adaptation of the extended look-ahead controllers that were designed in the previous chapters is developed using the input inversion technique on three control points: the center of gravity; the rear axle center; and the front axle center. Due to the nonlinearity of the single-track model, the inversion is determined numerically or approximated by Taylor series. Extensive simulation studies are performed to analyze the advantages and disadvantages of the aforementioned inversion methods and control points. From the viewpoint of computation time and tracking accuracy, it is shown that the second-order Taylor approximation yields the best results among the inversion methods. From the

viewpoint of implementation, the center of gravity control point is recommended. It is then concluded that we are able to adapt the extended look-ahead controllers in this thesis to actual vehicles.

The extended look-ahead concept and its derivative designs and developments in this thesis are shown to handle the main problem in a vehicle following approach, which is corner-cutting, achieving a satisfactory level of performance in simulations and experiments.

6.2 Recommendations for future research

Based on obtained insights and presented results in this thesis, there are several recommendations that are needed to be taken into accounts for future research directions.

Analyzing string stability: Throughout this thesis, it is demonstrated that the extended look-ahead approach compensates for corner-cutting. However, string stability, which is an important aspect of vehicle platooning, is not considered in this thesis. Although longitudinal string stability can be guaranteed by the constant time-gap spacing policy for a case when the platoon maneuvers on a straight path, it may not be guaranteed for a platoon maneuvers on a path with varying curvatures. Moreover, the lateral string stability of this extended look-ahead also needs to be studied. The string stability in a lateral sense focuses on the propagation of the lateral states (e.g., yaw rate, steering angle rate, etc) along the vehicle platoon. Since most existing literature provides the definition of string stability in the frequency-domain (see, e.g., Ge and Orosz (2014), Naus et al. (2010b), Ploeg (2014), Sheikholeslam and Desoer (1993), Zhang and Orosz (2016)), we first recommend analyzing lateral string stability in the time-domain based on Lyapunov stability, along the lines of Feng et al. (2019), Solyom et al. (2013). To simultaneously analyze both lateral and longitudinal string stability, we recommend to investigate the mesh stability of the interconnected system (Pant et al. (2001)).

Taking imperfect measurements and unavailability of states into account: The performance of the extended look-ahead was demonstrated using simulation and experiment studies. In experiments with E-puck mobile robots, the information about global positions, velocities, accelerations, and curvatures of all vehicles can be obtained, and the imperfect measurement of the orientation can be handled by an observer used in Chapter 4. However, for the actual implementation, it is recommended to also use observers for states that cannot be reliably measured. For the unavailability of states, the curvature rate in the experimental setup is approximated by the backward Euler's method. The method, however, is not robust against noises and disturbances. Hence, it is recommended to use the second-order method, e.g., Heun's method, Beeman's algorithm, etc, or a more reliable approximation of the curvature rate. Moreover, it is difficult to measure the lateral velocity of a vehicle, which is needed for the system inversion

in case of the extended look-ahead control in the global coordinate system. It is recommended to use an observer (see, e.g., Farrelly and Wellstead (1996), Park and Kim (1999), Pettersson (2008)) to estimate the lateral velocity of the vehicle.

Incorporating control reconfiguration methods for controller switching: The extended look-ahead approach in this thesis, which is based on the vehicle following approach, can be considered as an alternative control system in a case where the path information for the path following approach is not available. The main advantage of the vehicle following approach, as has been discussed in the previous chapters, is the cost-effectiveness and the ease in implementation. However, the proposed controller needs to be used in conjunction with other controllers, such as Electronic Stability Control (ESC), or Anti-lock Braking System (ABS), to ensure the stability of the vehicle. Thus, it is recommended to implement control reconfiguration methods as switching and decision mechanism between controllers.

Involving delays in communication: Throughout this thesis, it is assumed that the information from the V2V communication can be obtained without delays. Obviously, this will not be the case in practical implementation. As shown in experiments, delay in the Bluetooth communication affects the tracking accuracy of mobile robots. Moreover, string stability can be also affected by communication delays. It is recommended to consider a predictor based control for the time-delay nonlinear system, such as a Smith Predictor, along the lines of Alvarez Aguirre (2011), Chen and Serrani (2007), Oguchi and Nijmeijer (2005), Xing et al. (2019).

Incorporating heterogeneous vehicles in the platoon: It is assumed that the platoon consists of homogeneous vehicles, thus essentially assuming that identical control parameters can be applied, resulting in identical dynamic behavior. However, this is not the case in practical implementation. Therefore, the proposed control approach is required to be robust against these variations. The solution to this is to apply the low-level controller to achieve a near-identical behavior. The heterogeneity of vehicles in a platoon can be considered as a type of uncertainty, where the nominal system is homogeneous and the uncertainty is bounded (Zheng et al. (2019)). We recommend using a disturbance observer-based control approach to handle the uncertainty of the heterogeneous platoon.

Appendix to Chapter 3

A.1 Proof of Proposition 3.1

To prove Proposition 3.1, we first have to show that given the condition (3.12), the input (3.8) is well defined such that $z_{34,i}(t)$ remains bounded, using the following lemma.

Lemma A.1. *Let $z_{34,i} = [z_{3,i}, z_{4,i}]^T$, $\xi_i = [\xi_{1,i}, \xi_{2,i}]^T$, and consider the dynamics*

$$\dot{z}_{34,i} = - \begin{bmatrix} \frac{h_i v_i + r_i \cos^2 \theta_i}{h_i(r_i + h_i v_i)} & \frac{r_i \sin \theta_i \cos \theta_i}{h_i(r_i + h_i v_i)} \\ \frac{r_i \sin \theta_i \cos \theta_i}{h_i(r_i + h_i v_i)} & \frac{h_i v_i + r_i \sin^2 \theta_i}{h_i(r_i + h_i v_i)} \end{bmatrix} z_{34,i} + \xi_i, \tag{A.1}$$

with v_i and θ_i as in (3.1), and input ξ_i as a piecewise continuous function, bounded by $\|\xi_i\| \leq \xi_i^{\max}$. Let $\varepsilon > 0$ be given, and assume that $0 < \varepsilon < v_{i-1}^{\min} \leq v_{i-1}(t) \leq v_{i-1}^{\max}$.

1. *If*

$$\|z_{34,i}(0)\| \leq \left(\frac{r_i}{\varepsilon} + h_i \right) \xi_i^{\max} \leq v_{i-1}^{\min} - \varepsilon, \tag{A.2}$$

   then $v_i(t) \geq \varepsilon$.

2. *If, additionally,*

$$\lim_{t \to \infty} \|\xi_i(t)\| = 0, \tag{A.3}$$

   then $\lim_{t \to \infty} \|z_{34,i}(t)\| = 0$.

Proof. Consider the set $\Omega_c = \{\|z_{34,i}\| \leq v_{i-1}^{\min} - \varepsilon\}$. In Ω_c, we have

$$\varepsilon^2 \leq \left(v_{i-1}^{\min} - \|z_{34,i}\| \right)^2 \leq \left(v_{i-1} - \sqrt{z_{3,i}^2 + z_{4,i}^2} \right)^2$$

$$= v_{i-1}^2 - 2 v_{i-1} \sqrt{z_{3,i}^2 + z_{4,i}^2} + z_{3,i}^2 + z_{4,i}^2. \tag{A.4}$$

Define $c := [\cos \theta_{i-1}, \sin \theta_{i-1}]^T$. With this particular definition of c, while using the Cauchy-Schwarz inequality, we have

$$2 \|z_{34,i}\| \|c\| \geq \|z_{34,i} + c\|^2 - \|z_{34,i}\|^2 - \|c\|^2$$
$$2\sqrt{z_{3,i}^2 + z_{4,i}^2} \geq 2z_{3,i} \cos \theta_{i-1} + 2z_{4,i} \sin \theta_{i-1}. \tag{A.5}$$

Substituting (A.5) into (A.4), while using (3.5c) and (3.5d), yields

$$\varepsilon^2 \leq (v_{i-1} \cos \theta_{i-1} - z_{3,i})^2 + (v_{i-1} \sin \theta_{i-1} - z_{4,i})^2$$
$$\leq v_i^2, \tag{A.6}$$

which implies that inside Ω_c we have $v_i(t) \geq \varepsilon > 0$. Now we have to show that when a trajectory starts in Ω_c, i.e., $\|z_{34,i}(0)\| \leq v_{i-1}^{\min} - \varepsilon$, it will stay in Ω_c for all $t > 0$. Consider to this end a Lyapunov function $V = z_{3,i}^2 + z_{4,i}^2$. The derivative of V along the trajectory of the system (A.1) is then given by

$$\dot{V} = \phi + 2\xi_{1,i}z_{3,i} + 2\xi_{2,i}z_{4,i}, \tag{A.7}$$

with

$$\phi := -\frac{2v_i}{r_i + h_i v_i} \left(z_{3,i}^2 + z_{4,i}^2 + \frac{r_i}{h_i}(z_{3,i} \cos \theta_i + z_{4,i} \sin \theta_i)^2 \right).$$

Note that, since $v_i \geq \varepsilon > 0$, in the set Ω_c,

$$\phi \leq -\frac{2v_i}{r_i + h_i v_i}(z_{3,i}^2 + z_{4,i}^2) = -\frac{2v_i}{r_i + h_i v_i} \|z_{34,i}\|^2.$$

Moreover, by the Cauchy-Schwarz inequality we have

$$\|\xi_i + z_{34,i}\|^2 - \|\xi_i\|^2 - \|z_{34,i}\|^2 \leq 2 \|z_{34,i}\| \|\xi_i\|$$
$$2\xi_{1,i}z_{3,i} + 2\xi_{2,i}z_{4,i} \leq 2 \|z_{34,i}\| \|\xi_i\|.$$

Consequently,

$$\dot{V} \leq -\frac{2v_i}{r_i + h_i v_i} \|z_{34,i}\|^2 + 2 \|z_{34,i}\| \|\xi_i\|$$
$$= -\frac{v_i}{r_i + h_i v_i} \|z_{34,i}\|^2 - \frac{v_i}{r_i + h_i v_i} \left(\|z_{34,i}\| - \frac{r_i + h_i v_i}{v_i} \|\xi_i\| \right)^2 + \frac{r_i + h_i v_i}{v_i} \|\xi_i\|^2$$
$$\leq -\frac{v_i}{r_i + h_i v_i} \left(\|z_{34,i}\|^2 - \left(\frac{r_i + h_i v_i}{v_i} \xi_i^{\max} \right)^2 \right), \tag{A.8}$$

and it follows that the negative definiteness of $\dot{V}$ is determined by v_i and $\|z_{34,i}\|$. Note that by (A.2) and by the fact that $v_i \geq \varepsilon$, we have $(\frac{r_i}{v_i} + h_i)\xi_i^{\max} \leq (\frac{r_i}{\varepsilon} + h_i)\xi_i^{\max} \leq v_{i-1}^{\min} - \varepsilon$. Now let us consider two sets, $\Omega_u = \{\|z_{34,i}\| < (\frac{r_i}{v_i} + h_i)\xi_i^{\max}\}$ and $\Omega_s = \{(\frac{r_i}{v_i} + h_i)\xi_i^{\max} \leq \|z_{34,i}\| \leq v_{i-1}^{\min} - \varepsilon\}$. Inside Ω_u (which is a subset of Ω_c, according to condition (A.2)), we have $v_i \geq \varepsilon > 0$ and $\dot{V} > 0$. Consequently, a trajectory starting in Ω_u will move in a direction of increasing V until it reaches the lower bound $(\frac{r_i}{v_i} + h_i)\xi_i^{\max}$ of Ω_s. Inside Ω_s (which is also a subset of Ω_c), $v_i \geq \varepsilon > 0$ and it follows from (A.8) that $\dot{V}$ is negative in Ω_s. Hence, a trajectory

that starts in Ω_s will also converge to the lower bound of Ω_s. Since $v_i \geq \varepsilon$ implies that $(\frac{r_i}{v_i} + h_i)\xi_i^{\max} \leq (\frac{r_i}{\varepsilon} + h_i)\xi_i^{\max}$, we can conclude that for $\|z_{34,i}(0)\| \leq \left(\frac{r_i}{\varepsilon} + h_i\right)\xi_i^{\max} \leq v_{i-1}^{\min} - \varepsilon$ we have $\|z_{34,i}(t)\| \leq \left(\frac{r_i}{\varepsilon} + h_i\right)\xi_i^{\max} \leq v_{i-1}^{\min} - \varepsilon$.

Now we want to prove the second statement of Lemma A.1. Let $\lim_{t \to \infty} \|\xi_i(t)\| = 0$. Since $\|z_{34,i}(t)\|$ converges to $(\frac{r_i}{v_i} + h_i)\xi_i$ (which follows from (A.8) in the previous analysis), we have $\lim_{t \to \infty} \|z_{34,i}(t)\| = 0$. □

To conclude the proof, we have to show that ξ_i is bounded and converges to zero, given the condition (3.13). From (3.10), it can be observed that the boundedness of ξ_i depends on the boundedness of $H_{i-1}[a_{i-1}, \omega_{i-1}]^T$ (which is given by (3.12)), boundedness of G_i, and the initial condition $z_{12,i}(0)$. From (3.11), it can be observed that the Frobenius norm of G_i is bounded by $\|G_i\|_{\mathrm{F}} \leq 1/h_i$. By having sufficiently small initial velocity error $z_{34,i}(0)$, we can guarantee that all the future trajectories of $z_{34,i}(t)$ will be in the set Ω_s in which the velocity v_i is always positive, thus the input (3.8) is well defined. Since the input is well defined, then we also have $\lim_{t \to \infty} \|z_{12,i}(t)\| = 0$. In addition, under the condition (3.13) and sufficiently small initial position error $z_{12,i}(0)$, from (3.10) we have that ξ_i is bounded and converges to zero as $t \to \infty$. Therefore, by the second statement of Lemma A.1 it can be concluded that $\lim_{t \to \infty} \|z_{34,i}(t)\| = 0$.

A.2   Proof of Proposition 3.2

First we need to study the internal dynamics (3.38b). By substituting H_{i-1}, $\beta_{1,i}$, $\beta_{2,i}$, $\Gamma_{34,i}$, $\Gamma_{12,i}^{-1}$, separating the translational and rotational dynamics, and noting that $\omega_{i-1} = v_{i-1}\kappa_{i-1}$, we are able to rewrite (3.38b) into

$$\begin{bmatrix} \dot{z}_{3,i} \\ \dot{z}_{4,i} \end{bmatrix} = -G_i \begin{bmatrix} z_{3,i} \\ z_{4,i} \end{bmatrix} - \kappa_{i-1}\left(Q_i \begin{bmatrix} z_{3,i} \\ z_{4,i} \end{bmatrix} - f_{v,i}\right) + \zeta_i, \tag{A.9}$$

where

$$f_{v,i} = \begin{bmatrix} -v_{i-1}\sin\theta_{i-1} \\ v_{i-1}\cos\theta_{i-1} \end{bmatrix} v_{i-1} - \begin{bmatrix} -v_i\sin(\theta_i + \alpha) \\ v_i\cos(\theta_i + \alpha) \end{bmatrix} v_i \tag{A.10}$$

$$\zeta_i = h_{\kappa,i}\dot{\kappa}_{i-1} + \begin{bmatrix} \cos\theta_{i-1} \\ \sin\theta_{i-1} \end{bmatrix} a_{i-1} - \Gamma_{34,i}\Gamma_{12,i}^{-1} \begin{bmatrix} k_1 z_{1,i} \\ k_2 z_{2,i} \end{bmatrix} \tag{A.11}$$

$$h_{\kappa,i} = v_i(r + h_i v_i)\cos^2\alpha_i \begin{bmatrix} \sin(\theta_i + \alpha_i) \\ -\cos(\theta_i + \alpha_i) \end{bmatrix}$$
$$+ \frac{\cos\alpha_i - 1}{\kappa_{i-1}^2}\Gamma_{34}\Gamma_{12}^{-1} \begin{bmatrix} \sin\theta_{i-1} \\ -\cos\theta_{i-1} \end{bmatrix} \tag{A.12}$$

$$Q_i = \frac{r_i + h_i v_i}{\mu_i} \begin{bmatrix} q_{11} & q_{12} \\ q_{21} & q_{22} \end{bmatrix} \tag{A.13}$$

$$q_{11} = \cos \alpha_i \sin (\theta_{i-1} - \theta_i) \left(r_i \cos^2 \theta_i + h_i v_i\right)$$
$$+ h_i v_i \sin (\theta_i + \alpha_i) \left[\cos \theta_{i-1} - \cos \alpha_i \cos \theta_i\right] - r_i \sin \theta_i \cos \theta_i$$
$$q_{12} = \cos \alpha_i \sin (\theta_{i-1} - \theta_i) \left(r_i \sin \theta_i \cos \theta_i\right)$$
$$- h_i v_i \sin (\theta_i + \alpha_i) \left[- \sin \theta_{i-1} + \cos \alpha \sin \theta_i\right] - r_i \sin^2 \theta_i - h_i v_i$$
$$q_{21} = \cos \alpha_i \sin (\theta_{i-1} - \theta_i) \left(r_i \sin \theta_i \cos \theta_i\right)$$
$$- h_i v_i \cos (\theta_i + \alpha_i) \left[\cos \theta_{i-1} - \cos \alpha_i \cos \theta_i\right] + r_i \cos^2 \theta_i + h_i v_i$$
$$q_{22} = \cos \alpha_i \sin (\theta_{i-1} - \theta_i) \left(r_i \sin^2 \theta_i + h_i v_i\right)$$
$$+ h_i v_i \cos (\theta_i + \alpha_i) \left[- \sin \theta_{i-1} + \cos \alpha_i \sin \theta_i\right] + r_i \sin \theta_i \cos \theta_i,$$

with μ_i as in (3.37), and G_i as in (11). It can be observed that if the platoon maneuvers on a straight path (i.e., $\kappa_{i-1} = 0$ and $\omega_{i-1} = 0$), the subsystem (A.9) reduces to (9b), thus for tracking a straight path we can again use Proposition 3.1. The term ζ_i can be considered as external inputs that are decaying to zero. Given that κ_{i-1} is bounded by (3.39) and the condition (3.40) is satisfied, we first prove that the subsystem (A.9) is stable by the following lemma.

Lemma A.2. *Let* $z_{34,i} = [z_{3,i}, z_{4,i}]^T$, $\zeta_i = [\zeta_{1,i}, \zeta_{2,i}]^T$, *and consider the dynamics (A.9) where* κ_{i-1} *is bounded by (3.39) and input* ζ_i *is a continuous function, bounded by* $\|\zeta_i\| \leq \zeta_i^{\max}$. *Let* $\varepsilon > 0$ *be given, and assume that* $0 < \varepsilon < v_{i-1}^{\min} \leq v_{i-1}(t) \leq v_{i-1}^{\max}$.

1. *If*
$$\|z_{34,i}(0)\| \leq 2 \left(\frac{r_i}{\varepsilon} + h_i\right) \zeta_i^{\max} \leq v_{i-1}^{\min} - \varepsilon, \tag{A.14}$$

   then $v_i(t) \geq 0$.

2. *If, additionally,*
$$\lim_{t \to \infty} \|\zeta_i(t)\| = 0, \tag{A.15}$$

   then $\lim_{t \to \infty} \|z_{34,i}(t)\| = 0$.

Proof. Let us consider the set $\Omega_c = \left\{\|z_{34,i}\| \leq v_{i-1}^{\min} - \varepsilon\right\}$, with $\varepsilon > 0$. Inside Ω_c, we have

$$\varepsilon^2 \leq \left(v_{i-1}^{\min} - \|z_{34,i}\|\right)^2 \leq \left(v_{i-1} - \sqrt{z_{3,i}^2 + z_{4,i}^2}\right)^2$$
$$= v_{i-1}^2 - 2 v_{i-1} \sqrt{z_{3,i}^2 + z_{4,i}^2} + z_{3,i}^2 + z_{4,i}^2$$
$$\leq \left(v_{i-1} \cos \theta_{i-1} - z_{3,i}\right)^2 + \left(v_{i-1} \sin \theta_{i-1} - z_{4,i}\right)^2$$
$$= v_i^2. \tag{A.16}$$

Moreover, it directly follows from (3.19c) and (3.19d) that

$$
\begin{aligned}
v_i^2 &= (v_{i-1}\cos\theta_{i-1} - z_{3,i})^2 + (v_{i-1}\sin\theta_{i-1} - z_{4,i})^2 \\
&= v_{i-1}^2 - 2v_{i-1}z_{3,i}\cos\theta_{i-1} - 2v_{i-1}z_{4,i}\sin\theta_{i-1} + \|z_{34,i}\|^2 \\
&\le v_{i-1}^2 + v_{i-1}^2\cos^2\theta_{i-1} + z_{3,i}^2 + v_{i-1}^2\sin^2\theta_{i-1} + z_{4,i}^2 + \|z_{34,i}\|^2 \\
&= 2v_{i-1}^2 + 2\|z_{34,i}\|^2 \le 2\left(v_{i-1} + \|z_{34,i}\|\right)^2.
\end{aligned}
\tag{A.17}
$$

As a result from (A.16) and (A.17), v_i is bounded by

$$
0 < \varepsilon \le v_i \le \sqrt{2}\left(v_{i-1}^{\max} + v_{i-1}^{\min} - \varepsilon\right)
\tag{A.18}
$$

in Ω_c. Now consider a quadratic Lyapunov function $V = z_{3,i}^2 + z_{4,i}^2$. By using (3.19c, 3.19d), we can rewrite $f_{v,i}$ in (A.10) as

$$
f_{v,i} = \begin{bmatrix} -v_{i-1}\sin\theta_{i-1} \\ v_{i-1}\cos\theta_{i-1} \end{bmatrix}(v_{i-1} - v_i) + v_i\begin{bmatrix} -z_{4,i} \\ z_{3,i} \end{bmatrix},
\tag{A.19}
$$

such that the derivative of V along the trajectory (A.9) is given by

$$
\begin{aligned}
\dot{V} = &-2\begin{bmatrix} z_{3,i} \\ z_{4,i} \end{bmatrix}^T G_i \begin{bmatrix} z_{3,i} \\ z_{4,i} \end{bmatrix} - 2\kappa_{i-1}\begin{bmatrix} z_{3,i} \\ z_{4,i} \end{bmatrix}^T Q_i \begin{bmatrix} z_{3,i} \\ z_{4,i} \end{bmatrix} \\
&+ 2\kappa_{i-1}(v_{i-1} - v_i)\begin{bmatrix} z_{3,i} \\ z_{4,i} \end{bmatrix}^T \begin{bmatrix} -v_{i-1}\sin\theta_{i-1} \\ v_{i-1}\cos\theta_{i-1} \end{bmatrix} + 2\begin{bmatrix} \zeta_{i,i} \\ \zeta_{i,2} \end{bmatrix}^T \begin{bmatrix} z_{3,i} \\ z_{4,i} \end{bmatrix}.
\end{aligned}
\tag{A.20}
$$

By substituting G_i and Q_i into (A.20) and by noting that

$$
\sin\alpha_i = \kappa_{i-1}(r_i + h_i v_i)\cos\alpha_i,
$$

which directly follows from (3.21) and (3.22), we can rewrite $\dot{V}$ as

$$
\begin{aligned}
\dot{V} = &-\tfrac{2v_i}{\gamma_i(r_i + h_i v_i)}\left(z_{3,i}^2 + z_{4,i}^2 + \tfrac{r_i}{h_i v_i}(z_{3,i}\cos\theta_i + z_{4,i}\sin\theta_i)^2\right) \\
&+ \tfrac{2r_i\kappa_{i-1}}{\gamma_i h_i}(z_{3,i}\sin\theta_i - z_{4,i}\cos\theta_i)(z_{3,i}\cos\theta_i + z_{4,i}\sin\theta_i) \\
&- \tfrac{2v_i\kappa_{i-1}}{\gamma_i}f_{34,i}(z_{3,i}\cos\theta_{i-1} + z_{4,i}\sin\theta_{i-1}) \\
&+ \tfrac{2v_i\kappa_{i-1}\cos\alpha_i}{\gamma_i}f_{34,i}(z_{3,i}\cos\theta_i + z_{4,i}\sin\theta_i) \\
&+ 2\kappa_{i-1}v_{i-1}(v_{i-1} - v_i)(-z_{3,i}\sin\theta_{i-1} + z_{4,i}\cos\theta_{i-1}) \\
&+ 2\zeta_{1,i}z_{3,i} + 2\zeta_{2,i}z_{4,i},
\end{aligned}
\tag{A.21}
$$

where

$$
f_{34,i} = (z_{3,i}\sin(\theta_i + \alpha_i) - z_{4,i}\cos(\theta_i + \alpha_i))
\tag{A.22}
$$
$$
\gamma_i = 1 - \sin\alpha_i\sin(\theta_{i-1} - \theta_i).
\tag{A.23}
$$

Note that we can also apply the Cauchy-Schwarz inequality (in the same manner as (A.5)) to all terms in (A.21) that are dependent on $z_{3,i}$ and $z_{4,i}$. As a result,

those terms are always less than or equal to $\|z_{34,i}\|$. Moreover, by applying the inequality to (3.19c) and (3.19d) we also have $v_{i-1} - v_i \leq \|z_{34,i}\|$. Since $\gamma_i \leq 2$ by definition (A.23), it follows from (A.8) that

$$
\begin{aligned}
\dot{V} \leq &- \left(\tfrac{v_i}{r_i + h_i v_i} \right) \|z_{34,i}\|^2 - \kappa_{i-1} \left(-\tfrac{r_i}{h_i} \right) \|z_{34,i}\|^2 \\
&- v_i \kappa_{i-1} \|z_{34,i}\|^2 + v_i \kappa_{i-1} \cos \alpha_i \|z_{34,i}\|^2 \\
&+ 2\kappa_{i-1} v_{i-1} \|z_{34,i}\|^2 + 2 \|z_{34,i}\| \|\zeta_i\| ,
\end{aligned} \tag{A.24}
$$

and we need to show that $\dot{V} \leq 0$. Let us denote

$$
\Delta_i = \tfrac{v_i}{2(r_i + h_i v_i)} + \kappa_{i-1} \left(-\tfrac{r_i}{h_i} + v_i \left(1 - \cos \alpha_i \right) - 2v_{i-1} \right), \tag{A.25}
$$

such that we can rewrite (A.24) as

$$
\begin{aligned}
\dot{V} \leq &- \Delta_i \|z_{34,i}\|^2 - \tfrac{v_i}{2(r_i + h_i v_i)} \|z_{34,i}\|^2 + 2 \|z_{34,i}\| \|\zeta_i\| \\
= &- \Delta_i \|z_{34,i}\|^2 - \tfrac{v_i}{4(r_i + h_i v_i)} \|z_{34,i}\|^2 + \tfrac{4(r_i + h_i v_i)}{v_i} \|\zeta_i\|^2 \\
&- \tfrac{v_i}{4(r_i + h_i v_i)} \left(\|z_{34,i}\| - \tfrac{4(r_i + h_i v_i)}{v_i} \|\zeta_i\| \right)^2 \\
\leq &- \Delta_i \|z_{34,i}\|^2 - \tfrac{v_i}{4(r_i + h_i v_i)} \left[\|z_{34,i}\|^2 - \left(\tfrac{4(r_i + h_i v_i)}{v_i} \zeta_i^{\max} \right)^2 \right] ,
\end{aligned} \tag{A.26}
$$

and it follows that the negative definiteness of $\dot{V}$ is determined by v_i, $\|z_{34,i}\|$, and Δ_i. First we want to analyze the term Δ_i. Note that by using (3.22), and by using a Taylor expansion we can bound the term $(1 - \cos \alpha_i)$ by

$$
\begin{aligned}
1 - \cos \alpha_i &= \frac{\sqrt{1 + \kappa_{i-1}^2 \left(r_i + h_i v_i \right)^2} - 1}{\sqrt{1 + \kappa_{i-1}^2 \left(r_i + h_i v_i \right)^2}} \\
&\leq \frac{1}{2} \kappa_{i-1}^2 \left(r_i + h_i v_i \right)^2 .
\end{aligned} \tag{A.27}
$$

Moreover, due to the fact that $v_{i-1} \geq v_{i-1}^{\min} > 0$, it follows from (A.25) that

$$
v_i - 2 \left| \kappa_{i-1} \right| \left(r_i + h_i v_i \right) \left(-\tfrac{r_i}{h_i} + \tfrac{1}{2} v_i \left| \kappa_{i-1} \right|^2 \left(r_i + h_i v_i \right)^2 \right) > 0 \tag{A.28}
$$

is a sufficient condition for the first term in (A.26) to be negative. Using condition (3.39) and the bound of v_i from (A.18), we have

$$
\left| \kappa_{i-1} \right| \leq \frac{1}{r_i + h_i \sqrt{2} \left(v_{i-1}^{\max} + v_{i-1}^{\min} - \varepsilon \right)} \leq \frac{1}{r_i + h_i v_i}, \tag{A.29}
$$

where the second inequality follows from the upper bound of v_i in (A.18). By substituting (A.29) into (A.28), we obtain

$$
v_i - 2 \left(-\tfrac{r_i}{h_i} + \tfrac{1}{2} v_i \right) = \tfrac{2r_i}{h_i} > 0,
$$

from which we can conclude that Δ_i is positive for all κ_{i-1} satisfying (3.39). Now we want to show that the second term of (A.26) is negative. Note by (A.14) and by the fact that $v_i \geq \varepsilon$ from (A.18), we have $2(\frac{r_i}{v_i} + h_i)\zeta_i^{\max} \leq 2\left(\frac{r_i}{\varepsilon} + h_i\right)\zeta_i^{\max} \leq v_{i-1}^{\min} - \varepsilon$. Now let us consider two subsets of Ω_c, denote by $\Omega_u = \{\|z_{34,i}\| < 2(\frac{r_i}{v_i} + h_i)\zeta_i^{\max}\}$ and $\Omega_s = \{2(\frac{r_i}{v_i} + h_i)\zeta_i^{\max} \leq \|z_{34,i}\| \leq v_{i-1}^{\min} - \varepsilon\}$. By using the same reasoning as Lemma A.1, we can also conclude that for $\|z_{34,i}(0)\| \leq 2\left(\frac{r_i}{\varepsilon} + h_i\right)\zeta_i^{\max} \leq v_{i-1}^{\min} - \varepsilon$ we have $\|z_{34,i}(t)\| \leq 2\left(\frac{r_i}{\varepsilon} + h_i\right)\zeta_i^{\max} \leq v_{i-1}^{\min} - \varepsilon$, given that κ_{i-1} is strictly bounded by (3.39).

The second statement of Lemma A.2 can be proven directly using the same reasoning as the one in Lemma A.1. $\square$

From Lemma A.2, we have the result that the subsystem (A.9) is stable, under the condition that κ_{i-1} is bounded, and also under the condition that ζ_i is bounded by

$$\zeta_i(t) \leq \frac{v_{i-1}^{\min} - \varepsilon}{2\left(\frac{r_i}{\varepsilon} + h_i\right)}, \tag{A.30}$$

with ζ_i as in (A.11), and can be considered as external inputs that are decaying to zero. To conclude the stability proof of this system, we need to check the boundedness of $\Gamma_{34,i}\Gamma_{12,i}^{-1}$ and $h_{\kappa,i}$. From (3.21) and (3.22), we have

$$\cos^2 \alpha_i = \frac{\sin \alpha_i \cos \alpha_i}{\kappa_{i-1}\left(r_i + h_i v_i\right)}. \tag{A.31}$$

Substituting (A.31) into δ_i in (3.31) and taking (3.30) into account, we eventually obtain $\Gamma_{34,i}\Gamma_{12,i}^{-1}$ as

$$\Gamma_{34}\Gamma_{12}^{-1} = \frac{1}{\mu_i}\begin{bmatrix} \gamma_{11} & \gamma_{12} \\ \gamma_{21} & \gamma_{22} \end{bmatrix}, \tag{A.32}$$

with

$$\gamma_{11} = (r_i + h_i v_i)\cos\theta_i\cos(\theta_i + \alpha_i) + h_i v_i\sin(\theta_i + \alpha_i)p_1$$
$$\gamma_{12} = (r_i + h_i v_i)\sin\theta_i\cos(\theta_i + \alpha_i) - h_i v_i\sin(\theta_i + \alpha_i)p_2$$
$$\gamma_{21} = (r_i + h_i v_i)\cos\theta_i\sin(\theta_i + \alpha_i) - h_i v_i\cos(\theta_i + \alpha_i)p_1$$
$$\gamma_{22} = (r_i + h_i v_i)\sin\theta_i\sin(\theta_i + \alpha_i) + h_i v_i\cos(\theta_i + \alpha_i)p_2$$
$$p_1 = \sin\theta_i + \sin\alpha_i\cos\theta_{i-1} - \sin\alpha_i\cos\alpha_i\cos\theta_i$$
$$p_2 = \cos\theta_i - \sin\alpha_i\sin\theta_{i-1} + \sin\alpha_i\cos\alpha_i\sin\theta_i,$$

and μ_i as in (3.37). Applying the fact that $(1 - \sin\alpha_i\sin(\theta_{i-1} - \theta_i)) \leq 2$ into μ_i, we have

$$\left\|\Gamma_{34,i}\Gamma_{12,i}^{-1}\right\|_2 \leq \left\|\Gamma_{34,i}\Gamma_{12,i}^{-1}\right\|_F \leq \frac{2}{h_i}, \tag{A.33}$$

where $\|\cdot\|_F$ is the Frobenius norm. Thus, $\Gamma_{34,i}\Gamma_{12,i}^{-1}$ is bounded. Now we want to show that $h_{\kappa,i}$ is also bounded. Note that by substituting (3.22) and (A.27) into

(A.12), we can rewrite $h_{\kappa,i}$ as

$$h_{\kappa,i} \le \frac{v_i \left(r_i + h_i v_i \right)}{1 + \kappa_{i-1}^2 \left(r_i + h_i v_i \right)^2} \begin{bmatrix} \sin \left(\theta_i + \alpha_i \right) \\ -\cos \left(\theta_i + \alpha_i \right) \end{bmatrix}$$
$$+ \frac{1}{2} \left(r_i + h_i v_i \right)^2 \Gamma_{34} \Gamma_{12}^{-1} \begin{bmatrix} \sin \theta_{i-1} \\ -\cos \theta_{i-1} \end{bmatrix}. \tag{A.34}$$

By substituting (A.33) into (A.34), for a trajectory starting in Ω_c (which follows from (A.18)) we obtain

$$\|h_{\kappa,i}\|_2 \le v_i \left(r_i + h_i v_i \right) - \frac{1}{h} \left(r_i + h_i v_i \right)^2$$
$$\le \frac{r_i^2}{h_i} + h_i \sqrt{2} \left(v_{i-1}^{\max} + v_{i-1}^{\min} - \varepsilon \right) = h_{\kappa,i}^{\max}. \tag{A.35}$$

Since we have that $\dot{\kappa}_{i-1}$, a_{i-1} and $z_{12,i}$ converge to zero as $t \to \infty$, thus we have $\lim_{t\to\infty} \|z_{34,i}(t)\| = 0$.

Appendix to Chapter 4

B.1 Derivation of equilibrium point δ

In this appendix we show the derivation in obtaining the equilibrium point of δ. Consider $\delta = \theta - \theta_r + \alpha_r$, as in (4.14). By differentiating it with respect to time, we obtain

$$\dot{\delta} = \omega - \omega_r + \dot{\alpha}_r. \tag{B.1}$$

Substituting ω as in (4.17) and (4.7) into (B.1) eventually yields

$$\dot{\delta} = -\left(1 - \cos\delta\right)\omega_r - \frac{v_r}{d}\sin\delta + \zeta_r, \tag{B.2}$$

where

$$\zeta_r = \frac{k_1 \sin\delta}{d} z_1 - \frac{k_2 \cos\delta}{d} z_2 + \left(\frac{h_{\kappa,1}}{d}\sin\delta - \frac{h_{\kappa,2}}{d}\cos\delta + \frac{2d}{\sqrt{4 - d^2\kappa_r^2}}\right)\dot{\kappa}_r, \tag{B.3}$$

(z_1, z_2) as in (4.12), and $(h_{\kappa,1}, h_{\kappa,2})$ as in (4.16). In a steady state condition, which implies that $z_1 = z_2 = 0$ and $\dot{\kappa}_r = 0$, we have

$$\dot{\delta} = -\left(1 - \cos\delta\right)\omega_r - \frac{v_r}{d}\sin\delta. \tag{B.4}$$

By noting that $\kappa_r = \omega_r/v_r$ and $\sin^2\delta = 1 - \cos^2\delta$, the equilibrium points of (B.4) are determined by

$$\left(1 + d^2\kappa_r^2\right)\cos^2\delta - 2d^2\kappa_r^2\cos\delta + \left(d^2\kappa_r^2 - 1\right) = 0,$$

and given by

$$\delta^\star = 2n\pi \tag{B.5}$$

$$\delta^\star = \arctan\left(\frac{-2d\kappa_r}{d^2\kappa_r^2 - 1}\right) + 2n\pi, \tag{B.6}$$

where $n = 0, \pm 1, \pm 2, \ldots$.

B.2 Derivation of β

In this appendix we show how β is derived mathematically, such that z_3 has equilibrium points at $[0, \pi]$. Consider

$$z_3 = \theta - \theta_r + \alpha_r + \beta, \tag{B.7}$$

where $\beta : [-2\pi, 2\pi] \to [-1, 1]$. Taking the input ω as in (4.17) into account, the derivative of z_3 is given by

$$
\begin{aligned}
\dot{z}_3 = &-\frac{1}{d} \sin\left(\theta - \theta_r + \alpha\right) \left(-k_1 z_1 + v_r - \dot{\kappa}_r h_{\kappa,1}\right) \\
&+ \frac{1}{d} \cos\left(\theta - \theta_r + \alpha\right) \left(-k_2 z_2 + d\omega_r - \dot{\kappa}_r h_{\kappa,2}\right) \\
&- \omega_r + \dot{\alpha}_r + \dot{\beta}.
\end{aligned} \tag{B.8}
$$

In the equilibrium we have

$$\dot{z}_3 = -\frac{v_r}{d} \sin\left(z_3 - \beta\right) + \omega_r \cos\left(z_3 - \beta\right) - \omega_r, \tag{B.9}$$

and we want $\dot{z}_3 = 0$ for $z_3 = 0$ and $z_3 = \pi$, i.e.,

$$
\begin{aligned}
z_3 = 0 \qquad &\Rightarrow \sin\beta = -d\kappa_r \cos\beta + d\kappa_r \\
z_3 = \pi \qquad &\Rightarrow \sin\beta = -d\kappa_r \cos\beta - d\kappa_r
\end{aligned}
$$

which can be rewritten as

$$\sin\beta = d\kappa_r \cos z_3 - d\kappa_r \cos\beta. \tag{B.10}$$

By substituting (B.7) into (B.10), and noting that $\delta = \theta - \theta_r + \alpha_r$, we have

$$
\begin{aligned}
\sin\beta &= d\kappa_r \left(\cos\delta \cos\beta - \sin\delta \sin\beta - \cos\beta\right) \\
\sin\beta \left(1 + d\kappa_r \sin\delta\right) &= \cos\beta \left(d\kappa_r \cos\delta - d\kappa_r\right) \\
\frac{\sin\beta}{\cos\beta} &= \frac{d\kappa_r \cos\delta - d\kappa_r}{1 + d\kappa_r \sin\delta},
\end{aligned} \tag{B.11}
$$

resulting in $\sin\beta$ and $\cos\beta$ as in (4.21a) and (4.21b).

B.3 Boundedness of $\bar{v}_r$ and ξ_r

In this section the claim on the boundedness of $\bar{v}_r$ and ξ_r is proven.

Proof. First we want to show the lower and upper bound of $\bar{v}_r$. We can rewrite (4.29) as

$$
\begin{aligned}
\Delta &= d^2 \kappa_r^2 \left(1 - \cos\delta\right)^2 + \left(1 + d\kappa_r \sin\delta\right)^2 \\
&= 2d^2 \kappa_r^2 \left(1 - \cos\delta\right) + 2d\kappa_r \sin\delta + 1 \tag{B.12} \\
&= 2d^2 \kappa_r^2 + 1 + 2\left(d\kappa_r \sin\delta - d^2 \kappa_r^2 \cos\delta\right). \tag{B.13}
\end{aligned}
$$

To obtain the lower- and upper-bound of Δ, let us define an angle γ, characterized by $\sin\gamma = d\kappa_r/\sqrt{d^2\kappa_r^2+1}$ and $\cos\gamma = 1/\sqrt{d^2\kappa_r^2+1}$ such that we can write (B.13) as

$$\Delta = 2d^2\kappa_r^2 + 1 + 2d\kappa_r\sqrt{d^2\kappa_r^2+1}\left(\cos\gamma\sin\delta - \sin\gamma\cos\delta\right)$$
$$= 2d^2\kappa_r^2 + 1 + 2d\kappa_r\sqrt{d^2\kappa_r^2+1}\left(\sin\left(\delta-\gamma\right)\right).$$

Since $|\sin\left(\delta-\gamma\right)| \le 1$, we have

$$\Delta \ge 2d^2\kappa_r^2 + 1 - 2\left|d\kappa_r\sqrt{d^2\kappa_r^2+1}\right| \text{ and}$$
$$\Delta \le 2d^2\kappa_r^2 + 1 + 2\left|d\kappa_r\sqrt{d^2\kappa_r^2+1}\right|$$
$$\Rightarrow 3 - 2\sqrt{2} \le \Delta \le 3 + 2\sqrt{2}, \tag{B.14}$$

as the lower- and upper-bound of Δ, where the extreme value is obtained for $|d\kappa_r| = 1$. To show that $N > 0$, note that we can rewrite (4.28) as

$$N = \frac{1}{4}d^2\kappa_r^2\left(3 - \cos\delta\right)\left(1 - \cos\delta\right) + \left(1 + \frac{1}{2}d\kappa_r\sin\delta\right)^2. \tag{B.15}$$

Since $N > 0$, by taking (B.12) into account, we can also rewrite (4.28) as

$$N = \sqrt{\left(d^2\kappa_r^2\left(1 - \cos\delta\right) + d\kappa_r\sin\delta + 1\right)^2}$$
$$= \sqrt{\Delta + \left(d^2\kappa_r^2\left(1 - \cos\delta\right) + d\kappa_r\sin\delta\right)^2}. \tag{B.16}$$

Moreover, since $\Delta > 0$ (which follows directly from (4.29)), by substituting (B.16) into (4.26) we obtain

$$\bar{v}_r = v_r\sqrt{1 + \frac{1}{\Delta}\left(d^2\kappa_r^2\left(1 - \cos\delta\right) + d\kappa_r\sin\delta\right)^2}$$
$$= v_r\sqrt{1 + \frac{(N-1)^2}{\Delta}} \ge v_r, \tag{B.17}$$

which is the lower bound of $\bar{v}_r$. Note also that by using (B.12), we can rewrite N as

$$N = \frac{1}{2}\left(\Delta + 1\right). \tag{B.18}$$

By substituting (B.18) into (B.17), and taking the upper bound of Δ in (B.14) into account, we eventually obtain

$$\bar{v}_r = v_r\sqrt{\frac{(\Delta+1)^2}{4\Delta}} \le v_r\sqrt{2}, \tag{B.19}$$

which is the upper bound of $\bar{v}_r$.

To show the upper bound of ξ_r, note that we can rewrite N/Δ as

$$
\begin{aligned}
\frac{N}{\Delta} &= \frac{d^2 \kappa_r^2 \left(1 - \cos\delta\right) + d\kappa_r \sin\delta + 1}{2d^2 \kappa_r^2 \left(1 - \cos\delta\right) + 2d\kappa_r \sin\delta + 1} \\
&= \tfrac{1}{2}\left(1 + \tfrac{1}{\Delta}\right) \le \tfrac{1}{2}\left(1 + \tfrac{1}{\Delta^{\min}}\right) \\
&\le \tfrac{1}{2}\left(1 + \tfrac{1}{3-2\sqrt{2}}\right) = \frac{2 - \sqrt{2}}{3 - 2\sqrt{2}} = 2 + \sqrt{2},
\end{aligned}
\tag{B.20}
$$

where we use the lower bound of Δ in (B.14). Moreover, we also have

$$
|g_\kappa| = \left| \frac{N}{\Delta} f_r \left(\delta, d, \kappa_r\right) - \frac{d\left(1 - \cos\delta\right)}{\Delta} \right| < \frac{7}{9}d,
\tag{B.21}
$$

where the bound on $|g_\kappa|$ is obtained by evaluating the function and the maximum value is obtained for $\kappa_r = 1/d$ and $\delta = \frac{3}{4}\pi$. By using the triangle inequality and substituting (B.20), (B.21) into (4.27), we have

$$
\begin{aligned}
\xi_r &= \frac{N}{\Delta d}\begin{bmatrix} \sin\delta & -\cos\delta \end{bmatrix}\begin{bmatrix} k_1 z_1 \\ k_2 z_2 \end{bmatrix} + g_\kappa \dot{\kappa}_r \\
|\xi_r| &\le \tfrac{2+\sqrt{2}}{d}\left(k_1 \left|z_1\right| + k_2 \left|z_2\right|\right) + \tfrac{7}{9}d\left|\dot{\kappa}_r\right|,
\end{aligned}
\tag{B.22}
$$

which is the bound of $|\xi_r|$. $\qquad\square$

B.4   Proof of Proposition 4.1

Proof. From (4.19), we have $\|z_{12}(t)\| \le \|z_{12}(0)\|$. Since $|\dot{\kappa}_r(t)| \le K$, from (4.33) we have

$$
\begin{aligned}
|\xi_r(t)| &\le \tfrac{2+\sqrt{2}}{d}\sqrt{k_1^2 + k_2^2}\,\|z_{12}(t)\| + \tfrac{7d}{9}K \\
&\le \tfrac{2+\sqrt{2}}{d}\sqrt{k_1^2 + k_2^2}\,\|z_{12}(0)\| + \tfrac{7d}{9}K \\
&\le \tfrac{v_r^{\min}}{d}\varepsilon + \tfrac{7d}{9}K =: \xi_r^{\max},
\end{aligned}
\tag{B.23}
$$

where we use (4.34). Consider a positive-definite function

$$
V_3(z_3) = 1 - \cos z_3.
\tag{B.24}
$$

The time derivative of $V_3(z_3)$ along the trajectory (4.24), by taking (4.32) into account, is given by

$$
\begin{aligned}
\dot{V}_3\left(z_3\right) &= -\frac{\bar{v}_r}{d}\sin^2 z_3 + \xi_r \sin z_3 \\
&\le -\frac{v_r}{d}\sin^2 z_3 + |\xi_r|\,|\sin z_3| \\
&\le -\tfrac{v_r^{\min}}{2d}\left[\sin^2 z_3 + \left(|\sin z_3| - \tfrac{d}{v_r^{\min}}\,|\xi_r|\right)^2 - \left(\tfrac{d}{v_r^{\min}}\,|\xi_r|\right)^2\right] \\
&\le -\tfrac{v_r^{\min}}{2d}\left[\sin^2 z_3 - \left(\tfrac{d}{v_r^{\min}}\,|\xi_r|\right)^2\right].
\end{aligned}
\tag{B.25}
$$

Let us define $\Omega_u = \{z_3 \in \mathbb{R} \mid |\sin z_3| \leq \frac{d}{v_r^{\min}} \xi_r^{\max}\}$, where $\xi_r^{\max}$ is as defined in (B.23). By noting that $|\xi_r(t)| \leq \xi_r^{\max}$, solutions starting outside Ω_u move in the direction of decreasing V_3, since $\dot{V}_3 < 0$ outside Ω_u, and eventually will be inside and cannot leave Ω_u as $t \to \infty$, which corresponds to (4.35) when substituting $\xi_r^{\max}$ from (B.23) in the definition for Ω_u. This proves claim (a).

Moreover, for

$$\lim_{t \to \infty} z_1(t) = 0, \qquad \lim_{t \to \infty} z_2(t) = 0, \qquad \lim_{t \to \infty} \dot{\kappa}_r(t) = 0,$$

we have $\xi_r(t) \to 0$ as $t \to \infty$, according to (4.33). From claim (a), we have that any solution of z_3 will be inside and cannot leave Ω_u as $t \to \infty$, which means that $\sin z_3(t) \to \frac{d}{v_r^{\min}} \xi_r(t)$ as $t \to \infty$. Since $d > 0$, $v_r^{\min} > 0$, we have $\sin z_3(t)$ converges to zero if and only if $\xi_r(t)$ converges to zero, hence proving claim (b).

It is important to note that for a platoon with more than 2 vehicles, $v(t)$ will become the reference for the next vehicle. Thus, we also need the condition of $v(t) \geq v^{\min} > 0$. From (4.37) we have $|\sin z_3(0)| \leq \frac{7}{18} - \frac{8}{27}\varepsilon$, so using (4.38), we start in the set Ω_u and stay in the set Ω_u, which implies $|\sin z_3(t)| \leq \frac{7}{18} - \frac{8}{27}\varepsilon$ and $\cos z_3(t) \geq \sqrt{1 - \left(\frac{7}{18} - \frac{8}{27}\varepsilon\right)^2} > 0$ for all $t \geq 0$.

From (4.17), we have

$$v = v_r \left(\cos \delta + d\kappa_r \sin \delta\right) - \left(k_1 z_1 \cos \delta + k_2 z_2 \sin \delta\right)$$
$$- \dot{\kappa}_r \left(h_{\kappa,1} \cos \delta + h_{\kappa,2} \sin \delta\right). \tag{B.26}$$

Let us denote $\eta := \cos \delta + d\kappa_r \sin \delta$. Note that by using (4.22) we have

$$\eta = \cos z_3 \sqrt{d^2 \kappa_r^2 \left(1 - \cos \delta\right)^2 + \left(1 + d\kappa_r \sin \delta\right)^2}$$
$$= \cos z_3 \sqrt{2d\kappa_r \left(d\kappa_r - d\kappa_r \cos \delta + \sin \delta\right) + 1}$$
$$= \sqrt{2d\kappa_r \sin z_3 \cos z_3 \eta + \cos^2 z_3}. \tag{B.27}$$

By noting that $|\kappa_r| < 1/d$, we solve (B.27) with respect to η as

$$\eta = \cos z_3 \left(d\kappa_r \sin z_3 + \sqrt{d^2 \kappa_r^2 \sin^2 z_3 + 1}\right)$$
$$\geq \left(-1 + \sqrt{2}\right) \cos z_3. \tag{B.28}$$

Moreover, from (4.16) we have

$$|h_{\kappa,1}| \leq \frac{d^2}{2\sqrt{3}} =: h_{\kappa,1}^{\max} \tag{B.29a}$$

$$|h_{\kappa,2}| \leq d^2 \left(\frac{4 - \sqrt{3}}{2\sqrt{3}}\right) =: h_{\kappa,2}^{\max}. \tag{B.29b}$$

Thus, from (B.26), by substituting (4.37), (4.38), and (B.29), we obtain

$$
\begin{aligned}
v(t) &\geq v_r \left(-1 + \sqrt{2} \right) \cos z_3(t) - \sqrt{k_1^2 + k_2^2} \, \| z_{12}(t) \| \\
&\quad - K \sqrt{ \left| h_{\kappa,1}^{\max} \right|^2 + \left| h_{\kappa,2}^{\max} \right|^2 } \\
&\geq v_r^{\min} \left(-1 + \sqrt{2} \right) \sqrt{ 1 - \left(\tfrac{7}{18} - \tfrac{8}{27}\varepsilon \right)^2 } - \tfrac{v_r^{\min}\varepsilon}{2+\sqrt{2}} \\
&\quad - v_r^{\min} \left(\tfrac{1}{2} - \tfrac{5}{3}\varepsilon \right) \sqrt{ \tfrac{5 - 2\sqrt{3}}{3} } \\
&\geq \varepsilon v_r^{\min},
\end{aligned}
\tag{B.30}
$$

i.e., for $|\dot{\kappa}_r(t)| \leq K$, where K is given in (4.38), we have $v(t) \geq \varepsilon v_r^{\min} > 0$. Moreover, due to $\cos z_3(t) \geq \sqrt{ 1 - \left(\tfrac{7}{18} - \tfrac{8}{27}\varepsilon \right)^2 } > 0$ for all $t \geq 0$, we can guarantee that $z_3(t)$ does not converge to π. Thus, the claim of $\sin z_3(t) \to 0$ also implies that $z_3(t) \to 0$ (modulo 2π), as $t \to \infty$. This proves claim (c). $\qquad\square$

B.5 Proof of Proposition 4.2

Proof. Let $\zeta = (\zeta_x, \zeta_y, \zeta_c, \zeta_s)$. Differentiating the positive definite Lyapunov function candidate

$$
V_1(\zeta) = \frac{l_3}{2}\zeta_x^2 + \frac{l_4}{2}\zeta_y^2 + \frac{1}{2}\zeta_c^2 + \frac{1}{2}\zeta_s^2,
\tag{B.31}
$$

along solutions of (4.42) results in

$$
\begin{aligned}
\dot{V}_1(\zeta) &= l_3 \zeta_x v \zeta_c - l_1 l_3 \zeta_x^2 + l_4 \zeta_y v \zeta_s - l_2 l_4 \zeta_y^2 \\
&\quad - \omega \zeta_c \zeta_s - l_3 v \zeta_x \zeta_c + \omega \zeta_c \zeta_s - l_4 v \zeta_y \zeta_s \\
&= -l_1 l_3 \zeta_x^2 - l_2 l_4 \zeta_y^2 \leq 0,
\end{aligned}
\tag{B.32}
$$

which is negative semi-definite. We can conclude that the origin of (4.42) is uniformly globally stable (UGS). Moreover, we can not only conclude that ζ_x, ζ_y, ζ_c, and ζ_s are bounded, but using (4.42) that also $\dot{\zeta}_x$, $\dot{\zeta}_y$, $\dot{\zeta}_c$, and $\dot{\zeta}_s$ are bounded, and therefore also $\ddot{\zeta}_x$, and $\ddot{\zeta}_y$ (which follows by differentiating (4.42), and by using the fact that $\dot{v}$ and $\dot{\omega}$ are bounded).

Differentiating the bounded function

$$
V_2(\zeta) = -\dot{\zeta}_x \zeta_x - \dot{\zeta}_y \zeta_y
\tag{B.33}
$$

along the solutions of (4.42) results in

$$
\begin{aligned}
\dot{V}_2(\zeta) &= -\ddot{\zeta}_x \zeta_x - (v\zeta_c - l_1 \zeta_x)^2 - \ddot{\zeta}_y \zeta_y - (v\zeta_s - l_2 \zeta_y)^2 \\
&= -v^2 \left(\zeta_c^2 + \zeta_s^2 \right) + 2 l_1 v \zeta_c \zeta_x + 2 l_2 v \zeta_s \zeta_y \\
&\quad - l_1^2 \zeta_x^2 - l_2^2 \zeta_y^2 - \ddot{\zeta}_x \zeta_x - \ddot{\zeta}_y \zeta_y \\
&\leq -v_{\min}^2 \left(\zeta_c^2 + \zeta_s^2 \right) + M_x |\zeta_x| + M_y |\zeta_y|,
\end{aligned}
\tag{B.34}
$$

for certain constants M_x and M_y, where we used the previously derived boundedness of signals. Using Matrosov's theorem (Loría et al. (2005, Theorem 1), cf. Lefeber et al. (2017, Theorem 2)), we can conclude that (4.42) is UGAS. $\qquad\square$

Bibliography

Alam, A. A., Gattami, A., and Johansson, K. H. (2010). An experimental study on the fuel reduction potential of heavy duty vehicle platooning. In *13th International IEEE Conference on Intelligent Transportation Systems*, pages 306–311. IEEE.

Alvarez Aguirre, A. (2011). *Remote Control and Motion Coordination of Mobile Robots*. PhD thesis, Eindhoven University of Technology.

Attia, R., Orjuela, R., and Basset, M. (2012). Coupled longitudinal and lateral control strategy improving lateral stability for autonomous vehicle. *American Control Conference*, pages 6509–6514.

Bayuwindra, A., Aakre, Ø. L., Ploeg, J., and Nijmeijer, H. (2016). Combined lateral and longitudinal CACC for a unicycle-type platoon. *IEEE Intelligent Vehicles Symposium, Proceedings*, (4):527–532.

Bayuwindra, A., Lefeber, E., Ploeg, J., and Nijmeijer, H. (2019a). Extended Look-ahead Tracking Controller with Orientation-Error Observer for Vehicle Platooning. *IEEE Transactions on Intelligent Transportation Systems*, pages 00–00 (submitted).

Bayuwindra, A., Ploeg, J., Lefeber, E., and Nijmeijer, H. (2019b). Combined Longitudinal and Lateral Control of Car-Like Vehicle Platooning With Extended Look-Ahead. *IEEE Transactions on Control Systems Technology*, pages 1–14.

Beumer, T. P. (2017). *Control of Platooning Mobile Robots: Experimental Validation*. Master's thesis, Eindhoven University of Technology.

Bom, J., Thuilot, B., Marmoiton, F., and Martinet, P. (2005). A global control strategy for urban vehicles platooning relying on nonlinear decoupling laws. *2005 IEEE/RSJ International Conference on Intelligent Robots and Systems, IROS*, pages 1995–2000.

Braun, P. (2014). Three pieces of car tech you shouldn't leave the dealership without. https://www.digitaltrends.com/cars/road-rave-three-pieces-car-tech-shouldnt-leave-dealership-without/.

Brent, R. (1973). *Algorithms for Minimization without Derivatives*. Prentice-Hall, New Jersey.

Browand, F., McArthur, J., and Radovich, C. (2004). Fuel Saving Achieved in the Field Test of Two Tandem Trucks. Technical report.

Caarls, J. (2009). *Pose estimation for mobile devices and augmented reality*. phdthesis, Delft University of Technology, the Netherlands.

Canudas de Wit, C. (1998). Trends in mobile robot and vehicle control. In *Control Problems in Robotics and Automation*, pages 151–175. Springer-Verlag, London.

Chatzikomis, C. I. and Spentzas, K. N. (2009). A path-following driver model with longitudinal and lateral control of vehicle's motion. *Forschung im Ingenieurwesen/Engineering Research*, 73(4):257–266.

Chen, X. and Serrani, A. (2007). Smith Predictors in Nonlinear Systems - Application to ISS-based Leader/follower Trailing Control. In *American Control Conference*, pages 4506–4511, New York.

Commision of the European Communities (2006a). Europe Road Safety Action Programme - Mid-Term Review. Technical report, Brussels.

Commision of the European Communities (2006b). Keep Europe moving - Sustainable mobility for our continent - Mid-term review of the European Commission's 2001 Transport White Paper. Technical report, Brussels.

Commision of the European Communities (2006c). On the Intelligent Car Initiative - "Raising Awareness of ICT for Smarter, Safer and Cleaner Vehicles". Technical report, Brussels.

Englund, C., Chen, L., Ploeg, J., Semsar-Kazerooni, E., Voronov, A., Bengtsson, H. H., and Didoff, J. (2016). The Grand Cooperative Driving Challenge 2016: Boosting the introduction of cooperative automated vehicles. *IEEE Wireless Communications*, 23(4):146–152.

ENSEMBLE (2018). Platooning ENSEMBLE. https://platooningensemble.eu/.

ERSO (2016). Advanced driver assistance systems. Technical report.

Eyre, J., Yanakiev, D., and Kanellakopoulos, I. (1998). A Simplified Framework for String Stability Analysis of Automated Vehicles. *Vehicle System Dynamics*, 30(5):375–405.

Fahmy, H. M., Ghany, M. A. E., and Baumann, G. (2018). Vehicle Risk Assessment and Control for Lane-Keeping and Collision Avoidance at Low-Speed and High-Speed Scenarios. *IEEE Transactions on Vehicular Technology*, 67(6):4806–4818.

Farrelly, J. and Wellstead, P. (1996). Estimation of Vehicle Lateral Velocity. In *IEEE International Conference on Control Applications*, Dearborn, Miami.

Federal Highway Administration (2000). Roundabouts: An Informational Guide. Technical Report June.

Feng, S., Zhang, Y., Eben, S., Cao, Z., Liu, H. X., and Li, L. (2019). String stability for vehicular platoon control: Definitions and analysis methods. *Annual Reviews in Control*, 47:81–97.

Fujioka, T. and Omae, M. (1998). Vehicle Following Control in Lateral Direction for Platooning. *Vehicle System Dynamics*, 29:422–437.

Fukao, T., Aoki, T., Sugimachi, T., Yamada, Y., and Kawashima, H. (2013). Preceding Vehicle Following Based on Path Following Control for Platooning. *IFAC Proceedings Volumes*, 46(21):47–51.

Ge, J. I. and Orosz, G. (2014). Dynamics of connected vehicle systems with delayed acceleration feedback. *Transportation Research Part C*, 46:46–64.

Gehrig, S. K. and Stein, F. J. (1998). A trajectory-based approach for the lateral control of car following systems. *SMC'98 Conference Proceedings. 1998 IEEE International Conference on Systems, Man, and Cybernetics*, 4:3596–3601.

Gehring, O. and Fritz, H. (1997). Practical results of a longitudinal control concept for truck platooning with vehicle to vehicle communication. *Proceedings of Conference on Intelligent Transportation Systems*, pages 117–122.

Godbole, D. N. and Lygeros, J. (1994). Longitudinal Control of the Lead Car of a Platoon. *IEEE Transactions on Vehicular Technology*, 43(4):1125–1135.

Hassanain, I. (2017). *String-stable automated steering in cooperative driving applications.* Master's thesis, Delft University of Technology.

Huang, J. (2012). Vehicle Longitudinal Control. In *Handbook of Intelligent Vehicles*, pages 167–190. Springer London, London.

Huppe, X., Lafontaine, J. D., Beauregard, M., and Michaud, F. (2003). Guidance and control of a platoon of vehicles adapted to changing environment conditions. In *SMC'03 Conference Proceedings. 2003 IEEE International Conference on Systems, Man and Cybernetics. Conference Theme - System Security and Assurance (Cat. No.03CH37483)*, volume 4, pages 3091–3096.

Iguchi, M., Miyazaki, T., and Aoki, M. (1996). Promotion of the Program of Advanced Safety Vehicles for 21st Century. *IFAC Proceedings Volumes*, 29(1):7856–7861.

Isidori, A. (1995). *Nonlinear Control Systems.* Communications and Control Engineering. Springer London, London.

Jabil (2019). Advanced Driver Assistance Systems: Driving Safety Forward. https://www.jabil.com/solutions/by-industry/consumer/automotive-electronics-components/advanced-driver-assistance-systems-automotive-transportation.html.

Jakubiak, J., Lefeber, E., Tchon, K., and Nijmeijer, H. (2002). Two observer-based tracking algorithms for a unicycle mobile robot. *International Journal of Applied Mathematics and Computer Science*, 12(4):513–522.

Jakubiak, J., Nijmeijer, H., and Lefeber, E. (1999). Observer based tracking controllers for a mobile car. Technical report.

Jiang, Z.-P. and Nijmeijer, H. (1997). Tracking Control of Mobile Robots: A Case Study in Backstepping. *Automatica*, 33(7):1393–1399.

Kanayama, Y., Kimura, Y., Miyazaki, F., and Noguchi, T. (1990). A stable tracking control method for an autonomous mobile robot. In *Proceedings., IEEE International Conference on Robotics and Automation*, volume 30, pages 384–389. IEEE Comput. Soc. Press.

Khalil, H. K. (2002). *Nonlinear systems*. Prentice Hall, 3rd edition.

Kianfar, R. (2014). *On Cooperative Control of Automated Driving Systems from a Stability and Safety Perspective*. Phd thesis, Chalmers University of Technology.

Kianfar, R., Ali, M., Falcone, P., and Fredriksson, J. (2014). Combined longitudinal and lateral control design for string stable vehicle platooning within a designated lane. In *17th International IEEE Conference on Intelligent Transportation Systems (ITSC)*, pages 1003–1008. IEEE.

Lauer, M. (2011). Grand Cooperative Driving Challenge 2011. *IEEE Intelligent Transportation Systems Magazine*, 3(3):38–40.

Lefeber, E., Ploeg, J., and Nijmeijer, H. (2017). A Spatial Approach to Control of Platooning Vehicles: Separating Path-Following from Tracking. *IFAC-PapersOnLine*, 50(1):15000–15005.

Lim, E. H. M. and Hedrick, J. K. (1999). Lateral and longitudinal vehicle control coupling for automated vehicle operation. In *Proceedings of the 1999 American Control Conference (Cat. No. 99CH36251)*, volume 5, pages 3676–3680.

Loría, A. and Panteley, E. (2005). Cascaded Nonlinear Time-Varying Systems: Analysis and Design. In *Lecture Notes in Control and Information Science*, pages 23–64.

Loría, A., Panteley, E., Popovic, D., and Teel, A. R. (2005). A nested Matrosov theorem and persistency of excitation for uniform convergence in stable nonautonomous systems. *IEEE Transactions on Automatic Control*, 50(2):183–198.

Mondada, F. and Bonani, M. (2007). E-puck education robot. http://www.e-puck.org.

Morales, A. and Nijmeijer, H. (2016). Merging strategy for vehicles by applying cooperative tracking control. *IEEE Transactions on Intelligent Transportation Systems*, 17(12):3423–3433.

Morales Medina, A. I. (2018). *Cooperative Intersection Control for Autonomous Vehicle.* phdthesis, Eindhoven University of Technology.

Morales Medina, A. I., Van De Wouw, N., and Nijmeijer, H. (2018). Cooperative Intersection Control Based on Virtual Platooning. *IEEE Transactions on Intelligent Transportation Systems*, 19(6):1727–1740.

Morin, P. and Samson, C. (2008). Motion Control of Wheeled Mobile Robots. *Springer Handbook of Robotics*, pages 799–826.

Naus, G. J. L., Ploeg, J., Vugts, R. P. A., van de Molengraft, M. J. G., and Steinbuch, M. (2010a). Cooperative adaptive cruise control, design and experiments. In *2010 American Control Conference*, volume 1, pages 6145–6150.

Naus, G. J. L., Vugts, R. P. A., Ploeg, J., van de Molengraft, M. J. G., and Steinbuch, M. (2010b). String-stable CACC design and experimental validation: A frequency-domain approach. *IEEE Transactions on Vehicular Technology*, 59(9):4268–4279.

NHTSA (2017). Automated Driving Systems 2.0: A Vision for Safety. https://www.nhtsa.gov/sites/nhtsa.dot.gov/files/documents/13069a-ads2.0_090617_v9a_tag.pdf.

Nijmeijer, H. and van der Schaft, A. J. (1990). *Nonlinear Dynamical Control Systems.* Springer-Verlag, New York.

Noijen, S. P. M., Lambrechts, P. F., and Nijmeijer, H. (2005). An observer-controller combination for a unicycle mobile robot. *International Journal of Control*, 78(2):81–87.

Oguchi, T. and Nijmeijer, H. (2005). Control of non-linear systems with time-dealy using state predictor based on synchronization. In *EUROMECH nonlinear dynamics conference*, number August, pages 7–12, Eindhoven.

OICA (2018). Production Statistics. http://www.oica.net/category/production-statistics/2018-statistics/.

Omae, M., Fujioka, T., Hashimoto, N., and Shimizu, H. (2006). The Application of RTK-GPS and Steer-By-Wire Technology to the Automatic Driving of Vehicles and and Evaluation of Driver Behavior. *IATSS Research*, 30(2):29–38.

Pant, A., Seiler, P., Koo, T., and Hedrick, K. (2001). Mesh stability of unmanned aerial vehicle clusters. In *American Control Conference*, pages 62–68 vol.1, Arlington.

Panteley, E., Lefeber, E., Loría, A., and Nijmeijer, H. (1998). Exponential Tracking Control of a Mobile Car Using a Cascaded Approach. *IFAC Workshop on Motion Control*, 31(27):201–206.

Park, J. H. and Kim, J. H. (1999). Estimation of Vehicle Lateral Velocity With a Nonlinear Sliding-Mode Observer. In *14th World Congress of IFAC*, pages 8172–8177. Elsevier.

Pascual, J. P. C. (2009). *Advanced Driver Assistance System based on Computer Vision using Detection, Recognition and Tracking of Road Signs.* Ph.d. thesis, Charles III University of Madrid, Madrid, Spain.

Petrov, P. (2008). A mathematical model for control of an autonomous vehicle convoy. *WSEAS Transactions on Systems and Control*, 3(9):835–848.

Petrov, P. (2009). Nonlinear Adaptive Control of a Two-Vehicle Convoy. *The Open Cybernetics & Systemics Journal*, 3(2):70–78.

Pettersson, P. (2008). *Estimation of Vehicle Lateral Velocity.* Master's thesis, Lund University, Sweden.

Pham, M. and Wang, D. (2006). Unified Control Design for Autonomous Car-Like Vehicle Tracking Maneuvers. *Autonomous Mobile Robots*, pages 295–329.

Plaskonka, J. (2015). Different Kinematic Path Following Controllers for a Wheeled Mobile Robot of (2,0) Type. *Journal of Intelligent and Robotic Systems*, 77(3-4):481–498.

Ploeg, J. (2014). *Analysis and design of controllers for cooperative and automated driving.* PhD thesis, Eindhoven University of Technology.

Ploeg, J., Scheepers, B. T. M., van Nunen, E., van de Wouw, N., and Nijmeijer, H. (2011). Design and experimental evaluation of cooperative adaptive cruise control. In *2011 14th International IEEE Conference on Intelligent Transportation Systems (ITSC)*, pages 260–265.

Ploeg, J., Semsar-Kazerooni, E., Morales Medina, A. I., De Jongh, J. F., Van De Sluis, J., Voronov, A., Englund, C., Bril, R. J., Salunkhe, H., Arrue, A., Ruano, A., Garcia-Sol, L., Van Nunen, E., and Van De Wouw, N. (2018). Cooperative Automated Maneuvering at the 2016 Grand Cooperative Driving Challenge. *IEEE Transactions on Intelligent Transportation Systems*, 19(4):1213–1226.

Ploeg, J., Shladover, S. E., Nijmeijer, H., and van de Wouw, N. (2012). Introduction to the Special Issue on the 2011 Grand Cooperative Driving Challenge. In *IEEE Transactions on Intelligent Transportation Systems*, volume 13, pages 989–993.

Ploeg, J., van de Wouw, N., and Nijmeijer, H. (2014). Lp string stability of cascaded systems: Application to vehicle platooning. *IEEE Transactions on Control Systems Technology*, 22(2):786–793.

Rajamani, R. (2012). *Vehicle Dynamics and Control.* Springer New York, 2nd edition.

Rajamani, R. and Shladover, S. E. (2001). An experimental comparative study of autonomous and co-operative vehicle-follower control systems. *Transportation Research Part C: Emerging Technologies*, 9(1):15–31.

Rajamani, R., Tan, H. S., Law, B. K., and Zhang, W. B. (2000). Demonstration of integrated longitudinal and lateral control for the operation of automated vehicles in platoons. *IEEE Transactions on Control Systems Technology*, 8(4):695–708.

Rajamani, R. and Zhu, C. (2002). Semi-autonomous adaptive cruise control systems. *IEEE Transactions on Vehicular Technology*, 51(5):1186–1192.

Ramsey, M. (2015). Self-Driving Cars Could Cut Down on Accidents, Study Says. https://www.wsj.com/articles/self-driving-cars-could-cut-down-on-accidents-study-says-1425567905.

Ranjitkar, P., Nakatsuji, T., Gurusinghe, G. S., and Azuta, Y. (2002). Car-Following Experiments Using RTK GPS and Stability Characteristics of Followers in Platoon. In *Applications of Advanced Technologies in Transportation*, pages 608–615, Reston, VA. American Society of Civil Engineers.

Ren, D., Zhang, J., and Du, C. (2007). Variable structure adaptive control for vehicle longitudinal following in a platoon. *2007 IEEE International Conference on Robotics and Biomimetics, ROBIO*, (05):1906–1910.

Rodrigue, J.-P. (2017). *The Geography of Transport System*. Routledge, New York.

Royal Haskoning (2009). Roundabouts - Application and design. Technical Report June.

Santo, D. (2016). Autonomous Cars' Pick: Camera, Radar, Lidar? https://www.eetimes.com/author.asp?section_id=36&doc_id=1330069#.

Shaw, E. and Hedrick, J. K. (2007). Controller design for string stable heterogeneous vehicle strings. In *Proceedings of the IEEE Conference on Decision and Control*, pages 2868–2875.

Sheikholeslam, S. and Desoer, C. A. (1990). Longitudinal Control of a Platoon of Vehicles. In *1990 American Control Conference*, pages 291–296. IEEE.

Sheikholeslam, S. and Desoer, C. A. (1992a). A System Level Study of the Longitudinal Control of a Platoon of Vehicles. *Journal of Dynamic Systems, Measurement, and Control*, 114(2):286.

Sheikholeslam, S. and Desoer, C. A. (1992b). Combined Longitudinal and Lateral Control of a Platoon of Vehicles. *1992 American Control Conference*, 1:1763–1767.

Sheikholeslam, S. and Desoer, C. A. (1993). Longitudinal control of a platoon of vehicles with no communication of lead vehicle information: A system level study. *IEEE Transactions on Vehicular Technology*, 42(4):546–554.

Shladover, S. E. (1995). Review of the state of development of advanced vehicle control systems (AVCS). *Vehicle System Dynamics*, 24(6-7):551–595.

Shladover, S. E. (2006). Automated vehicles for highway operations (automated highway systems). *Proceedings of the Institution of Mechanical Engineers, Part I: Journal of Systems and Control Engineering*, 219(1):53–75.

Shladover, S. E. (2008). Longitudinal Control of Automotive Vehicles in Close-Formation Platoons. *Journal of Dynamic Systems, Measurement, and Control*, 113(2):231.

Shladover, S. E., Desoer, C. A., Hedrick, J. K., Tomizuka, M., Walrand, J., Zhang, W. B., McMahon, D. H., Peng, H., Sheikholeslam, S., and McKeown, N. (1991). Automatic vehicle control developments in the PATH program. *IEEE Transactions on Vehicular Technology*, 40(1 pt 1):114–130.

Silverman, L. (1969). Inversion of multivariable linear systems. *IEEE Transactions on Automatic Control*, 14(3):270–276.

Solyom, S., Idelchi, A., and Salamah, B. B. (2013). Lateral control of vehicle platoons. In *2013 IEEE International Conference on Systems, Man, and Cybernetics*, pages 4561–4565. Chalmers University of Technology, Göteborg, Sweden.

Stern, R. E., Cui, S., Delle Monache, M. L., Bhadani, R., Bunting, M., Churchill, M., Hamilton, N., Haulcy, R., Pohlmann, H., Wu, F., Piccoli, B., Seibold, B., Sprinkle, J., and Work, D. B. (2018). Dissipation of stop-and-go waves via control of autonomous vehicles: Field experiments. *Transportation Research Part C: Emerging Technologies*, 89:205–221.

Sugiyama, Y., Fukui, M., Kikuchi, M., Hasebe, K., Nakayama, A., Nishinari, K., Tadaki, S. I., and Yukawa, S. (2008). Traffic jams without bottlenecks-experimental evidence for the physical mechanism of the formation of a jam. *New Journal of Physics*, 10.

Swaroop, D. and Hedrick, J. K. (1999). Constant Spacing Strategies for Platooning in Automated Highway Systems. *Journal of Dynamic Systems, Measurement, and Control*, 121(3):462.

Swaroop, D., Hedrick, J. K., and Choi, S. B. (2001). Direct adaptive longitudinal control of vehicle platoons. *IEEE Transactions on Vehicular Technology*, 50(1):150–161.

Tientrakool, P., Ho, Y. C., and Maxemchuk, N. F. (2011). Highway capacity benefits from using vehicle-to-vehicle communication and sensors for collision avoidance. *IEEE Vehicular Technology Conference*, pages 0–4.

Toyota (2014). Toyota to Bring Vehicle-Infrastructure Cooperative Systems to New Models in 2015.

Tunçer, Ö., Güvenç, L., Coskun, F., and Karsligil, E. (2010). Vision based lane keeping assistance control triggered by a driver inattention monitor. In *Conference Proceedings - IEEE International Conference on Systems, Man and Cybernetics*, pages 289–297. IEEE.

Unsal, C. (1998). *Intelligent navigation of autonomous vehicles in an automated highway system: Learning methods and interacting vehicles approach.* Phd thesis, Virginia Polytechnic Institute and State University.

Vahidi, A. and Eskandarian, A. (2003). Research advances in intelligent collision avoidance and adaptive cruise control. *IEEE Transactions on Intelligent Transportation Systems*, 4(3):143–153.

van den Broek, T. H. A., van de Wouw, N., and Nijmeijer, H. (2009). Formation control of unicycle mobile robots: a virtual structure approach. In *Joint 48th IEEE Conference on Decision and Control and 28th Chinese Control Conference*, pages 8328–8333. IEEE.

van Nunen, E., Kwakkernaat, M. R. J. A. E., Ploeg, J., and Netten, B. D. (2012). Cooperative Competition for Future Mobility. *IEEE Transactions on Intelligent Transportation Systems*, 13(3):1018–1025.

Varaiya, P. (1993). Smart cars on smart roads: Problems of control. *IEEE Transactions on Automatic Control*, 38(2):195–207.

Vugts, R. P. A. (2010). *String-Stable CACC Design and Experimental Validation.* PhD thesis, Eindhoven University of Technology.

Warnick, S. C. and Rodriguez, A. A. (1994). Longitudinal control of a platoon of vehicles with multiple saturating nonlinearities. *Proceedings of 1994 American Control Conference - ACC '94*, 1.

Williams, M. (1988). PROMETHEUS - The European research programme for optimising the road transport system in Europe. *IEE Colloquium on Driver Information*, pages 1–9.

Xing, H., Ploeg, J., and Nijmeijer, H. (2019). Compensation of communication delays in CACC. *IEEE Transactions on Vehicular Technology*.

Yamasaki, T. and Balakrishnan, S. N. (2010). Sliding mode-based pure pursuit guidance for unmanned aerial vehicle rendezvous and chase with a cooperative aircraft. *Proceedings of the Institution of Mechanical Engineers, Part G: Journal of Aerospace Engineering*, 224(10):1057–1067.

Yamasaki, T., Enomoto, K., Takano, H., Baba, Y., and Balakrishnan, S. (2012). Advanced Pure Pursuit Guidance via Sliding Mode Approach for Chase UAV. (August):1–16.

Yanakiev, D. and Kanellakopoulos, L. (1998). Nonlinear spacing policies for automated heavy-duty vehicles. *IEEE Transactions on Vehicular Technology*, 47(4):1365–1377.

Zhang, L. and Orosz, G. (2016). Motif-Based Design for Connected Vehicle Systems in Presence of Heterogeneous Connectivity Structures and Time Delays. *IEEE Transactions on Intelligent Transportation Systems*, 17(6):1638–1651.

Zhao, J., Oya, M., and Kamel, A. E. (2009). A safety spacing policy and its impact on highway traffic flow. *IEEE Intelligent Vehicles Symposium, Proceedings*, pages 960–965.

Zheng, Y., Bian, Y., Li, S., and Li, S. E. (2019). Cooperative Control of Heterogeneous Connected Vehicles with Directed Acyclic Interactions. *IEEE Intelligent Transportation Systems Magazine*, pages 1–12.

Acknowledgements

This thesis concluded the years of my research at Dynamics and Control group of Mechanical Engineering, Eindhoven University of Technology. A long, winding journey, but feels like a glance. At the end, it is not the title that matters the most, but the experiences and the personal development along the way. I am genuinely grateful for the opportunity to work with great people in an amazingly dynamic environment. I would have never been able to complete my thesis without the guidance and help of many special people, to whom I would like to express my appreciation and gratitude.

First of all, I would like to express my appreciation and gratitude to my supervisor, Prof. Henk Nijmeijer. Dear Henk, I am very grateful for having you as my tremendous mentor. I sincerely thank you for your constant encouragement, guidance, patience, and valuable advice throughout this research, which became invaluable sources of inspiration for me during my research years. I enjoyed our discussions and countless meetings.

I extend my gratitude to my co-supervisors, Jeroen Ploeg and Erjen Lefeber. Dear Jeroen, thanks for your guidance, constant support, and advice during my PhD research. I very much appreciate your prompt response to my papers and reports at any time, even during your weekends and holidays. This greatly helps me to develop my technical writing skills. Dear Erjen, I would like to thank you for your endless guidance and valuable suggestions to improve my research on the theoretical side. I have benefited greatly from your mathematical and theoretical knowledge, and I am grateful for the countless hours of our discussions in front of the whiteboard. Dear Jeroen and Erjen, I truly appreciate your efforts in pointing out the weak points of my research and being critical throughout these years.

I would also like to extend my sincere gratitude to my doctorate committee members, Prof. Rudy Negenborn, Prof. Jan Huissoon, Prof. Bayu Jayawardhana, and Prof. Johan Lukkien for their critical reading, evaluation of my thesis, and for their valuable comments and feedback.

My gratitude is further extended to the Indonesian Ministry of Finance, through the Indonesia Endowment Fund for Education (LPDP), for their full financial

Curriculum vitae

Anggera Bayuwindra was born on July 12, 1984, in Bandung, Indonesia. After finishing the bachelor's degree in Electrical Engineering (Control Engineering) in 2006 at Institut Teknologi Bandung, Indonesia, he worked as an Engineer in Infineon Technologies, Batam, Indonesia. In 2011, he studied Control & Intelligent System in the department of Electrical Engineering at Institut Teknologi Bandung, Indonesia, and obtained Master of Science degree (cum laude) in 2012. His master thesis focused on the sliding mode control design of the Anti-lock Braking System.

In 2013, he started his PhD research in the Dynamics and Control group, at the department of Mechanical Engineering in Eindhoven University of Technology, working on the look-ahead tracking controllers for integrated longitudinal and lateral control of vehicle platoons. During the period 2013-2014, he took graduate courses at the Dutch Institute of Systems and Control (DISC) and received the DISC certificate. The main results of his PhD research are presented in this dissertation.